
On the relevance of PS exposure as a regulatory event for
ADAM10-mediated substrate release

Dissertation
zur Erlangung des Doktorgrades
der Mathematisch-Naturwissenschaftlichen Fakultät
der Christian-Albrechts-Universität zu Kiel

vorgelegt von
Florian Bleibaum
Kiel, 2018

Erster Gutachter: Prof. Dr. Thomas Roeder

Zweiter Gutachter: Prof. Dr. Karina Reiss

Tag der mündlichen Prüfung: 28.05.2018

Zum Druck genehmigt:

Gez. Prof. Dr. Natascha Oppelt, Dekanin

Table of contents

1. Introduction	7
1.1 Classification of ADAM proteases	7
1.1.1 Structure of ADAM10 and ADAM17	8
1.2 Physiological and pathophysiological roles of ADAM10.....	11
1.2.1 ADAM10 expression, trafficking, and function	11
1.2.2 ADAM10 substrates	12
1.2.1 ADAM10 roles in disease models.....	13
1.2.2 ADAM10 mechanism of activation.....	16
1.3 ADAM10 in the context cell membrane (re)organisation.....	17
1.3.1 Scramblase-mediated phospholipid transport.....	18
2. Aim of the thesis:.....	22
3. Material and Methods.....	23
3.1 Consumables and equipment.....	23
3.2 Chemicals	25
3.3 Kits.....	27
3.4 Software.....	27
3.5 Stimuli and inhibitors	28
3.6 Primary and secondary antibodies	28
3.7 Plasmids	29
3.8 General buffers	30
3.9 Cells and cell lines.....	32
3.10 Cell and cell culture cultivation and passaging	32
3.10.1 Cell counting	33
3.10.2 Cell culture cryopreservation	33
3.11 Rabbit erythrocyte – pVCC model.....	33
3.11.1 Isolation and preparation of rabbit erythrocyte from whole blood.....	33
3.11.2 Rabbit erythrocyte – pVCC hemolysis assay.....	34
3.11.3 Rabbit erythrocytes – pVCC Western Blot samples.....	34
3.12 ADAM10 stalk mutants.....	35
3.12.1 ADAM10 stalk mutants primer design	35
3.12.2 ADAM10 plasmid mutagenesis	35
3.12.3 Production of chemically competent <i>E.coli</i> cells	36
3.12.4 ADAM10 Stalk mutant transformation, cultivation, and purification.....	36
3.12.5 Bacterial glycerol stocks of ADAM10 stalk mutants	36
3.12.6 ADAM10 stalk mutants sequencing and analysis	37
3.13 Western Blot analysis of ADAM10 shedding assays.....	37
3.13.1 Protein concentration determination	37

3.13.2	Sodium dodecyl sulfate (SDS) polyacrylamide gel electrophoresis.....	37
3.13.3	Western Blot transfer and analysis	38
3.13.4	Antibody detection of transferred proteins	38
3.13.5	Antibody removal and re-probing of PVDF membrane	39
3.14	Transient transfection of adherent cells	39
3.15	Alkaline phosphatase assays	39
3.15.1	Inhibition, stimulation, and analysis of alkaline phosphatase assays	40
3.16	Flow cytometry analysis	40
3.16.1	Flow cytometry analysis of Annexin-V labelled rabbit erythrocytes	41
3.16.2	Flow cytometry analysis of Annexin-V labelled cells COS7 cells	41
3.16.3	Flow cytometry analysis of ADAM10 expression	41
3.16.4	Flow cytometry analysis of CD23 and lactadherin labelling	42
3.17	Confocal microscopic analysis of Annexin-V labelled cells	42
3.18	ADAM10 fluorescent peptide substrate assay	43
3.19	Biophysical experiments with the ADAM10 stalk peptide.....	43
3.19.1	Preparation of lipid aggregates/liposomes.....	44
3.19.2	Acoustic wave biochip analyses	44
3.19.3	Fluorescence resonance energy transfer spectroscopy (FRET)	44
3.19.4	Isothermal Titration Calorimetry (ITC)	45
3.20	ADAM10 and ADAM17 – OPS interaction model	45
3.21	Statistical analysis.....	45
4.	Results.....	46
4.1	Stimulation with ADAM10 activators leads to PS exposure	46
4.2	OPS inhibits the shedding of overexpressed ADAM10 substrates.....	47
4.3	OPS inhibits ADAM10-mediated shedding of endogenously expressed substrates.....	50
4.4	ADAM10 constitutive <i>bona fide</i> enzymatic activity remains functional under OPS.....	53
4.5	PS exposure regulates ADAM10 shedding activity	54
4.6	TMEM16F/ANO6-related activity supports the functional role of PS in ADAM10-mediated shedding activity.....	60
4.7	Gain of function in TMEM16F/ANO6 PS scrambling activity drives ADAM10-mediated substrate release.....	66
4.8	Loss of function of TMEM16F/ANO6 PS scrambling impairs ADAM10 shedding activity.....	69
4.9	ADAM10 stalk domain interacts with PS, based on sequence and structural data analyses	73
4.10	ADAM10 stalk domain intercalates into PS liposomes via a biphasic mechanism of interaction.....	74
4.11	ADAM10 enhanced shedding activity depends on a positively charged stalk domain	77

4.12	ADAM10 enhanced <i>bona fide</i> enzymatic activity depends on a positively charged stalk domain	80
5.	Discussion.....	83
5.1	PS exposure regulates ADAM10 shedding activity	83
5.2	Phospholipid scramblase TMEM16F/ANO6 contributes to ADAM10 shedding activity through enhanced PS exposure	86
5.3	Loss of TMEM16F/ANO6 scrambling activity is related to impaired ADAM10-mediated substrate release	90
5.4	ADAM10 stalk domain facilitates the interaction with PS	91
5.5	The stalk domain of ADAM10 is essential for substrate shedding.....	93
5.6	A model behind PS regulation of ADAM10 shedding activity	95
6.	Outlook.....	100
7.	Summary.....	103
8.	Zusammenfassung.....	105
9.	References:.....	107
10.	List of figures.....	115
11.	List of tables	116
12.	Abbreviations	117
13.	Acknowledgments	120
14.	Erklärung.....	121
15.	Curriculum vitae	122

1. Introduction

Post-translational modification of proteins is a critical step to maintain proteostasis. Within the variety of post-translational modifications, proteolysis is the most significant modification, because it is irreversible and ubiquitous. It involves the breakdown of proteins to smaller metabolically active peptides, which emphasises the importance the role proteases have in cell fate. Although the percentage of the human genome that encodes for proteases is overall little (Turk, 2006), there is an enormous variety of proteases with an even more impressive diversity in functions (Puenta et al., 2003). One group of proteases with particular importance for many physiological processes are the metalloproteinases. Among these is the superfamily of metzincin proteases which comprises the physiologically significant group: the “*a disintegrin and metalloproteinases*” (ADAMs).

1.1 Classification of ADAM proteases

The metzincin family comprises the “*a disintegrin and metalloproteinases*” (ADAMs), the “*a disintegrin and metalloproteinases with a thrombospondin motif*” (ADAMTSSs) and the snake venom metalloproteinases (SVMPs, Fig. 1, Edwards et al., 2008). The members of the ADAM family are type I transmembrane proteases (Saftig and Lichtenthaler, 2015). The first ADAM protease (ADAM1, PH-30) which was firstly purified in 1987 by Primakoff et al. (1987) and described in 1992 in further detail by Blobel et al. (1992) established the base of this new protein family. Interestingly, while the identification of ADAM1 was essential for the establishment of this group of proteins *per se*, this protein turned out to be a proteolytically inactive member of the ADAM family. However, the inactive members of this family fulfil critical physiological functions as, e.g., sperm-egg cell adhesion proteins in fertilisation (Wong et al., 2001).

To date, 21 ADAM proteases are described in the human genome, of which 13 show proteolytic activity (ADAM: DEC-1, 8, 9, 10, 12, 15, 17, 19, 20, 21, 28, 30, 33, Edwards et al., 2008). Amongst these, ADAM10 and ADAM17 are the two most comprehensively studied proteases regarding their function in physiological and pathophysiological processes and the variety of substrates they cleave (Reiss and Saftig, 2009). The cleavage of the myelin basic protein was the first function of ADAM10 ever described (Chantry et al., 1989); however, this remained unknown until its amplification and cloning allowed its further characterisation (Howard et al., 1996). In addition to ADAM10, ADAM17 was first described as the protease mediating the proteolytic release of tumor necrosis factor-alpha (TNF- α) and named by its function: tumor necrosis factor-alpha converting enzyme (TACE, Black et al., 1997, Moss et al., 1997).

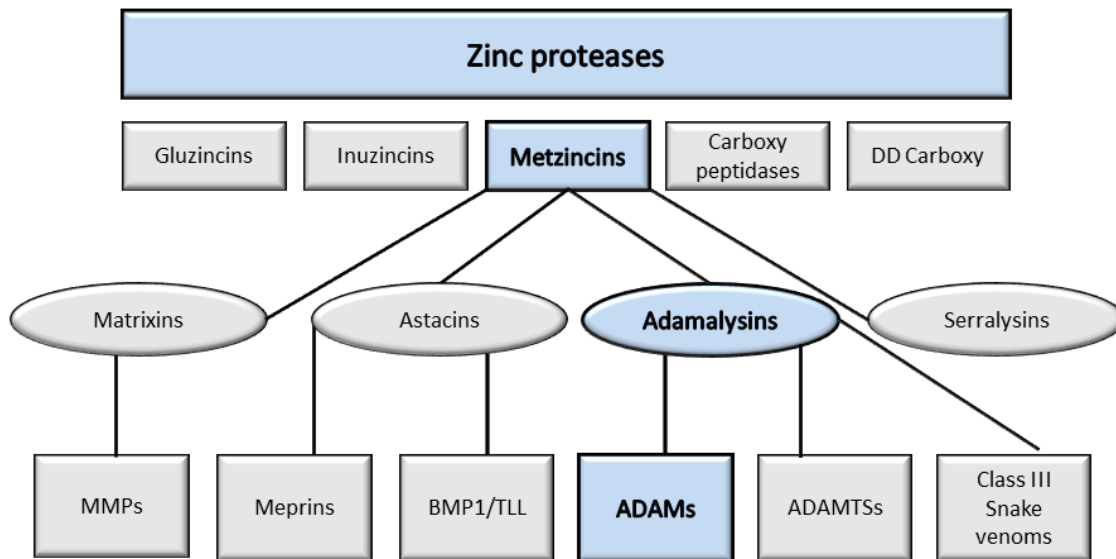


Figure 1. Overview of the zinc-dependent proteases superfamilies.

Zinc-dependent proteases are classified into the gluzincins, inuzincins, metzincins, carboxypeptidases and DD carboxy superfamilies. The superfamily of metzincin proteases summarises the proteases families: matrixins, astacins, adamalysins, and serralysins. The family of adamalysins contains three subgroups: the “*a disintegrin and metalloproteinases*” (ADAMs), the “*a disintegrin and metalloproteinases with a thrombospondin motif*” (ADAMTSs), and the snake venom metalloproteinases (class III snake venoms). Overview modified from Huxley-Jones et al. (2007).

1.1.1 Structure of ADAM10 and ADAM17

The direct comparison of the different domains of ADAM10 and ADAM17 demonstrates their high structural similarity (Fig. 2a). Both proteases contain a pro-domain, which in ADAM10 functions as a natural inhibitor of proteolytic activity (Moss et al., 2007). This domain is followed by a catalytic active metalloprotease domain, which mediates the enzymatic cleavage of substrates (Giebeler and Zigrino, 2016). It contains a zinc ion chelating multi histidine motif (HEXGHXXGXXHD) in its centre (Fig. 2b, upper and lower panel). This histidine motif is what differentiates ADAM10 and ADAM17 from other, non-catalytically active members of the ADAM protein family (e.g., ADAM22); where the histidine is almost entirely replaced (Fig. 2b, middle and lower panel, Liu et al., 2009). In addition to the proteolytically active metalloprotease domain, ADAM10 contains a disintegrin (D) and a cysteine-rich (C) domain. Part of the D domain and the entire C domain in ADAM17 are referred to as membrane-proximal domain (MPD, Fig. 2a, Lorenzen et al., 2012). The ADAM10 C domain contains a substrate recognition motif (Janes et al., 2005) while the ADAM17 MPD is involved in the regulation of the protease proteolytic activity (Sommer et al., 2016). The ADAM10 D+C domains and the ADAM17 MPD share further structural similarities. For instance, the MPD of ADAM17 contains a thioredoxin motif (CXXC) that can also be found in the C domain of ADAM10 (Atapattu et al., 2016). For ADAM17 it was shown that the protein-disulfide isomerase (PDI) reshuffles the cysteine connections of the CXXC motif and mediates the transition between the “open” and the “closed” form of the MPD. The PDI-mediated reassembling of the CXXC disulfide bounds closes/inactivate ADAM17 shedding activity

(Dusterhoft et al., 2013). However, although both proteases possess a thioredoxin motif, PDI-related effect could not be described for ADAM10. Interestingly, mutation of the CXXC motif in ADAM10 led to a reduced antibody binding to the C domain, suggesting that this motif is of similar importance in ADAM10 (Atapattu et al., 2016). The C domain of ADAM10 and the MPD of ADAM17 are followed by a flexible stalk domain, which for ADAM17 is referred to as “conserved ADAM17 dynamic interaction sequence” (CANDIS, Dusterhoft et al., 2014). The CANDIS in ADAM17 shows properties of an amphipathic alpha helix that interacts with the plasma membrane (Dusterhoft et al., 2015), and it is also involved in the recognition of the substrates IL-6R and IL-1RII (Dusterhoft et al., 2014, Dusterhoft et al., 2015). In ADAM10, the flexible stalk domain can interact with tetraspanin 15 (Tspan15), as indicated by co-immunoprecipitation of Tspan15 using an overexpressed ADAM10 stalk-only mutant (Noy et al., 2016). Both, the CANDIS in ADAM17 and the flexible stalk in ADAM10, are followed by their transmembrane domain (TMD), which is suggested to be necessary for the dimerisation (Deng et al., 2014) of ADAM10 and for substrate shedding in ADAM17 (Li et al., 2007). The structure of ADAM10 and ADAM17 ends with a cytoplasmic domain, which is described to be necessary for homo-dimerisation in both proteases (Xu et al., 2012, Deng et al., 2014). However, this cytoplasmic domain is preferably an inhibitor than a promotor of ADAM10 shedding activity and is completely negligible for stimulated substrate shedding (Maretzky et al., 2015). Independently of the asserted importance of the different domains of ADAM10 and ADAM17, described in both *in vitro* and *in vivo* experiments, a complete understanding of their function requires a full three-dimensional model of the proteases. The latest three-dimensional structure of ADAM10 comprises the disintegrin, cysteine-rich and metalloproteinase domain and only lacks parts of the stalk domain and the entire transmembrane and cytoplasmic domain (Seegar et al., 2017). Nevertheless, this structure provides essential insight on how substrate recognition and cleavage by ADAM10 is facilitated. Despite the physiological importance of both proteases, little is known about the mechanisms regulating ADAM10 shedding activity.

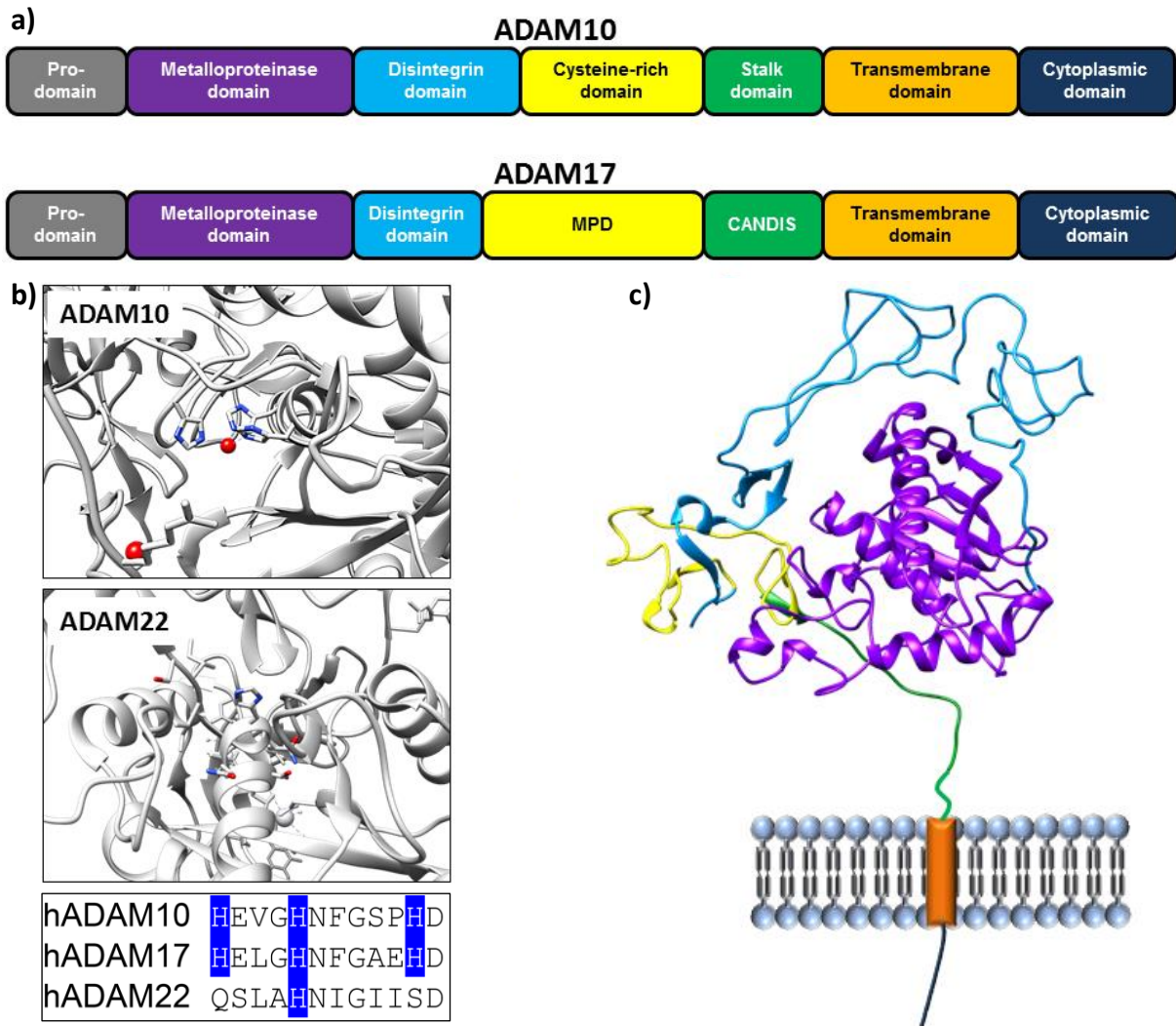


Figure 2. Structural overview and characteristics of ADAM10.

a) ADAM10 and ADAM17 show a highly conserved domain structure. **b)** ADAM10 metalloproteinase domain (upper picture) indicate three histidine side chains (blue) chelating a zinc ion (red). Proteolytically inactive ADAM22 shows an impaired histidine motif and no ion binding (middle picture). A sequence alignment of human ADAM10 (hADAM10), human ADAM17 (hADAM17), and human ADAM22 (hADAM22) indicates a conserved multi histidine motif (blue) for the proteolytically active proteases ADAM10 and ADAM17. The multi histidine motif is absent in the proteolytically inactive ADAM22 (lower picture). The histidine motif is highly conserved among proteolytically active metalloproteinases like ADAM10 and ADAM17. **c)** The three-dimensional ribbon structure highlights the spatial coordination of the different extracellular domains of ADAM10. The metalloproteinase domain (M, purple), disintegrin domain (D, blue), and cysteine domain (C, yellow) and partially the stalk domain (green) represent the spatial resolution of the available ADAM10 structure (PDB: 6BDZ). Unresolved/missing structural parts of ADAM10 (parts of the stalk domain - green, transmembrane domain - orange, and cytoplasmic domain - dark blue) were manually added to the ADAM10 ribbon structure. Pro-domain is not shown. Colours in c represent the different domains highlighted according to the basic scheme in a.

1.2 Physiological and pathophysiological roles of ADAM10

The most critical function of ADAM10 is the proteolytic release of metabolically active extracellular domains of membrane-anchored or type I or II transmembrane proteins from the cell surface. This process is referred to as ectodomain shedding (Arribas and Borroto, 2002). Before ADAM10-mediated substrate shedding takes place, the protease undergoes various intracellular modifications which define the maturation and trafficking of ADAM10 to the cell surface where substrate shedding takes place.

1.2.1 ADAM10 expression, trafficking, and function

The metalloproteinase ADAM10 is ubiquitously expressed (Weber and Saftig, 2012) and translated as a pro-form, with the pro-peptide sequence located at its N-terminus. The peptide pro-domain of ADAM10 works, on the one hand, as a natural inhibitor of its enzymatic activity and, on the other hand, as chaperone-like protein preventing its degradation (Moss et al., 2007). Mutants of ADAM10 lacking the pro-domain tend to be faster degraded while overexpression of the pro-domain, only in this setup, prevents the protease from degradation (Anders, 2001). The ADAM10 pro-form is transported through the endoplasmatic reticulum (ER) to the Golgi apparatus, where cleavage of the pro-domain leads to its maturation. The proprotein convertase 7 and furin were shown to cleave the pro-domain of ADAM10 (Reiss and Saftig, 2009). The Golgi apparatus is also the cellular compartment where the highest accumulation of ADAM10 is found (Moss et al., 2007). Besides the removal of the pro-domain, other modifications to ADAM10, e.g., glycosylation, are also required to ensure its correct folding and trafficking. ADAM10 contains four N-linked-glycosylation sites which all seem to go through post-translational modification with high-mannose and complex-type glycans (Saftig and Lichtenthaler, 2015). Mutagenesis of these glycosylation sites leads to reduced ADAM10 activity and higher susceptibility to degradation by other proteases (Escreveinte et al., 2008). Although all these modifications are necessary to prevent the degradation of ADAM10, they seem to be insufficient to explain how the protease is transported through the secretory pathway to the cell surface. It seems more intuitive, regarding membrane localisation and substrate specificity, that other proteins which are tightly attached to ADAM10 would be guiding the protease through the different steps of processing in the secretory pathway. For example, the protein SAP97 aids trafficking of ADAM10 to synaptic spines (Saraceno et al., 2014). Additionally, proteins of the tetraspanin family are attached to ADAM10 in many intracellular compartments (Jouannet et al., 2016). In particular proteins of the TspanC8 (Tspan: 5, 10, 14, 15, 17, 33/Penumbra), which contain eight cysteine residues at their large extracellular domain, are associated with ADAM10 trafficking and function (Matthews et al., 2017b). Different TspanC8 proteins guide ADAM10 from the ER to the cell surface, similarly to what is described for iRhom 1 and 2 with ADAM17 (Matthews et al., 2017a). At the cell surface, ADAM10 requires tight binding to Tspans for substrate cleavage as overexpression of Tspan5 or Tspan15 enhances ADAM10-mediated Notch signalling and APP or N-cadherin cleavage, respectively (Dornier et al., 2012, Noy et al., 2016). This evidence supports the broad functional importance of Tspans for ADAM10 not only in trafficking but

also in substrate cleavage. Nevertheless, the contribution of Tspans to ADAM10 shedding activity seems to be rather indirect through enhanced maturation and/or stabilization of the protease on the cell surface.

1.2.2 ADAM10 substrates

To date, there are numerous substrates known to be cleaved by ADAM10 (Pruessmeyer and Ludwig, 2009), and this number is continuously rising. Table 1 summarises typical ADAM10 substrates and their function. Unknowingly, the identification of ADAM10 as the protease cleaving the myelin basic protein revealed its general importance in the neuronal context (Chantry et al., 1989). More critical within the context of neuronal development is the role of ADAM10 in Notch signalling (Groot and Vooijs, 2012). The different Notch (Notch 1-4) signalling pathways are susceptible to ADAM10-mediated cleavage. The protease cleaves the extracellular domain of Notch-1 (Zhuang et al., 2015) which is related to lateral inhibition during neurodevelopment (Jorissen et al., 2010). Furthermore, the Notch-2 signalling in the marginal zone B cell development is sharply reduced in ADAM10 deficient B-cells (Gibb et al., 2010). Another influential group of substrates cleaved by ADAM10 are cell junction proteins, e.g., neuronal cadherin (N-cadherin, Reiss et al., 2005), epithelial cadherin (E-cadherin, Maretzky et al., 2005) and vascular endothelial cadherin (VE-cadherin, Schulz et al., 2008). Cadherins are essential for cell to cell contact and tissue integrity (Halbleib and Nelson, 2006), they exemplify best the role of ADAM10-mediated cleavage for cell signalling processes. The extracellular soluble fragment then can act as receptor ligand leading to downstream signalling (e.g. soluble E-Cad, Brouxhon et al., 2014). This remaining part of the cleaved cadherin is then susceptible to further proteolytic cleavage and signalling (Fig. 3, Marambaud et al., 2002). The group of substrates cleaved by ADAM10 (mainly cell adhesion proteins) distinguishes itself from those that are cleaved by ADAM17 (mainly EGFR receptor ligands). However, some substrates can be cleaved by both proteases, like APP, TGF- α (Hinkle et al., 2003) and IL6-R (Garbers et al., 2011). ADAM10 also cleaves EGFR receptor ligands betacellulin (BTC, Sanderson et al., 2005) and epidermal growth factor (EGF, Sahin et al., 2004). Although the activity of both proteases is crucial for cell survival, the lack of ADAM10 seems to be more critical. This is highlighted by knock-out experiments in mice, where the ADAM10 gene is deleted. As a consequence mice die at embryonal day 9.5 with obvious phenotypical developmental problems related to missing Notch signalling (Hartmann et al., 2002). Whereas, ADAM17 deficiency has been actually described in patients. They survive even though they show severe phenotypical characteristics related to missing ADAM17-EGFR signalling (Blaydon et al., 2011). A similar case for ADAM10 deficiency has not been described; this underlines the importance of ADAM10, in particular for Notch signalling, in the early stages of neuronal development. Another comprehensively studied substrate of ADAM10 is the low affinity IgE binding receptor (CD23, Weskamp et al., 2006). CD23 is mostly known for its role in the adaptive immune system as a negative regulator in IgE production (Yu et al., 1994) and is also involved in cell to cell adhesion (Moulder et al., 1993). In contrast to most substrates of ADAM10, CD23 is a type II transmembrane protein (Weskamp et al., 2006).

Summarizing the substrates shed by ADAM10, the majority are essential in the neuronal context, either in development or brain-related diseases. In the latter, ADAM10-related cleavage of the amyloid precursor protein (APP) and the cellular prion protein (PrP^c) is an essential posttranslational modification in both proteins (Postina et al., 2004, Altmeppen et al., 2015). Independently of the large number of substrates that are cleaved by ADAM10, the analysis of a potential ADAM10 substrate is sometimes difficult due to their low expression. Interestingly to note in this context is that some pore-forming toxins (e.g., pVCC), which modulate ADAM activity (Reiss and Bhakdi, 2012), can be cleaved also by ADAMs (Valeva et al., 2004). This proteolytic modulation makes some of these toxins favourable substrates to measure ADAM activity. The *Vibrio cholerae* cytolysin (VCC) is a toxin of the cholera pathogen, which penetrates the cell membrane and leads to cell lysis. The VCC exists as a pro-form (pVCC) and forms a heptameric pore, once its pro-domain is cleaved off (Olson and Gouaux, 2005, De and Olson, 2011). The pVCC can be cleaved by a variety of proteases including ADAM proteases, as metalloproteinase inhibitor TAPI inhibits ADAM-mediated cleavage of cell-bound pVCC (Valeva et al., 2004). The combination of pVCC with a cell type that dominantly expresses ADAM10 makes this a favourable model to measure the activity of the protease. Independently of the physiological importance of ADAM10-mediated substrate shedding, its altered expression or activity can be an indicator of a transition between physiology and pathophysiology.

1.2.1 ADAM10 roles in disease models

The importance of ADAM10 in pathophysiology is partially related to its reduced activity or its overexpression. In addition to Notch signalling, ADAM10 also cleaves the neurologically important APP (Kuhn et al., 2010). The cleavage of APP is mainly mediated by two different proteases (α -secretase ADAM10 and β -secretase BACE), each cleaving APP at different positions which lead to two different soluble APP peptides (Cai et al., 2001, Chow et al., 2009). The shedding of APP through α -secretase ADAM10 results in the production of a soluble APP-alpha peptide (sAPP- α), which is suggested to have neuroprotective properties (Barger and Harmon, 1997). Despite the importance of ADAM10 in cleaving APP, sAPP- α production is not entirely impaired in ADAM10 knock-out experiments (Hartmann et al., 2002). This goes in line with results showing that other metalloproteinases, like ADAM9 or 17, can also act as α -secretases processing APP (Asai et al., 2003). However, ADAM10 is suggested to be the major sheddase cleaving APP in the neuronal context (Endres and Fahrenholz, 2012).

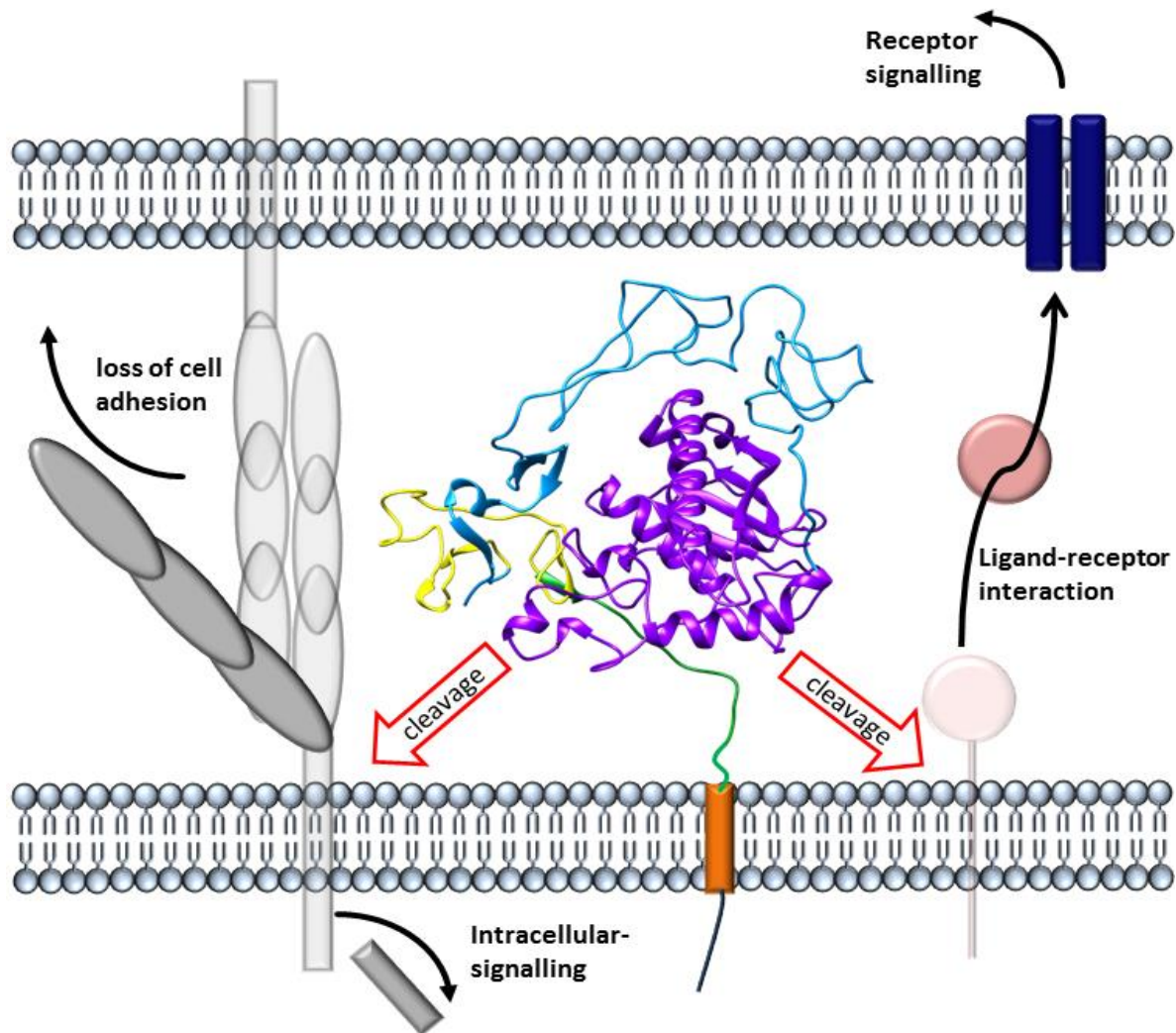


Figure 3. ADAM10-mediated substrate release and its implications for cell signalling.

ADAM10 cleaves various substrates (e.g., cadherins or EGF-receptor ligands) near the plasma membrane. The cleavage of cell adhesion molecules reduces cell-cell contacts and promotes cell migration (left). Soluble extracellular and intracellular domains function either as receptor ligands or directly enhance cellular processes, e.g., proliferation (right).

The same processing of APP by ADAM10 can be observed for the cleavage of the PrP^c (Checler and Vincent, 2002). The different proteolytic processing of the prion protein can also lead to the accumulation of neurotoxic plaques, which are a pathological characteristic of prion-related diseases like Creutzfeldt-Jakob in humans. The full-length PrP^c is cleaved by several proteases which leads to different soluble fragments of the PrP^c (Linsenmeier et al., 2017), similarly to what is observed in Alzheimer disease with sAPP α and sAPP β . However, the processing of the prion protein is highly complex; different proteases are involved in its cleavage, and the diverse roles of the released fragments remain partially unknown (Linsenmeier et al., 2017). However, proteolytic processing of the PrP^c has been suggested for a long time (Borchelt et al., 1993) and ADAM10 seems to be the only alpha secretase cleaving PrP^c in the brain (Linsenmeier et al., 2018). The expression and function of ADAM10 is not limited to the onset of neurological diseases. The protease is ubiquitously expressed and in contrast to its reduced activity in Alzheimer disease, its overexpression is seen in some cancer types (Lee et al.,

2010, Guo et al., 2012, Yang et al., 2012a, You et al., 2015). The therapeutic relevance of ADAM10 in cancer treatment is subject to a number reviews about ADAM10 as a target in cancer treatment (Crawford et al., 2009, Duffy et al., 2011, Saftig and Reiss, 2011). Indeed, numerous ADAM10 substrates are related to the pathology of different cancer types like Notch-1 in non-small cell lung cancer (Guo et al., 2012), CXCL16 in pancreatic cancer (Wente, 2010) and ErbB2 in adenocarcinoma and squamous cell carcinoma (Crawford et al., 2009). A general characteristic of cancer is an increased cell migration/metastasis and proliferation (Evan and Vousden, 2001); ADAM10 might be more directly involved in these processes since it cleaves a variety of cell adhesion proteins that lead to enhanced cell migration and increased proliferation (Crawford et al., 2009). Indeed, the shedding of E-cadherin and N-cadherin, both substrates of ADAM10, disrupts cell to cell contacts and enables higher cell migration, while intracellular enhanced β -catenin signalling acts as a transcription factor driving protein expression and thus proliferation (Maretzky et al., 2005, Reiss et al., 2005). Although many studies are focusing on the upregulation of ADAM10, it remains unclear whether overexpression of ADAM10 comes along with an increased shedding activity. Notably, a version of ADAM10 with a higher molecular weight is enhanced at the cell surface of cancer stem-like cells. The treatment of these cells with furin reduces the molecular weight of this high molecular weight form of ADAM10, indicating that it might be the pro-form of the protease that is expressed on the cell surface of these cancer stem-like cells (Atapattu et al., 2016). Besides the reduced activity of ADAM10 in severe neurological conditions and its upregulation in cancer, the mechanism how the activity of the proteases is regulated is poorly understood. This mechanism requires further investigation to understand the processes driving the protease function.

Table 1. Substrates released by ADAM10 and their relevance in diseases.

Name	Function	Disease	TM* Type	Reference
APP§	Unknown	Alzheimer disease	TM Type I	(Kuhn et al., 2010)
BTC	EGFR ligand	Cancer	TM Type I	(Sanderson et al., 2005)
CD23	IgE receptor	Cancer/allergy	TM Type II	(Weskamp et al., 2006)
E-cadherin	Cell adhesion	Cancer	TM Type I	(Maretzky et al., 2005)
N-cadherin	Cell adhesion	Cancer	TM Type I	(Reiss et al., 2005)
PrP ^c (prion protein)§	Receptor ligand	Prion disease	GPI anchor	(Altmeyen et al., 2015)
VE-cadherin	Cell adhesion	Cancer	TM Type I	(Schulz et al., 2008)

* TM=Transmembrane; §=not analysed in this thesis

1.2.2 ADAM10 mechanism of activation

ADAM10 shows, in addition to its constitutive shedding activity, an enhanced substrate cleavage upon stimulation with calcium ionophores, in comparison to other proteolytically active ADAMs (Horiuchi et al., 2006). A potent activator of ADAM10 is the calcium ionophore ionomycin. Ionomycin stimulation leads to irreversible changes in cell morphology and apoptosis as a consequence of increased calcium influx through depletion of intracellular calcium stores (Morgan and Jacob, 1994). The stimulation of ADAM10 with ionomycin, however, also seems to depend on extracellular calcium; since depletion of extra-cellular calcium abolishes ionomycin stimulated enhanced ADAM10-mediated shedding of BTC (Maretzky et al., 2015). Another potent stimulator of ADAM10 activity is melittin, a peptide part of bee venom, which can intercalate into plasma membranes (Lam et al., 2001). The stimulation with melittin leads to the release of ATP which in turn can activate P2 receptors and ADAM10-mediated shedding of E-cadherin (Sommer et al., 2012). The P2 receptor family is divided into five groups (P2X, P2Y, P2T, P2U, and P2Z), from these, the direct activation of P2X and P2Y is associated with enhanced shedding activity of ADAM10 and ADAM17 (Pupovac and Sluyter, 2016). The receptors of the P2X and the P2Y groups differ in the way they activate further cell signalling. The P2X receptors form a multimeric pore enabling direct ionic exchange between the extracellular and intracellular space, which underlines their function as ligand-gated ion channels (ionotropic receptors, North, 2002). In contrast, P2Y receptors are associated with heterotrimeric G-protein coupled receptors and indirectly activate other ion-transporter proteins or mediate direct downstream signalling (metabotropic receptors, von Kugelgen and Hoffmann, 2016). Both P2 receptor groups can be activated by extracellular nucleotides and can trigger the shedding activity of ADAM10 and ADAM17 (Pupovac and Sluyter, 2016). In particular, the activation of the P2X7 receptor (P2X7R), by adenosine triphosphate (ATP) or its potent analogue 3'-O-(4-benzoyl) benzoyl adenosine 5'-triphosphate (BzATP), was shown to directly activate ADAM10-mediated shedding of CD23 (Pupovac et al., 2015) and CXCL16 (Pupovac et al., 2013) on B-cells. Interestingly, the activation of the P2X7R stimulates not only ADAM10-mediated substrate shedding but also increases intracellular calcium levels (Adinolfi et al., 2005, Adinolfi et al., 2009, Pupovac and Sluyter, 2016). The elevated intracellular calcium levels seem to have no direct influence on ADAM10 or its ability to shed substrates since its shedding activity can be stimulated without its cytosolic tail (Maretzky et al., 2015), which could be susceptible to intracellular calcium. It is more likely that ATP-P2XR7 related increase of intracellular calcium levels leads to the activation of proteins requiring calcium for their activity, as it was shown for the phospholipid scrambling protein TMEM16F/anoctamin-6 (TMEM16F/ANO6, Ousingsawat et al., 2015). In this context, the stimulation of P2X7R with ATP or BzATP leads to enhanced translocation of the membrane phospholipid phosphatidylserine (PS) from the inner to the outer cellular leaflet, as indicated by the binding of Annexin-V to PS after stimulation. A similar PS binding of Annexin-V was observed in human erythrocytes stimulated with ionomycin (Lang et al., 2003) and in human keratinocytes stimulated with melittin (Sommer et al., 2016). This indicates that activators of ADAM10 increase intracellular calcium levels and enhance translocation of

PS from the inner to the outer plasma membrane leaflet. The altered phospholipid distribution, after stimulation, opens the possibility that the plasma membrane itself is involved in regulating ADAM10 shedding activity. Evidence for this hypothesis has been provided by recent data demonstrating a clear role of PS-exposure in regulating ADAM17 shedding activity, the protease that is structurally and functionally closely related to ADAM10 (Sommer et al., 2016).

1.3 ADAM10 in the context cell membrane (re)organisation

The plasma membrane and its different structural components regulate a variety of signalling processes that might be important for ADAM10 shedding activity. Indeed, alterations of the membrane composition, via cholesterol depletion, enhance ADAM10-mediated shedding of APP and PrP^c (Kojro et al., 2001, Hooper, 2005). Although, the artificial attachment of ADAM10, through a GPI anchor, into cholesterol-rich lipid rafts reduces shedding of APP (Harris et al., 2009). However, changes in membrane composition and fluidity alternate the localisation of the proteases and its respective substrate (Reiss et al., 2011), but they would be insufficient to explain how shedding is activated. The interaction between proteins and lipids is a common mechanism to enable protein function, but the sheer quantity of lipids in eukaryotic cells and therefore the variety of possible protein-lipid interactions is overwhelming. In this dimension of possible protein-lipid interactions, however, specific lipids seem to be more suitable than others in relation to their abundance. The majority of lipids in the plasma membrane are glycerophospholipids (van Meer et al., 2008), with their most common representatives: phosphatidylcholine (PC), phosphatidylethanolamine (PE), phosphatidylserine (PS) and phosphatidylinositol (PI) and sphingomyelin (SM, Table 2). The plasma membrane is asymmetrically constructed with PC, PI and SM located at the outer membrane leaflet and PE and PS localised at the inner leaflet (Devaux, 1991). PC and PE are the most abundant phospholipids in eukaryotic plasma membranes, and PI and PS to lesser degree (Leventis and Grinstein, 2010). Although the abundance of PS in eukaryotic membranes is low, its functional relevance for protein binding is of vital importance for physiological processes like blood clotting and apoptosis (Leventis and Grinstein, 2010). The recognition of PS by proteins occurs either in a calcium-dependent or independent way. The most common calcium-dependent binding proteins contain a C2 domain. The C2 domain resembles those first identified in the protein kinase C alpha (PKC- α). The C2 domain-related binding to PS is an exemplary mechanism for protein-phospholipid interaction (Lemmon, 2008). A diagnostically related calcium-dependent PS-binding protein is Annexin-V (van Engeland et al., 1996). Although Annexin-V exhibits characteristics of a C2 domain, it is structurally unrelated to PKC- α C2 domains (Lemmon, 2008). In contrast to calcium-dependent interactions, some proteins bind to PS in a calcium-independent way. In this group, the discoidin C2 domain (structurally not related to C2 domains) binds to PS in a stereospecific way (Lemmon, 2008). A specific protein that utilises this binding mechanism is lactadherin. The nature of the protein-PS interaction is either a stereospecific recognition of phospholipids and/or a charge dependent electrostatic interaction (Lemmon, 2008). Interestingly, some proteins (like HIV-1 Nef) contain several moieties of membrane interaction mechanisms. At the

cytosolic site, the negatively charged phospholipids attract the HIV-1 Nef protein near the inner plasma membrane leaflet. There, the myristate anchor of the HIV-1 Nef protein incorporates into the plasma membrane. Finally, a combination of an amphipathic helix and a poly-cationic motif of four positively charged amino acid residues enable electrostatic interaction and incorporation of the HIV-1 Nef protein into the plasma membrane (Gerlach et al., 2010). The HIV-1 Nef protein elucidates exemplarily that protein-membrane interaction may require several mechanisms. In fact, it requires several, but overall weaker mechanisms to bind more specifically (Gerlach et al., 2010). Noticeable, these processes take place at the cytosolic site, because under non-altered conditions PS is mainly localised in the cytosolic leaflet (Devaux, 1991). The translocation, however, is vital for a variety of processes that require PS on the extracellular leaflet. These processes include blood coagulation, synaptic pruning, and fertilisation. All of them highlight the importance of PS exposure in a non-apoptotic context.

Table 2. Eukaryotic plasma membrane phospholipids abundance and localisation*.

Phospholipid	% of total membrane phospholipid	% at the cytoplasmic (In) and exoplasmic (Out) leaflet
Phosphatidylserine (PS)	15	90 In; 10 Out
Phosphatidylcholine (PC)	27	30 In; 70 Out
Phosphatidylethanolamine (PE)	30	80 In; 20 Out
Phosphatidylinositol (PI)	<5	20 In; 80 Out
Sphingomyelin (SM)	23	15 In; 85 Out

*adapted from Nelson & Cox, Lehninger Principles of Biochemistry, 3rd ed., 2000

1.3.1 Scramblase-mediated phospholipid transport

A phospholipid interaction mechanism, regulating ADAM10 activity, would require the translocation of PS to the extracellular site. This is because the intracellular part of ADAM10 is dispensable for its shedding activity. The process of plasma membrane remodelling is fine-tuned via phospholipid transporters. Three different types of phospholipid transporters are currently described: Flippases, mediate the transport of phospholipids from extracytosolic site to the intracytosolic site, floppases, mediate the transport of phospholipids from intracytosolic site to the extracytosolic site and scramblases, which randomly transport phospholipids bidirectionally (Nagata et al., 2016). The flippases and floppases are ATP driven phospholipid transporters (Leventis and Grinstein, 2010), while scramblases function independent of ATP and require either calcium or caspase-mediated activation for their activity (Fig. 4a, Williamson, 2015). A variety of proteins are presumed to be phospholipid scrambling proteins.

Additionally to its physiological importance, PS exposure is described as a hallmark of apoptosis, though PS exposure itself was later suggested not to be the responsible trigger (Segawa et al., 2011). Nevertheless, PS exposure is a significant characteristic of apoptosis. A scramblase considered to be involved in apoptosis-related PS scrambling is Xkr8. This scramblase works in a calcium-independent way and is activated through caspase-3-mediated cleavage of its C-terminus (Suzuki et al., 2013, Suzuki et al., 2016).

The most studied group of scramblases are members of the TMEM16 protein family; they are multi-transmembrane containing proteins. The proteins of the TMEM16 family contain ten transmembrane domains (TMDs), but they were initially described to contain eight TMDs, which lead to their name: anoctamins (ANOs). The process of PS translocation has been extensively studied for the scramblase TMEM16F/ANO6 (Nagata et al., 2016). A structural analysis of the scramblase ortholog from the fungus *Nectria haematococca* indicates that human TMEM16F/ANO6 also consists of ten TMD and forms homodimers (Fig. 4b, Brunner et al., 2014). Furthermore, TMEM16F/ANO6 consists of a 35 amino acid long scrambling domain located at the transition between the 4th and 5th transmembrane domain (Fig. 4c) and several amino acid residues in the TMD segments 6-8, that can bind calcium (Nagata et al., 2016). These calcium-binding residues are highly conserved among the members of the anoctamin family and can also be found in the TMEM16 ortholog protein from *N. haematococca* (Nagata et al., 2016). A spontaneously introduced mutation of the calcium binding glutamate at position 409 to glycine leads to a hyperactive PS scrambling mutant of TMEM16F/ANO6 (TMEM16F/ANO6 D409G, Suzuki et al., 2010). Cells that expressed the hyperactive TMEM16F/ANO6 D409G mutant showed constant PS exposure under resting calcium conditions (Suzuki et al., 2010). Interestingly, the scrambling activity of the TMEM16F/ANO6 hyperactive mutant is reduced with the intracellular calcium chelator BAPTA-AM. This provides evidence that the scrambling mechanism of TMEM16F/ANO6 and hyperactive TMEM16F/ANO6 is calcium dependent (Suzuki et al., 2010). The TMEM16F/ANO6 D409G (respectively D408G for human TMEM16F/ANO6) represents a gain of function for TMEM16F/ANO6.

In contrast, the Scott syndrome, a bleeding disorder causing disease (named after the patient it was first identified) is related to a loss of function of TMEM16F/ANO6 (Lhermusier et al., 2011). Genetic analyses of patients with the Scott syndrome connect the bleeding disorder to impaired PS scrambling, which is essential for blood clotting (Toti et al., 1996). This genetic defect in TMEM16F/ANO6 activity affects red blood cells (Beverly et al., 1992), platelets (Rosing et al., 1985) and B-cells (Kojima et al., 1994) from Scott disease patients. However, the induction of apoptosis in Scott cells leads to enhanced PS exposure, indicating a general ability of these cells to expose PS (Kmit et al., 2013). In addition to TMEM16F/ANO6, TMEM16A/ANO1 is another calcium-activated protein from the anoctamin family. Although TMEM16F/ANO6 and TMEM16A/ANO1 show sequential similarities for the calcium binding domain, a scrambling activity has only been described for TMEM16F/ANO6 (Fig. 4d). The investigation of a three-dimensional structure of TMEM16A/ANO1 led to the assumption that the pore

formed by TMEM16A/ANO1 is unsuitable for the transport of large molecules like phospholipids (Fisher and Hartzell, 2017, Paulino et al., 2017). Indeed, most studies suggest TMEM16A/ANO1 as calcium-activated chloride channel (Sala-Rabanal et al., 2015). However, whether TMEM16A/ANO1 might indirectly contribute to phospholipid scrambling is still under debate. An indirect impact of TMEM16A/ANO1 on PS scrambling may be organised by interaction with other scramblases. Karl Kunzelmann (personal communication) suggested that a cross-talk between TMEM16A/ANO1 and TMEM16F/ANO6 represents such a way how TMEM16A/ANO1 indirectly affects TMEM16F/ANO6 scrambling activity. However, whether TMEM16F/ANO6 or TMEM16A/ANO1 could contribute to ADAM10 shedding activity is unknown. In light of recent results underlining that PS exposure regulates ADAM17 shedding activity, it is plausible that scrambling proteins like TMEM16F/ANO6 play an essential role for ADAM10 shedding activity.

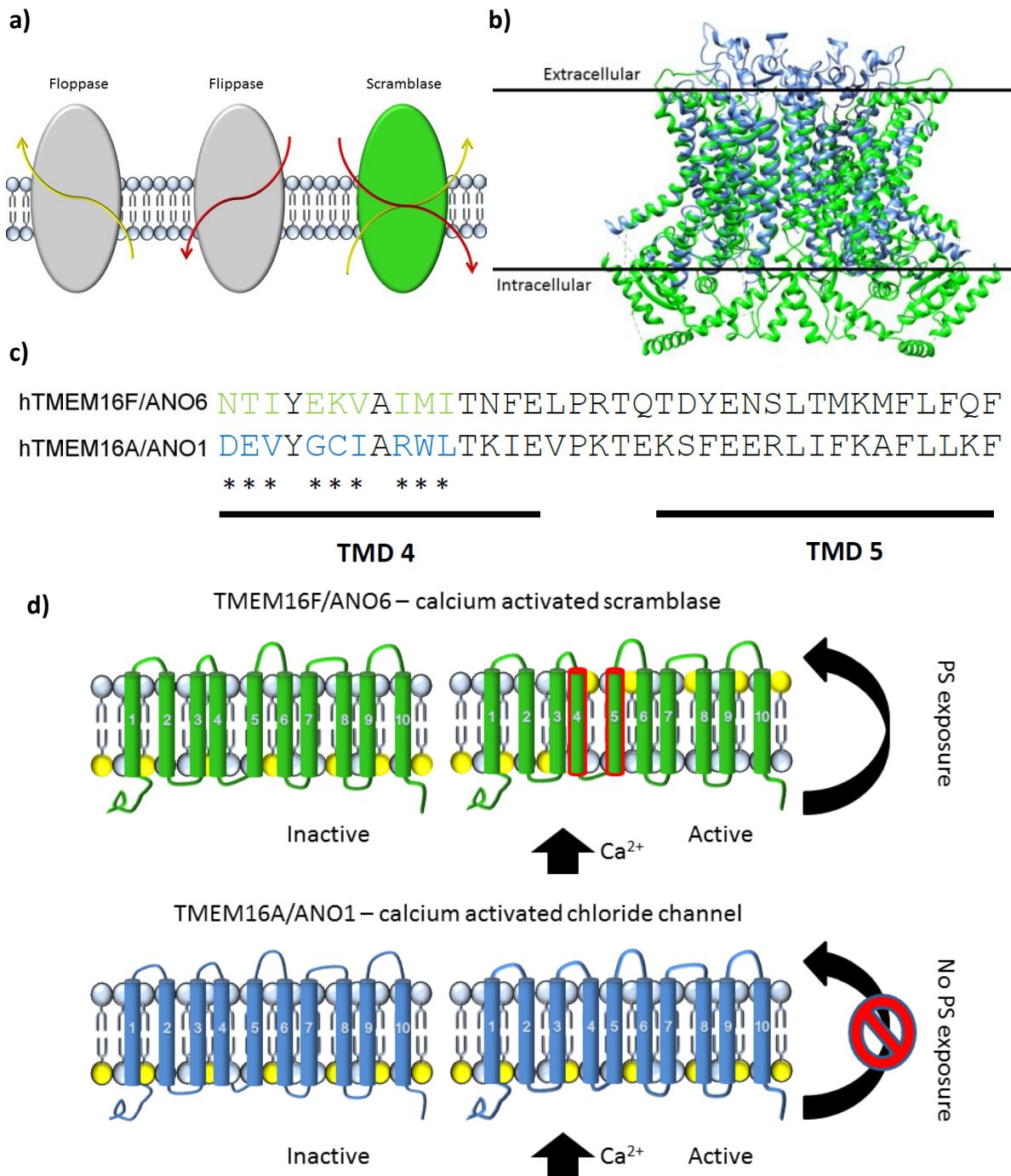


Figure 4. Anoctamins and phospholipid scrambling.

a) Cell membrane asymmetry and phospholipid transport are maintained by: floppases (from the inner to the outer leaflet, grey left), flippases (from the outer to the inner leaflet, grey centre) and scramblases (bi-directional transport, green right). **b)** Overlay of the ribbon structure of crystallographic resolved calcium-activated phospholipid scramblase homolog *Nectria hematococca* TMEM16 (nhTMEM16, PDB: 4WIS, green) and of crystallographic resolved mouse calcium-activated chloride channel TMEM16A/ANO1 (mTMEM16A, PDB: 6BGI, blue). Overlay indicates a high structural similarity between both anoctamins. **c)** Sequence alignment between human TMEM16F/ANO6 and human TMEM16A/ANO1. This indicates a phospholipid scrambling domain for human TMEM16F/ANO6 (asterisks indicate essential amino acids for the scrambling activity in human TMEM16F/ANO6, green highlighted amino acids) which is absent in human TMEM16A/ANO1 (respective amino acids are highlighted in blue) between the 4th and 5th transmembrane domains (TMD). **d)** Both ANOs are calcium-activated ion channels. Enhanced calcium influx activates TMEM16F/ANO6-mediated PS exposure (upper panel, green) and TMEM16A/ANO1 channel activity (lower panel, blue).

2. Aim of the thesis:

The variety of processes that require proteolytic modulation by ADAM10 is remarkable, but at the same time, the events that regulate the protease shedding activity are poorly understood. Given that the metalloproteinases ADAM10 and ADAM17 are involved in several physiological and pathophysiological processes, a better understanding of the mechanism regulating the shedding activity of both proteases is urgent. Within this context, the discovery that ADAM17 shedding activity is regulated by the interaction with the plasma membrane phospholipid PS at the extracellular site was an important addition to the understanding of how the shedding activity of this protease is regulated. Interestingly, various data for ADAM10 indicate that the regulatory mechanism might be similar to the one proposed for ADAM17. For example, the deletion of the cytosolic tail of ADAM10, like in ADAM17, does not influence ADAM10 shedding activity, indicating that also ADAM10 shedding activity is regulated extracellularly rather than intracellularly. These results raise the question whether the shedding activity of ADAM10, the closest relative of ADAM17, also requires PS exposure and membrane interaction.

Activators of ADAM10 lead, along with enhanced substrate shedding, to calcium increase, the breakdown of cell membrane asymmetry, and PS exposure. The first part of this thesis will, therefore, focus on assessing whether stimuli induced PS exposure is the primary regulatory event for enhanced ADAM10-mediated substrate shedding and whether this is facilitated through a direct interaction between PS and ADAM10. In this context, this part will try to answer the questions whether the headgroup of PS and a *de novo* rabbit erythrocyte-pVCC model can describe PS exposure as the primary regulatory event for ADAM10 shedding activity. The second part of this thesis will then focus on membrane modulating proteins and how they contribute to PS exposure and thereby to ADAM10 shedding activity. In particular scramblases, which randomly transport phospholipids along the plasma membrane have been comprehensively studied in recent years. Although their scrambling activity is yet not fully understood, overexpression of the calcium-dependent scramblase TMEM16F/ANO6 has been shown to enhance PS exposure. The second part of this thesis will therefore focus on whether phospholipid scramblases like TMEM16F/ANO6 contribute via PS exposure to ADAM10-shedding activity and whether a gain and loss of TMEM16F/ANO6 scrambling activity is characterised by a respective gain or loss of ADAM10 shedding activity. The last part of this thesis will build upon the previous ones to suggest a possible mechanism behind the interaction between ADAM10 and PS. Since ADAM17 seems to interact with PS via a triplet motif of cationic amino acids and ADAM10 contains a similar triplet of cationic amino acids in its stalk domain, a similar interaction mechanism with PS is expected for ADAM10. The last part of the thesis will, therefore, focus on the role of ADAM10 stalk domain and whether this part of ADAM10 interacts with PS. Through mutations of the stalk domain of ADAM10, it will be further analysed whether the cationic amino acids are relevant, particularly for ADAM10 enhanced shedding activity.

3. Material and Methods

3.1 Consumables and equipment

Table 3. Consumables.

Consumable	Provider
1.5 ml Reaction tube	Sarstedt (GER)
1.5 ml Reaction tube (low DNA bind)	Eppendorf (GER)
2.0 ml Cryo preservation tube	Sarstedt (GER)
5.0 ml Flow cytometry tubes	Sarstedt (GER)
96-well plates (flat bottom)	Sarstedt (GER)
Cell culture dishes (10 cm)	Sarstedt (GER)
Cell culture flask (75 cm ²)	Sarstedt (GER)
Cell culture plates (12-, 24-, 96-well)	Sarstedt (GER)
Cell scraper (16 cm, 25 cm)	Sarstedt (GER)
Cellometer Disposable Counting Chambers	Nexelom Bioscience (USA)
Coverslips	Hecht-Assistent (GER)
Falcon centrifuge tubes (15 ml, 50 ml)	Sarstedt (GER)
Glass flasks, 1000 ml, 300 ml	Schott (GER)
Microscope slides	Menzel-Gläser (GER)
Parafilm	American National Can Company (USA)
Pasteur pipettes (150 mm)	Th. Geyer (GER)
Pasteur pipettes (230 mm)	Hecht-Assistent (GER)
Petri dishes	Sarstedt (GER)
Plastic box (airtight)	EMSA (GER)
PVDF membrane (0.45 µm)	Carl Roth (GER)
Serological pipettes (5 ml, 10 ml, 25 ml)	Sarstedt (GER)
Syringe filter (0.45 µm pore size)	Sarstedt (GER)
Whatman paper (1.5mm)	Carl Roth (GER)

Table 4. Laboratory standard equipment.

Equipment	Manufacturer
80 °C Freezer Forma 900 Series	Thermo Fisher Scientific (USA)
Analytical balance S-603	Denver Instruments (USA)
Analytical balance XS205	Kern & Sohn (GER)
Biophotometer	Eppendorf (GER)
Bright Field Cell Counter	Nexelom Bioscience (USA)
Cellometer Auto 1000	Nexelom Bioscience (USA)
Centrifuge 5417R (Fixed angle rotor F45-30-11)	Eppendorf (GER)
Centrifuge 5424 (Fixed angle rotor FA45-24-11)	Eppendorf (GER)
Centrifuge 5804R (Fixed angle rotor F34-6-38)	Eppendorf (GER)
Centrifuge 5810R (swing-out rotor A-4-62)	Eppendorf (GER)
Centrifuge Heraeus Multifuge X3R Fixed angle rotor F14-6x250LE	Eppendorf (GER)
Chemiluminescence detector Fusion FX7	Peqlab (GER)
Exhaust pump (BVC professional)	Vacuubrand (GER)
Fluorescent microscope DMI3000B	Leica (GER)
Freezing container (Nalgene; Mr Frosty)	Thermo Fisher Scientific (USA)
Heating Block	Eppendorf (GER)
Incubator Hera cell 150	Thermo Fisher Scientific (USA)
Light microscope, inverse	Hund (GER)
Magnetic stirrer CB162	Stuart (USA)
Microwave oven	Samsung (GER)
NanoDrop 1000, spectrophotometer	Peqlab (GER)
pH-meter pH211	HANNA Instruments (GER)
Plate Reader EL800	Biotek Instruments (GER)
Plate reader FLx800	Biotek Instruments (GER)
Power Supply EV231	Peqlab (GER)
Power Supply PAC300	BioRad Laboratories (GER)
Semi-dry electroblotter, PerfectBlue	Peqlab, (GER)
Shaking incubator Minitron	Infors HT (GER)
Single-channel pipettes	Abimed GmbH (GER)
Sonicator	Bandelin electronic (GER)
Sterile work bench S1 laboratory	Köttermann (GER)

Sterile work bench S2 laboratory	Kleinfeld Labortechnik (GER)
Tank electro-blotter Web S	Peqlab (GER)
Thermocycler peqSTAR 96 universal	Peqlab (GER)
Tube rotator MACSmix™	Miltenyi Biotech (GER)
Tube rotator RS-TR10	Phoenix Instruments (GER)
Vortexer Vortex Genie	IKA (GER)
Water bath GFL1004	GFL (GER)
Water purification system, TKA GenPure	TKA (GER)

3.2 Chemicals

Table 5. Chemicals and provider.

Chemical	Provider
1,10- Phenanthroline	Carl Roth (GER)
1,2-dioleoyl-<i>sn</i>-glycero-3-phospho-L-serine (PtdSer)	Avanti Polar Lipids (USA)
1,2-dioleoyl-<i>sn</i>-glycero-3-phosphocholine (PtdCho)	Avanti Polar Lipids (USA)
2'(3')-O-(4-Benzoylbenzoyl)adenosine-5'-triphosphate tri(triethylammonium) salt (BzATP)	Tocris
4-(2-Aminoethyl)benzenesulfonyl fluoride hydrochloride (AEBSF)	Sigma Aldrich (GER)
Accutase®	Merck (GER)
ADAM10 Selective Substrate (Fluorogenic) PEPMCA001 (soluble)	BioZyme (USA)
Agar-Agar	Carl Roth (GER)
Ammoniumperoxidisulfate (APS)	Carl Roth (GER)
Ampicillin	Carl Roth (GER)
Annexin-V APC	Thermo Fisher Scientific (USA)
Annexin-V FITC	Enzo Life Sciences (USA)
Bovine serum albumin (BSA)	Sigma Aldrich (GER)
Biofreeze	Biochrome (GER)
Bromophenol blue	Carl Roth (GER)
Calciumchloride (CaCl₂)	Carl Roth (GER)
cOmplete®	Roche (CH)
Di-sodium phosphate (NH₂POH₄)	Carl Roth (GER)
Dimethyl sulfoxide (DMSO)	Carl Roth (GER)

Dithiothreitol (DTT)	Thermo Fisher Scientific (USA)
ECL Advanced	GE Healthcare (USA)
Ethylenediaminetetraacetic acid (EDTA)	Carl Roth (GER)
Egtazic acid (EGTA)	Carl Roth (GER)
Fetal bovine serum (FBS)	Thermo Fisher Scientific (USA)
GI254023X (GI)	Tocris Bioscience (UK)
Glucose	Carl Roth (GER)
Glycerin	Carl Roth (GER)
Glycine	Carl Roth (GER)
Lactadherine-FITC	Haematologic Technologies (USA)
HEPES	Carl Roth (GER)
Hydrochloric acid (HCl)	Carl Roth (GER)
Ionomycin (IO)	Merck /GER)
Isopropanol	Carl Roth (GER)
Magnesium chloride (MgCl₂)	Carl Roth (GER)
Magnesium sulfate (MgSO₄)	Merck (GER)
Marimastat (MM)	Tocris (UK)
Melittin (Mel)	Produced by J. Andrä (FZ Borstel)
Mercaptoethanol	Carl Roth (GER)
Methanol (MeOH)	Carl Roth (GER)
Milk powder	Carl Roth (GER)
O-phosphocholine (OPC)	TCI Deutschland GmbH (GER)
O-phosphoserine (OPS)	Sigma Aldrich (GER)
PhosSTOP®	Roche (CH)
Potassiumchloride (KCl)	Merck (GER)
Potassium dihydrogen phosphate (KH₂PO₄)	Carl Roth (GER)
PPADS tetrasodium salt	Sigma Aldrich (GER)
PageRuler™ Plus Prestained Protein Ladder 10 to 250 kDa	Thermo Fisher Scientific (USA)
Color Prestained Protein Standard, Broad Range 11 to 245 kDa)	New England Biolabs (USA)
Saccharose	Carl Roth (GER)
SDS pellets	Carl Roth (GER)
Sodiumchloride (NaCl)	Carl Roth (GER)
Sodiumdodecylsulfate (SDS)	Carl Roth (GER)

Tetramethylethylenediamine (TEMED)	Carl Roth (GER)
Transfection reagent <i>Turbofect</i>	Thermo Fisher Scientific (USA)
Tris(hydroxymethyl)aminomethane (Tris)	Carl Roth (GER)
Trypton/Pepton from casein	Carl Roth (GER)
Yeast extract	Carl Roth (GER)
Triton X-100	Carl Roth (GER)
TAPI-1 (TAPI)	Merck (GER)
Trypsin-EDTA (0.5 %)	Thermo Fisher Scientific (USA)
Ethanol 96 % (EtOH)	Carl Roth (GER)
Dulbecco´s Modified Eagle Medium (DMEM) High Glucose (4.5g/l)	Thermo Fisher Scientific (USA)
Tween®20	Carl Roth (GER)
Penicillin/Streptomycin (100x)	Thermo Fisher Scientific (USA)
Annexin Alexa 568	Thermo Fisher Scientific (USA)
Pierce™ 660nm Protein Assay Reagent	Thermo Fisher Scientific (USA)

3.3 Kits

Table 6. Commercial kits and provider.

Name	Provider
PureYield™ MidiPrep Kit	Promega (USA)
QuickChange® II Site-directed Mutagenesis XL	Agilent (USA)

3.4 Software

Table 7. Software and developer.

Software	Developer
Adobe Photoshop CS4	Adobe Systems (USA)
Bio1D	Vilber Lourmat (GER)
EndNote, X7	Thomson Reuters (USA)
FlowJo	FlowJo (USA)
FluoView FV10-ASW 4.0	Olympus Corporation (JPN)
Fusion 15.17	Vilber Lourmat (GER)
Geneious 6.2	Biomatters Inc. (USA)
GraphPad Prism 7	GraphPad Software (USA)

ImageJ 1.47m	NIH (USA)
Microsoft Office 365	Microsoft (USA)
UCSF Chimera 1.12	University of California (USA)

3.5 Stimuli and inhibitors

Table 8. Stimuli and inhibitors.

Name	Application	Final concentration
AEBSF	Serine proteases inhibitor	100 μ M
BzATP	P2X7 agonist	500 μ M
Fas receptor antibody (CH11)	Fas receptor activation	0.5 μ g/ml
GI254023X (GI)	Preferential ADAM10 inhibitor	3 μ M
Ionomycin (IO)	Calcium ionophore	1 μ M
Marimastat (MM)	Metalloproteases inhibitor	10 μ M
Melittin	Bee venom component	0.5 μ M
OPC	Control for OPS	10 mM*
OPS	Competitive inhibitor of PS-binding	10 mM*
PPADS	P2(X)-receptor inhibitor	100 μ M
TAPI-1	Metalloproteases inhibitor	10 μ M

*if not indicated differently

3.6 Primary and secondary antibodies

Table 9. Primary antibodies.

Name	Reactivity	Provider	Species	App.*	Conc.	Dilut.
CD23	h	BD Bioscience	mouse	FC	25 μ g/ml	1:100
E-cadherin	h, m, r, d	BD Bioscience	mouse	WB	250 μ g/ml	1:3000
GAPDH	h, m, r	Santa Cruz	rabbit	WB	200 μ g/ml	1:500
GFP	/	Roche	mouse	WB	400 μ g/ml	1:500
humanADAM10	h	Abcam	mouse	FC	500 μ g/ml	1:100
IgG1-APC isotype	/	BD Bioscience	mouse	FC	12,5 μ g/ml	1:50
IgG2a isotype	/	R&D	rat	FC	500 μ g/ml	1:100
IgG2b isotype	/	R&D	mouse	FC	500 μ g/ml	1:100
mouseADAM10	h, m	Abcam	rabbit	WB	1000 μ g/ml	1:1000
mouseADAM10	m	Abcam	rat	FC	500 μ g/ml	1:100
N-cadherin	h, m, r, ch	BD Bioscience	mouse	WB	250 μ g/ml	1:3000

P2X7R	h	BioLegend	mouse	WB	500 µg/ml	1:1000
VCC	/	Mainz	rabbit	WB		1:2000

Application *WB=Western Blot, FC=Flow cytometry, h=human, m=mouse, r=rat, d=donkey, ch=chicken

Table 10. Secondary antibodies.

Name	Coupling	Provider	App.*	Conc.	Dilut.
Donkey anti mouse	Alexa 488	Thermo FisherScientific	FC	2.000 µg/ml	1:500
Donkey anti rat IgG	Alexa 488	Thermo Fisher Scientific	FC	2.000 µg/ml	1:500
Goat-anti mouse IgG	HRP	Dianova	WB	15.000 µg/ml	1:10.000
Goat-anti rabbit IgG	HRP	Dianova	WB	15.000 µg/ml	1:10.000

Application *WB=Western Blot, FC=Flow cytometry

3.7 Plasmids

Table 11. Plasmids.

Name	Vector	Provider
BTC-AP	pcDNA3.1 (Invitrogen)	C. Blobel (HSS, New York, USA)
mADAM10 E/A	pcDNA3.1 (Invitrogen)	C. Blobel (HSS, New York, USA)
mADAM10 Stalk 1	pcDNA3.1 (Invitrogen)	Mutated ADAM10wt (generated in this thesis)
mADAM10 Stalk 2	pcDNA3.1 (Invitrogen)	Mutated ADAM10wt (generated in this thesis)
mADAM10 Stalk 3	pcDNA3.1 (Invitrogen)	Mutated ADAM10wt (generated in this thesis)
mADAM10wt	pcDNA3.1 (Invitrogen)	Thorsten Maretzky (UOI, Iowa City, USA)
TMEM16A/ ANO1-GFP	pcDNA3.1 (Invitrogen)	Karl Kunzelmann (UR, Regensburg, GER)
TMEM16F/ ANO6-GFP	pcDNA3.1 (Invitrogen)	Karl Kunzelmann (UR, Regensburg, GER)
TMEM16F/ ANO6 D408G GFP	pcDNA3.1 (Invitrogen)	Martin Veit (UKSH, Kiel, GER)
VE-cadherin-AP	pcDNA3.1 (Invitrogen)	C. Blobel (HSS, New York, USA)

3.8 General buffers

Table 12. Buffer recipes.

Buffer	Chemical composition
6x SDS sample buffer	0.75 M Tris 12 % (w/v) SDS 6.54 M Glycerin 6 mM EDTA 120 mM DTT 0.15 % (v/v) Bromphenole blue pH 6.8
Alkaline phosphatase (AP) buffer	100 mM NaCl 100 mM Tris 20 mM MgCl ₂ pH 9.5
Annexin binding buffer (ABB)	10 mM HEPES 140 mM NaCl 2.5 mM CaCl ₂ pH 7.4
Cell lysis buffer (AP-assays)	1 mM EDTA 10 mM 1,10-Phenantrolin 2.5 % (v/v) TritonX-100
CaCl₂-solution	0.1 mM CaCl ₂ 5 mM Tris 5 mM MgCl ₂
ADAM lysis buffer (Western blotting)	5 mM Tris 1 mM EGTA 250 mM Saccharose 1 % (v/v) TritonX-100 10 mM 1,10-Phenanthroline 1x Complete protease inhibitor mix 1x PhosStop phosphatase inhibitor mix
Erythrocyte lysis buffer	0.1 % (v/v) PBS
NaCl-medium	145 mM NaCl 5 mM KCl 5 mM Glucose 10 mM HEPES 0.1 % (w/v) BSA
Electrophoresis buffer	25.1 mM Tris 192 mM Glycin 0.1 % (w/v) SDS pH 8.8
PBS	137 mM NaCl 2.7 mM KCl

	1.8 mM KH ₂ PO ₄ 10.1 mM Na ₂ HPO ₄
Resolving gel buffer	1.5 M Tris 0.4 % (w/v) SDS pH 8.8
Stacking gel buffer	0.5 M Tris 0.4 % (w/v) SDS pH 6.8
Stripping buffer for PVDF membranes	62.5 mM Tris 20 % (w/v) SDS 0.7 % (v/v) 2-mercaptoethanol
TBST	20 M Tris 1.17 M NaCl 10 mM EDTA 0.1 % (v/v) Tween-20
Tris buffer	0.1 mM NaCl 5 mM Tris 5 mM MgCl ₂
Blocking Solution	5 % milk powder in TBST
Transfer buffer (Western blotting)	192 mM Glycin 25 mM Tris 10 % (v/v) MeOH pH 8.5
LB medium	171 mM NaCl 10 % (w/v) Trypton/Pepton 5 % (w/v) Yeast Extract
LB Agar plates	171 mM NaCl 10 % (w/v) Trypton/Pepton 5 % (w/v) Yeast Extract 15 g/l Agar-Agar 0.1 mg/ml Ampicillin
SOC-medium	0.5 g/l Yeast Extract 2 g/l Trypton 10 mM NaCl 2.5 mM KCl 10 mM MgCl ₂ 10 mM MgSO ₄ 20 M Glucose

3.9 Cells and cell lines

Table 13. Cells and cell lines used in this thesis.

Cell line/cells	Type	Culture medium
ADAM10/ADAM17-deficient HEK-293T	CRISP/Cas-9 modified Human Embryonic Kidney cells; A10/A17 knock-out. Kindly provided by Prof. Björn Rabe (CAU, Kiel, GER)	DMEM+10 % FBS+Pen/Strep*
COS7	SV40 transformed cell line from the kidney of <i>Ceercopithecus aethiops</i> , fibroblast-like cells	DMEM+10 % FBS+Pen/Strep*
HaCaT	Human keratinocytes, immortalized	DMEM+10 % FBS+Pen/Strep*
Human B-cells (control B-cells)	EBV-transformed B-lymphoblasts	RPMI+10 % FBS+Pen/Strep*
Murine embryonic fibroblasts (MEF)	Immortalized fibroblasts	DMEM+10 % FBS+Pen/Strep*
Rabbit Erythrocytes	Erythrocytes (freshly prepared from whole blood samples, blood samples were obtained from PreClinics, GER)	NaCl-medium+AEBSF+MM
Scott UK patient B-cells (Scott UK B-cells)	EBV-transformed B-lymphoblasts from a patient with Scott syndrome	RPMI+10 % FBS+Pen/Strep*

*Penicillin/Streptomycin: 100 U/ml, **AEBSF (100 μ M), MM (10 μ M)

3.10 Cell and cell culture cultivation and passaging

Adherent and suspension cells were cultivated in the Hera cell 150 Incubator, at 37 °C with 5 % CO₂ in a humidified atmosphere. COS7, HaCaT and A10/A17-deficient HEK-293T cells and MEFs (adherent cells) were cultivated in 10 cm dishes with Dulbecco's Modified Eagle Medium (DMEM), supplemented with 10 % fetal bovine serum (FBS) and Penicillin/Streptomycin (100 U/ml). B-cells (suspension cells) were cultivated in TC Flasks T75 with Roswell Park Memorial Institute medium (RPMI-1640), supplemented with 10 % FBS and Penicillin/Streptomycin (100 U/ml). Rabbit erythrocytes were kept in 15 ml tubes with NaCl-medium, supplemented with 10 μ M marimastat (MM) and 100 μ M AEBSF. Adherent and suspension cells were split every 2-4 days before the culture reached 90 % confluency/bottom layer and were then either seeded into new culture dishes or cell culture plates for the experimental procedures. For this, cells were washed once with PBS and incubated with Trypsin/EDTA and kept at 37 °C till complete detachment of the cells. Subsequently, the cells were resuspended in DMEM supplemented with 10 % FBS to halt trypsin incubation. Resuspended cells were split in a ratio of 1:10 and seeded onto new 10 cm culture dishes. Suspension cells were subcultured every 2-3 days. Cells were resuspended and split in a ratio of 1:5 into new culture flasks. All culture media were preheated to 37 °C before use.

3.10.1 Cell counting

Cell counting was performed whenever indicated before seeding and experimental procedure. Adherent cells were resuspended in DMEM medium supplemented with 10 % FBS and Pen/Strep antibiotics mix, and 50 µl of resuspended cells were mixed with 50 µl PBS with trypan blue (Table 11). For the counting of living (trypan blue negative) and dead (trypan blue positive cells) cells, 20 µl of the total 100 µl solution was filled into the Nexus counting chamber slides and counted by the Cellometer Auto 1000 (Nexus). For the estimation of the required cell number, only living cells were included in the counting.

3.10.2 Cell culture cryopreservation

Eukaryotic cells were washed once with PBS and incubated with Trypsin/EDTA till cells detached from the culture dish. Fresh DMEM with 10 % FBS and Pen/Strep mix was added to the culture dish and cells were suspended and transferred into 50 ml Falcon tubes. Centrifugation was carried out at 250 xg for 5 minutes at room temperature. After centrifugation DMEM culture medium was removed and cells were suspended in 1 ml BioFreeze (Biochrome) and transferred into 2 ml cryopreservation tubes. The cryopreservation tubes were then placed into containers with isopropanol and placed into -80 °C freezer to assure a slow freezing process. After 24 hours cryopreservation tubes were placed for long-time storage into liquid nitrogen.

3.11 Rabbit erythrocyte – pVCC model

In contrast to human erythrocytes, rabbit erythrocytes express functional ADAM10 (Reiss et al., 2011). This unique characteristic of rabbit erythrocytes cells represents a compelling *ex vivo* tool to analyse ADAM10 activity in a steady-state scenario. Reiss et al. (2011) combined for the first time rabbit erythrocytes with the pro-form of the *Vibrio cholera* cytolysin (pVCC) to analyse the activity of ADAM10 on rabbit erythrocytes. The pro-form of VCC incorporates into the rabbit erythrocytes plasma membrane. Although the pro-form of VCC can be cleaved by different proteases, the major protease on rabbit erythrocytes was suggested to be ADAM10. The cleavage of the pro-form of VCC by ADAM10 leads to the production of mature VCC monomers. These VCC monomers oligomerize and form a heptameric pore that leads to respective erythrocyte hemolysis. The erythrocyte hemolysis and the cleavage of pVCC can, therefore, be analysed directly in the context of ADAM10 activity.

3.11.1 Isolation and preparation of rabbit erythrocyte from whole blood

Whole rabbit blood samples were purchased from PreClinics (GER). The rabbit blood was combined with a 5 % dextran solution 1:1 and kept in 45° angle for 30 minutes to allow erythrocyte sedimentation. Subsequently, whole rabbit blood was centrifuged at 2,500 xg for 5 minutes. The supernatant (including plasma) was removed, and the sedimented erythrocytes were 3 x washed with PBS. After the last centrifugation, rabbit erythrocytes were kept in NaCl-medium containing metalloproteinase inhibitor marimastat (MM, 10 µM) and serine protease inhibitor AEBSF (100 µM) and kept for a maximum of 3 days at 4 °C.

3.11.2 Rabbit erythrocyte – pVCC hemolysis assay

For hemolysis assays, a 5 % erythrocyte solution was prepared and incubated with pVCC (3 µg/ml) for 30 minutes on ice. Subsequently, erythrocytes were washed once with NaCl medium and split into the different samples. The erythrocyte hemolysis experiments were split into two groups. In the first group it was analysed whether activation of the P2X7R leads to PS exposure, thus driving the cleavage of pVCC and related erythrocyte hemolysis. In the other group, it was analysed whether ADAM10 is the responsible protease for the cleavage of pVCC and related hemolysis. In both experimental groups, 50 µl of the pVCC incubated 5 % rabbit erythrocyte solution was combined with 50 µl of NaCl-medium with AEBSF (100 µM) and MM (10 µM). Both inhibitors were kept in the buffer during the blocking and the stimulation to prevent the cleavage of pVCC by metalloproteases and/or serine proteases during the stimulation. Afterwards, AEBSF remained in the buffer to further inhibit the activity of serine proteases, and only MM was removed to assure metalloproteinase activity. The control sample was incubated with PPADS (100 µM), and all samples were incubated for 10 minutes on ice. After the preincubation, 0.5 mM BzATP was added to the respective samples and incubated for 15 minutes at 37 °C. Subsequently, all samples were centrifuged for 30 seconds at 15,000 xg at 4 °C and filled up with NaCl-medium with AEBSF (100 µM). Additionally, PPADS (100 µM) in the respective control sample. The samples were then incubated for the indicated times. To determine the progress of hemolysis the respective samples were centrifuged at 15,000 xg for 30 seconds at the indicated time periods, and 14 µl supernatant was removed from each sample and combined with 120 µl NaCl-medium and filled in a 96 well plate. For the analysis of ADAM10-mediated cleavage of pVCC, rabbit erythrocytes incubated with pVCC were similarly prepared as described above. Samples were then incubated with either OPS or OPC (40 mM, 20 mM, 10 mM and 5 mM), TAPI-1 (TAPI, 10 µM) or GI254023X (GI, 3 µM) and incubated for 10 minutes on ice. Respective samples were then stimulated with BzATP (0.5 mM) at 37 °C in the presence of the respective ADAM10 modulating agents and AEBSF (100 µM) and MM (10 µM). After the stimulation, all samples were centrifuged at 15,000 xg for 30 seconds and filled up with NaCl-medium with AEBSF (100 µM). ADAM10 modulating agents were added again to the respective samples. The samples were then again incubated for the indicated times. As hemolysis controls for both experimental groups, unstimulated erythrocytes were used as a negative control while 14 µl of each sample was added to 120 µl H₂O at the end of the last sample collection as positive hemolysis control. Hemolysis was measured at 405 nm (TECAN Sunrise).

3.11.3 Rabbit erythrocytes – pVCC Western Blot samples

Rabbit erythrocytes were incubated with pVCC (3 µg/µl) and treated with P2X7R and ADAM10 modulating agents and times as described elsewhere (Chapter 3.11.3). To analyse the cleavage of pVCC, the differently treated erythrocytes were centrifuged at 2,500 xg for 5 minutes after the respective incubation time, and the supernatant was removed. All erythrocyte samples were repeatedly washed with 5x with 0.1 x PBS (Table 11) till the hemoglobin visually disappeared. Subsequently, the protein

concentration was determined as described elsewhere (Chapter 3.16.1) and equal amounts of protein homogenate were prepared for each sample. Afterwards, all samples were combined with 6x SDS sample buffer (Table 11). All samples were boiled for 5 minutes at 95 °C and further processed as described elsewhere (Chapter 3.13.2 – 3.13.4).

3.12 ADAM10 stalk mutants

To assess the functional relevance of cationic amino acids in the mouse ADAM10 stalk domain (AA: 647, 657, 659 and 660) site-specific point mutations were introduced to change the coding sequence (CDS) of murine ADAM10 wild-type (mADAM10wt) plasmid. Different mutants of mADAM10 were generated containing either: R647N (ADAM10 Stalk 1), R657N, K659N and K660N (ADAM10 Stalk 2) or a combination of both (ADAM10 Stalk 3). All mutagenesis reactions were carried out with the QuickChange® II Site-directed Mutagenesis XL (Agilent) according to the manufacturer's protocol.

3.12.1 ADAM10 stalk mutants primer design

For the introduction of site-specific mutations into the stalk domain, site-directed primers were designed using the Geneious software (Version 6.1.8) taking into account CDS of mADAM10 (Gene bank Entry: NM_007399.4). Primers were designed according to the Quick-change XL mutagenesis kit manual (Agilent). The mutagenesis primers were between 25 – 45bp, with a GC ratio >40 %. Primers were ordered from Sigma-Aldrich (Table 14).

Table 14. List of the ADAM10wt mutagenesis and sequencing primers.

Primer	Nucleotide sequence 5' – 3'
ADAM10 R647N forward	gtgatgtttcatgcggtgcaacttagtagaatgctgatggc
ADAM10 R647N reverse	gccatcagcattctactaagttgcaccgcatgaaacatcac
ADAM10 R657N forward	gatggcctctagctaactgaaaaagcc
ADAM10 R657N reverse	ggctttttcagattagctagagggccatc
ADAM10 K659N K660N forward	cctctagctaactgaacaacgccatttttag
ADAM10 K659N K660N reverse	ctaaaaatggcggtgttcagattagctagagg
pcDNA3.1BGHrev reverse	ctagaaggcacagtcgag

3.12.2 ADAM10 plasmid mutagenesis

The mADAM10wt plasmid (pcDNA 3.1 as the backbone) contained the entire CDS of mouse ADAM10 and was produced by Thorsten Maretzky (UOI, Iowa City, USA). Each mutation was introduced separately, which lead to the production of three murine ADAM10 stalk mutants. The plasmids were named as follow: mADAM10 Stalk1 (R647N), mADAM10 Stalk2 (R657N, K659N, and K660N) and mADAM10 Stalk3 (R647N, R657N, K659N, and K660N). The mADAM10wt plasmid was combined

with the forward and reverse primer for the specific mutation and a polymerase chain reaction (PCR) with PfuUltra HF was performed either for 16 or 18 cycles, depending on the total numbers of mutations that were introduced at the same time. After mutagenesis PCR, bacterial methylated plasmids were digested using endonuclease *DpnI*, and unmethylated plasmids were then used for the transformation into *E.coli* XL1 blue chemically competent cells (Agilent).

3.12.3 Production of chemically competent *E.coli* cells

For the production of chemically competent *E.coli* XL1 blue cells (Agilent) were treated with CaCl₂. The bacterial culture, grown overnight, was diluted with LB-medium (1:100) and incubated at 37 °C at 170 rpm. Upon an optical density (OD₆₀₀) of around 0.4-0.6 cells were incubated for 20 minutes on ice and subsequently centrifuged at 5000 xg for 5 minutes at 4 °C. After the supernatant was removed, the cell pellet was resuspended in 20 ml ice-cold Tris-buffer. The Tris-buffered cells were again centrifuged for 10 minutes at 5000 xg at 4 °C. The obtained cell pellet was then resuspended in 20 ml CaCl₂-solution and incubated for 20 minutes on ice. Once again, the cells were centrifuged for 10 minutes at 5000 xg at 4 °C and resuspended in 2 ml CaCl₂ solution. The cells in solution were again incubated on ice for 1 additional hour before 500 µl glycerin was added. Finally, the competent E-coli cells were transferred into liquid nitrogen and stored at aliquots of 50 µl at -80 °C.

3.12.4 ADAM10 Stalk mutant transformation, cultivation, and purification

Following *DpnI* digestion, ADAM10 stalk mutants plasmids were transformed separately into chemically competent *E.coli* XL1 blue (Agilent). Chemically competent *E.coli* XL1 blue cells were placed on ice and slowly thawed. For each transformation, 50 µl chemically competent *E.coli* XL1 blue were combined with 1 µl of the respective ADAM10 stalk mutant plasmid and kept for 30 minutes on ice. The transformation sample was then heated for 50 seconds at 42 °C and immediately placed back on the ice for 2 minutes. Transformed *E.coli* XL1 blue cells were then combined with 450 µl SOC medium (Table 11) and incubated for 90 minutes at 37 °C, at 170 rpm. After the 90 minutes incubation, 100 µl of the *E.coli* XL1 blue suspension was plated onto ampicillin containing LB-agar plates (Table 11) and incubated at 37 °C overnight. Colonies on the ampicillin containing LB-agar plates were picked and placed in reaction flasks containing 250 ml LB-medium (Table 11) with 0.1 % ampicillin. This culture was then grown for approx. 16 hours at 37 °C, at 170 rpm. Plasmids from the *E.coli* culture were then isolated with the PureYield MidiPrep kit (Promega) according to the protocol of the manufacturer. Plasmids were purified with nuclease free water (Promega). Plasmids concentration was determined with the NanoDrop 1000 (Thermo Fisher Scientific).

3.12.5 Bacterial glycerol stocks of ADAM10 stalk mutants

Transformed bacteria cells were kept as glycerol cryo-stocks for long-term storage, to allow fast plasmid purification. Bacterial cryo-stocks were produced as follows: 850 µl of 16 hours bacteria culture were

mixed with 150 μ l sterile glycerol and subsequently placed into liquid nitrogen. Stocks stored long-term were kept at -80 °C.

3.12.6 ADAM10 stalk mutants sequencing and analysis

Successful mutagenesis for all ADAM10 stalk mutant plasmids was confirmed via Sanger sequencing of each plasmid. 3 μ l from each plasmid (concentration of 100 ng/ μ l) were combined with 1 μ l sequencing primer pcDNA3.1BGHrev (Table 13) with a concentration of 4.8 μ M and sent to the Institute of Clinical Molecular Biology (IKMB, CAU, Kiel) for sequencing. Sequence data for the different ADAM10 stalk mutant plasmids were then compared with the sequencing data of mADAM10wt plasmid, using the Geneious software (Version 6.2).

3.13 Western Blot analysis of ADAM10 shedding assays

Unless indicated otherwise, samples from ADAM10 shedding assays were prepared as follows. Similar numbers of cells were seeded into 6 well plates. After 48 hours, the culture medium was removed and replaced with fresh medium without FBS and antibiotics. The cells were preincubated with OPS (10 mM), OPC (10 mM), MM (10 μ M) or TAPI-1 (TAPI, 10 μ M) and GI254023X (GI, 3 mM) 15 minutes before stimulation. Stimulation agent ionomycin (1 μ M) was then added to the respective cells for 20 minutes. After 20 minutes of incubation, the supernatant was removed, and cells were subsequently placed on ice. ADAM10 lysis buffer (Table 11), supplemented with PhosStop® (Roche) and cComplete® (Roche), was added to each sample. All samples were 3x frozen and thawed before the lysate was removed and transferred into 1.5 ml reaction tubes. All samples were kept on ice for 30 minutes and vortexed in between. Afterwards, all lysate samples were centrifuged at 13,000 xg for 5 minutes at 4 °C to separate proteins from cellular debris. Purified cell lysates were subsequently used to determine protein concentrations or stored at -20° for later analysis.

3.13.1 Protein concentration determination

Total protein concentrations of cell lysates were determined with the 660 nm protein assay (Thermo Fisher Scientific). For this, 6 μ l from each cell lysate sample was added to 100 μ l 660 nm protein assay reagent. 6 μ l lysis buffer was used as a control and subtracted from each sample concentration respectively. Sample sets were adjusted equally to a define concentration through interpolation into a BSA acquired standard curve. All sample concentrations were measured with Sunrise (Tecan) plate reader at 620 nm.

3.13.2 Sodium dodecyl sulfate (SDS) polyacrylamide gel electrophoresis

A SDS polyacrylamide gel provides a homolog net structure by which proteins can be separated according to their molecular weight. The addition of SDS to each lysate sample leads to a defined negative charge of all proteins. The separation requires an electric field through which the negatively charged proteins can be transported from cathode to anode. For the analysis of protein expression, the

defined total protein amounts were loaded for the different samples. For experiments with COS7, HaCaT, MEFs, control B-cells and Scott-UK B-cells 50 µg/sample protein homogenate was prepared. For experiments with rabbit erythrocytes 15µg/sample protein homogenate was prepared. All samples were combined with 1x SDS loading dye buffer and boiled at 95 °C for 5 minutes. Samples with overexpressed TMEM16A/ANO1 or TMEM16F/ANO6 were incubated at 30 °C for 1 hour. To determine protein molecular weight, 6 µl of protein marker *PageRuler Plus Prestained Protein Ladder* was loaded separately onto each gel. For the SDS gel-electrophoresis, a 10 % resolving gel and 4.5 % stacking gel (Table 15) were prepared. Samples were loaded onto the gel and electrophoresis was carried for the first 30 minutes at 90 V and for the remaining time at 150 V.

Table 15. SDS page composition.

Gel type	Composition
Stacking gel (4.5 %)	2.90 ml H ₂ O 1.25 ml stacking gel buffer 0.835 ml acrylamide 30 µl APS 15 µl TEMED
Resolving gel (10 %)	4.03 ml H ₂ O 2.50 ml resolving gel buffer 3.33 ml acrylamide 60 µl APS 30 µl TEMED

3.13.3 Western Blot transfer and analysis

Transfer of electrophoretically separated proteins from the SDS-gel onto polyvinylidene fluoride (PVDF) membrane was performed by semi-dry or tank blotting. Semi-dry blotting was used for the transfer and analysis of overexpressed mADAM10wt, mADAM10 Stalk 2, and pVCC while tank blotting was used for the transfer and analysis of N-cadherin, E-cadherin, TMEM16A/ANO1GFP, TMEM16F/ANO6GFP, and P2X7R. In both blotting methods, the PVDF membrane was activated in MeOH. The activated membrane and the gel were placed between two layers of *Whatman paper*. The PVDF membrane was placed in the direction of the anode while the PVDF membrane was placed in the direction of the cathode. Semi-Dry blotting was carried out at 1.5 mA/cm² for 2 hours, and tank blotting was performed at 85 mA for 13 hours.

3.13.4 Antibody detection of transferred proteins

The PVDF membrane was placed after Western Blot transfer into a blocking solution containing 5 % milk powder (Table 12). The membrane was blocked for 1 hour and subsequently incubated with the respective primary antibody (Table 9) diluted in blocking solution containing 5 % milk powder. The primary antibody incubation was carried out for 1 hour at room temperature under constant rotation. Afterwards, the antibody solution was removed, and the membrane was washed 3x for 10 minutes with

TBST washing buffer. The membrane was then placed into TBST containing the respective secondary antibody coupled with peroxidase (HRP) and incubated for 45 minutes at room temperature under constant rotation. The membrane was additionally washed 3x with TBST washing buffer. For detection, the membrane was placed on a glass plate and covered with ECL select reaction solution. Peroxidase induced a chemical luminescence reaction, which was visualized with a CCD camera (Fusion FX7, Peqlab).

3.13.5 Antibody removal and re-probing of PVDF membrane

For the removal of primary and secondary antibodies, the PVDF membrane was placed in an airtight box and incubated with Stripping buffer (Table 12) for 30 minutes at 65 °C. Afterwards, the membrane was washed 3x with TBST washing buffer. Control staining was then carried out analogously to Chapter 3.16.4 with primary GAPDH antibody and mouse peroxidase-coupled secondary antibody. Only if indicated, densitometric analysis of Western Blots was carried out with the Bio1D software (Vilber Lourmat).

3.14 Transient transfection of adherent cells

COS7 or ADAM10/ADAM17-deficient HEK-293T cells were transfected, unless indicated otherwise, as follows. GFP control vector (500 ng), TMEM16F/ANO6GFP (500 ng), TMEM16A/ANO1GFP, human TMEM16F/ANO6 D408G (500 ng), mock control vector (1000 ng), inactive mADAM10 E/A, mADAM10wt (1000 ng), mADAM10 Stalk1(1000 ng), mADAM10 Stalk2 (1000 ng) or mADAM10 Stalk3 (1000 ng) or co-transfected with a AP construct (250 ng per construct, Table 10). Cells were seeded 24 hours before the transfection and only transfected at confluency between 60-80 %. Respective plasmids were mixed in DMEM without FBS and Pen/Strep mix. For single transfections, plasmid 1 was added to 100µl DMEM and the transfection reagent Turbofect was added (1 µl/500 ng plasmid). For double-transfection plasmid 1 and plasmid 2 were combined in 100 µl DMEM and the transfection reagent Turbofect was added (1 µl/ 500 ng plasmid). The tubes with the respective plasmids were inverted multiple times, and the plasmid transfection reaction mix was incubated for 15 minutes at room temperature. DMEM culture medium was removed from the cells and replaced by DMEM+10 % FBS without Pen/Strep mix. After 15 minutes incubation, plasmid transfection mix was added dropwise to each indicated well. After 24 hours, transfected cells were used for the respective experimental approach.

3.15 Alkaline phosphatase assays

Alkaline phosphatase (AP) fused substrates were introduced as a reliable way to analyse ADAM10/ADAM17 shedding activity. The AP tag was added to the protein of interest, so the AP fused substrate could then be transfected into cells. ADAM10-mediated shedding activity led to cleavage and release of the substrate into the medium while the unprocessed substrate remained in the cell membrane.

Afterwards, supernatant and cell lysate were collected, and the ratio between the released and the lysed substrate was determined.

3.15.1 Inhibition, stimulation, and analysis of alkaline phosphatase assays

For the analysis of ADAM10 mediated shedding of AP-substrates, COS7 cells were transfected as described in chapter 3.14. 24 hours after the transfection, DMEM culture medium was removed and replaced by 400 μ l DMEM without FBS or Pen/Strep Mix. Transfected COS7 cells were then preincubated with either OPS (1 mM, 5 mM or 10 mM), OPC (1 mM, 5 mM, 10 mM), TAPI-1 (TAPI, 10 μ M) or GI254023X (GI, 3 μ M), for 15 minutes at 37 °C in the Hera cell 150 incubator. Transfected COS7 cells or transfected ADAM10/ADAM17-deficient HEK-293T cells were stimulated with either ionomycin (IO, 1 μ M) or melittin (0.5 μ M) for 30 minutes. Subsequently, after the stimulation, the 400 μ l supernatant of each sample was collected, and the cells were lysed in 400 μ l AP lysis buffer. The supernatant and lysate of each sample were then centrifuged at 13,000 xg for 5 minutes at 4 °C. Triplicates of 100 μ l from each supernatant and 10 μ l from each lysate were then filled into a 96 well chamber. The lysates were filled up with 90 μ l AP assay buffer (Table 11). To measure ADAM10-mediated shedding of the respective AP tagged substrates, supernatant, and lysate from each sample were incubated with 100 μ l of the colourless substrate p-nitrophenyl phosphate (p-NPP), solved in AP assay buffer (Table 11), which under AP enzymatic activity turns into yellow p-nitrophenol (p-NP). All incubated cells were then measured at 405 nm with the Sunrise (Tecan) plate reader. Untransfected cells were used as a control and subtracted from all sample values. Supernatant values were multiplied by the factor 4, and lysate values were multiplied by the factor 40. The ratio between the multiplied values of the supernatants and the respective multiplied values of the lysates were then calculated and transformed into % shedding.

3.16 Flow cytometry analysis

Flow cytometry allows a two-dimensional displaying of cells according to their size (FSC) and granularity (SSC). This separation provides further information about the morphological characteristics of a specific cell-type in a sample. Most experimental flow cytometry approaches additionally analyse the expression of one or more cell surface proteins to characterise the displayed cell type. For the specific detection analysis of one or more cell surface proteins, cells were incubated with antibodies either directly or indirectly fluorochrome-labelled. The fluorochromes were then detected with the respective lasers. This was done as in the analysis of ADAM10-mediated shedding of CD23 (Chapter 4.8). B-cells were incubated with a fluorochrome (APC) coupled antibody against CD23. This approach allows the assessment of the ratio between the total cell number and the number of antigen on these cells. In addition to the detection of surface proteins with respective antibodies, flow cytometry is often used to determine PS levels on the outer leaflet of cells. Fluorochrome coupled Annexin-V and lactadherin are standard techniques to label and visualise PS on the outer leaflet of cells. In this thesis, different cell

types were analysed for protein surface expression: B-cells (CD23 or ADAM10), ADAM10/ADAM17-deficient HEK-293T cells (retransfected ADAM10) or phosphatidylserine (PS) exposure with lactadherin-FITC (B-cells), Annexin-V FITC (rabbit erythrocytes) or Annexin-V APC (COS7 cells). Gates were set before the stimulation to Annexin-V/lactadherin negative cell populations. Adherent cells were detached with Accutase® before the respective antibody or PS staining. All samples were measured with the FACSVerse flow cytometer and obtained data were analysed with FlowJo (Version 10.4.2, FlowJo).

3.16.1 Flow cytometry analysis of Annexin-V labelled rabbit erythrocytes

For flow cytometry analysis 1 ml from the total rabbit erythrocytes in NaCl-medium with AEBSF (100 µM) and MM (10 µM) was removed and centrifuged at 4 °C for 30 seconds at 15,000 xg. From the centrifuged erythrocytes, a 1 % solution was prepared. For each sample, 20 µl from the 1 % rabbit erythrocytes solution was added to 70 µl NaCl medium. To analyse whether PS exposure is driven by the activation of the P2X7R, respective control samples were incubated with P2 receptor broad-spectrum inhibitor PPADS (100 µM) 10 minutes before or after the stimulation. For the activation of the P2X7R, respective samples were incubated for 15 minutes with BzATP (0.5 mM). All samples were filled up with NaCl medium and centrifuged at 4 °C for 30 seconds at 15,000 xg. After the supernatant was removed, each sample was filled up with 195 µl ABB. Subsequently, 5 µl Annexin-V FITC was added to the respective samples, and all samples were stained for 15 minutes at room temperature in the dark. Following the staining with Annexin-V FITC, all samples were filled up with ABB and centrifuged at 4 °C for 30 seconds at 15,000 xg. The cells were resuspended in ABB and analysed.

3.16.2 Flow cytometry analysis of Annexin-V labelled cells COS7 cells

COS7 cells were seeded in 10 cm dishes and transfected with 9000 ng of GFP, TMEM16F/ANO6GFP or TMEM16F/ANO6 D408G GFP. 24 hours after transfection the cells were detached and centrifuged at 250 xg for 5 minutes at room-temperature. Cells were resuspended in DMEM without FBS or Pen/Strep mix, and total cell number per sample was set to 200,000. GFP and TMEM16F/ANO6GFP transfected samples were then stimulated for 10 minutes with IO at room-temperature, and respective controls were incubated respectively without IO. Each sample was then stained with Annexin-V APC for 10 minutes at room temperature. Human TMEM16F/ANO6 D408G GFP cells were subsequently stained with Annexin-V-APC. Gates were set to Annexin-V APC negative control cells and only GFP positive cells were analysed for the IO-induced Annexin-V APC signal.

3.16.3 Flow cytometry analysis of ADAM10 expression

The surface levels of ADAM10 of control B-cells and Scott UK-B cells and from retransfected ADAM10/ADAM17-deficient HEK-293T cells (Chapter 3.14) were assessed as follows. Retransfected ADAM10/ADAM17 deficient HEK-293T cells, control B-cells and Scott UK B-cells were transferred into 1.5 ml reaction tubes and fixated with 1 % PFA in PBS for 10 minutes at room-temperature. All

samples were then washed once with PBS. After each wash step, the cells were centrifuged at 250 g for 5 minutes at 4 °C. Subsequently, after the centrifugation, the supernatant was removed, cells were resuspended in either PBS containing 1 % BSA or NaCl-medium containing 1 % BSA and incubated for 10 minutes on ice. The incubation with the first antibody against ADAM10 (Table 9) was carried out for 30 minutes on ice. Afterwards, the cells were washed 2x with PBS or NaCl-medium respectively. All samples were then resuspended again in either PBS or NaCl-medium and incubated with the respective secondary Alexa 488 coupled antibody for 30 minutes on ice, in the dark. After the incubation with the secondary antibody, the cells were rewashed with PBS and analyzed.

3.16.4 Flow cytometry analysis of CD23 and lactadherin labelling

For the analysis of PS exposure and CD23 shedding, control B-cells or Scott-UK B-cells were stimulated with BzATP for 30 minutes at 37 °C. Involvement of ADAM10 was analysed by preincubation of the different B-cell samples with GI254023X (GI, 3 µM). Lactadherin-FITC (8,53 nM) was added 5 minutes before the end of the stimulation. After the incubation, all samples were filled up again with NaCl-medium and subsequently centrifuged at 250 xg for 5 minutes and dissolved in 1 % PFA in PBS. The samples were kept for 10 minutes at room temperature and in complete darkness. Afterwards, all samples were filled up with PBS and again centrifuged at 250 xg for 5 minutes. The cells in each sample were then replenished in NaCl-medium containing 1 % BSA and then placed on ice. All cells were stained at the same time with the CD23-APC antibody and kept on ice and in complete darkness for 30 minutes, to avoid light-dependent bleaching of the fluorophore. After the incubation period, all samples were filled up again with NaCl-medium and centrifuged for 5 minutes at 250 xg. All samples were dissolved in NaCl-medium. Fas-Ab treatment (0.5 µg/ml) was performed for 6 hours at 37 °C in the Hera cell 150 incubator. Lactadherin-FITC was added to each sample 10 minutes before the end of the incubation time. All samples were removed from the incubator and filled up with RPMI medium without FBS or Pen/Strep mix and centrifuged and fixated for 10 minutes at room temperature with 1% PFA in PBS. Afterwards, all samples were filled up with PBS and centrifuged at 4 °C for 5 minutes at 250 xg. The cells were then resuspended in PBS with 3 % BSA and incubated for 10 minutes on ice before the CD22-APC, or respective isotype to the control was added. All samples were incubated for additional 30 minutes on ice. After the incubation with the primary antibody, the cells were filled up with PBS and centrifuged again at 4 °C for 5 minutes at 250 xg. All samples were resuspended in PBS and subsequently analyzed.

3.17 Confocal microscopic analysis of Annexin-V labelled cells

COS7 cells were seeded on glass coverslips coated with 0.25 % gelatin. COS7 with or without transfected TMEM16F/ANO6GFP, human TMEM16F/ANO6 D408G GFP or GFP control were stimulated after 24 hours with ionomycin (IO, 1 µM) or melittin (Mel, 0.5 µM) for 30 minutes before the labelling with Annexin-V Alexa 568. DMEM was removed from the cells, and all samples were

washed 1x with ABB (Table 12). The cells were then incubated with Annexin-V Alexa 568 in ABB (1:20) for 15 minutes at room temperature in the dark. After the staining, the cells were again washed 2x with ABB and 1x with PBS. Subsequently, the cells were fixated with 1 % PFA in PBS for 15 minutes and washed again 2x with PBS. Cells were covered in mounting solution with DAPI to visualise DNA and to preserve the cells. Annexin-V 568 labelled cells were analyzed with confocal microscope Fluoview FV1000 (Olympus) using a UPLSAPO 60x oil immersion objective. All images were acquired under the same laser and detection settings with separated channels. Each channel was equally adjusted with the FV10-ASW (Version 4.0, Olympus) program. Quantification of the Annexin-V Alexa 568 signals was performed with ImageJ (Version 1.47m). For quantification $n \geq 7$ pictures per sample were taken and analysed. Background fluorescence was set equally for each image. Total Annexin-V Alexa 568 signal was set in relation to total DAPI signals per image and displayed in $\mu\text{M}^2/\text{cell}$.

3.18 ADAM10 fluorescent peptide substrate assay

COS7 cells were seeded in 12-well plates and grown to confluency. Cells were mock treated or incubated with TAPI-1 (TAPI, 10 μM), preferential ADAM10 inhibitor GI254023X (GI, 3 μM), OPS (10 mM) or OPC (10 mM) for 15 min. ADAM10/ADAM17 deficient HEK-293T cells were transfected with control vector, inactive mADAM10-E/A, mADAM10wt or ADAM10 Stalk mutants (1-3). For the analysis of the effect of hyperactive human TMEM16F/ANO6 D408G on substrate cleavage, ADAM10/ADAM17 deficient HEK-293T were transfected either with inactive mADAM10-E/A, mADAM10wt or ADAM10 Stalk2 mutant together with empty control vector or human TMEM16F/ANO6 D408G vector. 24 hours after transfection, the culture medium was removed and replaced by serum-free DMEM. The cells were incubated with or without GI254023X (GI, 3 μM), 15 minutes before the ADAM10 fluorescent peptide substrate (Biozyme, 15 μM) was added to the samples. All samples were incubated for 30 minutes with the ADAM10 fluorescent peptide substrate. The supernatant of each sample was measured in triplicates at excitation 320/20 nm and emission 400/30 with FLx800 (BioTek) fluorescence reader. The values from respective incubated ADAM10 fluorescent peptide substrate without cells was used as a control and subtracted from each sample for the analysis.

3.19 Biophysical experiments with the ADAM10 stalk peptide

The biophysical experiments analysing the interaction of the ADAM10 stalk peptide to PS and PC rich liposomes (Chapter 3.19.1-3.19.4) were carried out by the AG Gutschmann (Research centre Borstel). Namely, the isothermal titration calorimetry (ITC) experiments with the ADAM10 stalk peptide were carried out by Dr Wilmar-Alexander Correa-Vargas (Chapter 3.19.4). The surface acoustic wave (SAW) and fluorescence resonance energy transfer (FRET) experiments with the ADAM10 stalk peptide were carried out by Dr Christian Nehls (Chapter 3.19.2 and 3.19.3). The ADAM10 stalk peptide was ordered from Biosyntan (GER). The peptide represented the following amino acid sequence: CRLVDADGPLARLKKAIIFSGSGSGK-OH.

3.19.1 Preparation of lipid aggregates/liposomes

Liposomes were prepared as 1 mg ml⁻¹ (SAW, FRET) or 1 mM (ITC) aqueous dispersions of the phospholipids as follows. Lipids were dissolved in chloroform to a concentration of 10 mg ml⁻¹. After the solvent was evaporated under a stream of nitrogen and buffer was added, sonication with a Heinemann tip sonicator (G. Heinemann Ultraschall- und Labortechnik, Germany) for 4 min ml⁻¹ (1 ml solution) was used to achieve homogeneous liposome formation. Subsequently, the preparation was cooled for 30 min at 4 °C and two times heated for 30 min at 60 °C and cooled to 4 °C. Preparations were stored at 4 °C overnight before measurements.

3.19.2 Acoustic wave biochip analyses

Gold-coated chips (S-sens K5 Biosensor Quartz Chips, SAW Instruments GmbH, GER) were functionalized as described by Andra et al. (2008). Biomolecular interaction processes on the surface of the sensor chip can affect phase and amplitude of the surface guided acoustic wave. Changes of these parameters correlate with mass loading and viscosity changes on the chip surface. Measurements were performed as described by Sommer et al. (2016). To ensure a complete vesicle spreading process on the surface functionalization, the liposomes were prepared and dissolved in 5 mM HEPES buffer containing 150 mM NaCl. However, after membrane formation, the buffer was displaced by 5 mM HEPES, pH 7.4. Since capturing of the liposomes is induced by electrostatic attraction between the positively charged PLL coupled to the sensor surface and negatively charged lipids, the immobilisation of pure PC liposomes was not possible in this setup. Therefore, a low amount of PS was added to PC. Following the immobilization of liposomes (300 µg ml⁻¹ PS liposomes or PC:PS (9:1 [M:M]) liposomes) on the positively ionised sensor chip surface, 100 µl of 100 µg ml⁻¹ solution of the ADAM10 peptide in 5 mM HEPES were injected. Changes of phase and amplitude induced by the interaction of ADAM10 with the lipid bilayer were recorded over time. All biosensor measurements were performed at 22 °C

3.19.3 Fluorescence resonance energy transfer spectroscopy (FRET)

Intercalation of the ADAM10 peptide into liposomes was determined by FRET spectroscopy applied as a probe dilution assay using a Fluorolog 3 fluorescence spectrometer (HORIBA Jobin Yvon, USA). Liposomes were labelled by addition of 0.5 % NBD-phosphatidylethanolamine (NBD-PE) as donor dye and 0.5 % Rhodamine-DHPE as acceptor dye (molar ratio) to the chloroform lipid solution. The peptide was titrated 10 times in 10 µl injections of 1 mg ml⁻¹ to 900 µl 10 µg ml⁻¹ liposome dispersions (PS or PC:PS (9:1) in 5 mM HEPES, pH 7.4) at 37 °C, which led to a 3:2 lipid:protein molar ratio after the last injection. By excitation of the system at 470 nm, the intercalation could be monitored as an increase of the ratio between donor intensity I_d at 531 nm and acceptor intensity I_a at 593 nm (FRET signal) in a time-dependent manner.

3.19.4 Isothermal Titration Calorimetry (ITC)

The interaction of the ADAM10 peptide with PC or PS liposomes was analysed by Isothermal Titration Calorimetry measurements on an ITC200 (GE Healthcare, UK). 0.5 mM solutions of the ADAM10 peptide in 5 mM HEPES were titrated 20 times in 2 µl injections to 250 µl 0.1 mM PS or PC liposome dispersions – leading to a 4:3 lipid:protein molar ratio after the last injection. The heat of dilution was determined in control experiments by injecting peptide solution into a buffer (5 mM HEPES, pH 7.4). Enthalpy changes were recorded over time; measurements were performed at 37 °C.

3.20 ADAM10 and ADAM17 – OPS interaction model

The Swiss server (www.swissdock.ch/docking, Grosdidier et al., 2011) was used to predict the docking of OPS to ADAM10 and ADMA17. Before docking, the C-terminal part of the available ADAM10 structure (PDB:6BE6) was extended using the Chimera program (Version 1.12) and missing amino acids of the conserved ADAM10 stalk domain were added based on the prediction of their secondary structure (www.compbio.dundee.ac.uk/jpred, Drozdetskiy et al., 2015). The extended ADAM10 and the available structure of ADAM17 (PDB:2M2F) were docked to O-phospho-L-serine (ZINC03869280, zinc.docking.org, Irwin et al., 2012).

3.21 Statistical analysis

Unless otherwise indicated, statistical analyses were performed using the Prism software (Version 7). Generally, results were shown as means± s.e.m. based on experiments with an $n \geq 3$. Differences among groups were assessed using One-way ANOVA and Bonferroni multiple comparison post-hoc test. P-values <0.05 were considered statistically significant. A significant increase was indicated with *, and a significant decrease was indicated by #. The relationship between Annexin-V APC and substrate release was assessed by means of a linear regression model. Normality and model fitting was visualized inspecting the residuals of the model. Analysis was carried out with R Statistical Software package Ver. R-3.3.3 (R Core, 2017).

4. Results

The plasma membrane phospholipid phosphatidylserine (PS) is suggested to be a significant regulator of ADAM17 shedding activity. The probability that ADAM17 and ADAM10 share PS exposure as a common mechanism regulating their shedding activity is high, given the high structural and functional similarity between both proteases. However, whether PS regulates ADAM10 shedding activity remains unknown. Interestingly, a variety of stimuli have been shown to activate ADAM17 and ADAM10 shedding activity. Given that these stimuli activate both ADAM17 and ADAM10, and ADAM17 shedding is PS regulated, those stimuli are expected to induce PS exposure; which would be the first prerequisite to ascertain that PS also regulates ADAM10 shedding activity.

4.1 Stimulation with ADAM10 activators leads to PS exposure

To analyse whether PS exposure was enhanced by activators of ADAM10, COS7 cells were seeded onto coverslips and stimulated with either calcium ionophore ionomycin (IO) or the P2 receptor activator melittin (Mel). Stimulation with IO or Mel respectively was carried out for either 15 or 30 minutes after which the cells were stained with DAPI (blue) and Annexin-V Alexa 568 (red) to visualise cell DNA and PS externalisation, respectively. To evaluate a potential increase in PS exposure under both stimuli, the Annexin-V Alexa 568 signal of unstimulated control cells was set as a reference.

Confocal microscopic analysis of unstimulated COS7 cells stained with Annexin-V Alexa 568 revealed only minimal levels of external PS for both controls (Fig. 5a, upper and lower panel). Stimulation of COS7 cells with IO for 15 minutes led to a detectable enhancement of the Annexin-V Alexa 568 signal, indicating that the cells exposed PS under IO stimulation (Fig. 5a, upper panel). Moreover, IO stimulated cells showed a shrunk DAPI signal, indicating the stimulation lead to cell shrinkage. The analysis of the 30 minutes IO stimulated COS7 cells showed a similar shrunk DAPI signal while the Annexin-V Alexa 568 signal was more pronounced compared to the Annexin-V Alexa 568 signal for the 15 minutes IO stimulated cells (Fig. 5a, upper panel). Quantification of the Annexin-V Alexa 568 signal of all IO stimulated COS7 cells and respective control corroborated that levels of PS continuously increased over time (Fig. 5b).

A different result was obtained for COS7 cells stimulated with Mel. The stimulation with Mel for 15 minutes led to an increase of the Annexin-V 568 signal but showed no altered DAPI signal, compared to the Annexin-V Alexa 568 and DAPI signal from the unstimulated control cells (Fig. 5a, lower panel). Indicating that the stimulation with Mel led to PS exposure without affecting the cellular morphology. Interestingly, COS7 cells stimulated with Mel for 30 minutes showed a less pronounced Annexin-V Alexa 568 signal compared to the 15 minutes Mel stimulated cells (Fig. 5a, lower panel). Quantification of the different Annexin-V Alexa 568 signals for Mel stimulated, and respective control cells confirmed that the stimulation with Mel led to a transient exposure of PS (Fig. 5c). Although the quantification of the IO or Mel induced Annexin-V Alexa 568 signals showed that both stimuli led to PS exposure, it

appears that IO leads to a constant increasing PS signal, while stimulation with Mel leads to a transient PS exposure.

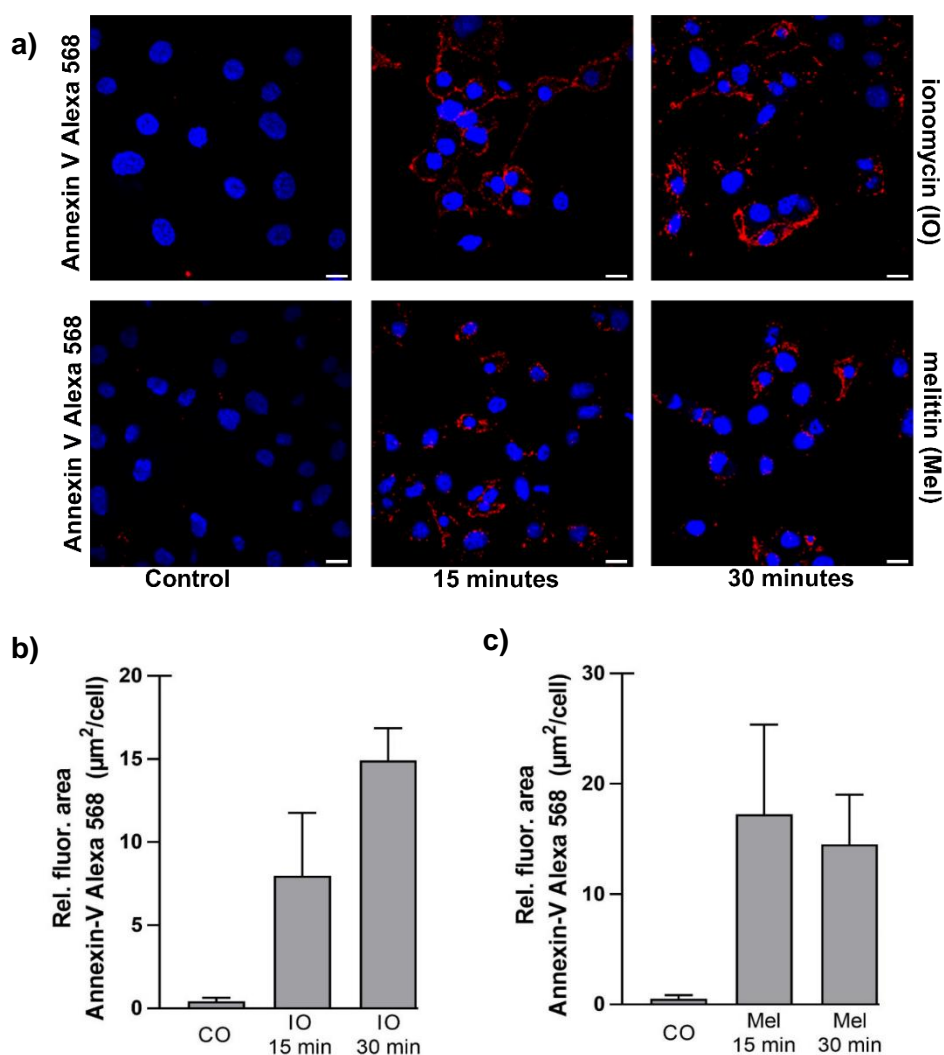


Figure 5. COS7 cells expose PS under ionomycin and melittin stimulation.

a) COS7 cells were treated with ionomycin (IO, 1 μM , a, upper panel) or melittin (Mel, 0.5 μM , a, lower panel) for 15 or 30 minutes and stained with Annexin-V Alexa 568 (red) and DAPI (blue) to visualise PS exposure and DNA respectively. The Annexin-V Alexa 568 signal for IO or Mel stimulated and respective control cells were analysed via confocal microscopy. Quantification of the **b)** IO-induced Annexin-V Alexa 568 signal and **c)** Mel-induced Annexin-V Alexa 568 signal was performed with ImageJ analysis software. One representative image for each treatment is shown. Quantification of the Annexin-V Alexa 568 signal after IO stimulation ($n=4$) or after Mel stimulation ($n=3$). Scale bar (white) shows 10 μm .

4.2 OPS inhibits the shedding of overexpressed ADAM10 substrates

The previous results showed that stimulation with two different activators of ADAM17 and ADAM10 led to PS exposure. However, it is not known whether stimuli-induced PS exposure regulates ADAM10 shedding activity. Therefore, COS7 cells were transfected with the ADAM10 substrate betacellulin

(BTC). The substrate was fused to an alkaline phosphatase (BTC-AP), which allowed to determine the ratio between the shed and released substrate in the supernatant as well as the substrate remaining in the cell lysate. The BTC-AP transfected cells were then stimulated with either IO or Mel for 30 minutes, given that this time of stimulation led to PS exposure thus assuring that ADAM10-mediated shedding would take place. Indeed, IO and Mel stimulation of the BTC-AP transfected COS7 cells led to the enhanced release of the substrate (BTC-AP) into the supernatant (Fig. 6 a&b). To confirm this was a result of ADAM10 shedding activity, BTC-AP expressing cells were incubated with the metalloproteinase inhibitor TAPI-1 (TAPI) or the ADAM10 inhibitor GI254023X (GI); before the stimulation with either stimulus. Both inhibitors led to a significant reduction of BTC-AP release into the supernatant, confirming that ADAM10-mediated shedding of the substrate was the reason for the enhanced BTC-AP levels in the supernatant (Fig. 6 a&b). To further assess whether stimuli induced PS exposure led to the enhanced ADAM10-mediated substrate release, BTC-AP transfected cells were incubated with different concentrations of O-phosphoserine (OPS, 1, 5 and 10mM) before the stimulation with either IO or Mel. OPS, the head group of PS, was reported to act as a competitive inhibitor of protein-lipid interaction (Spiegel et al., 2004). Thus, to confirm OPS specificity, BTC-AP transfected COS7 cells were also incubated with respective concentrations of O-phosphocholine (OPC), the headgroup of phosphatidylcholine. The outcome indicated that OPS had a direct inhibitory effect on ADAM10-mediated BTC-AP release (Fig. 6 a&b). This inhibitory effect was enhanced with increasing concentrations, i.e., 10 mM OPS led to a significant reduction of BTC-AP release (Fig. 6 a&b). In contrast, BTC-AP expressing COS7 cells, incubated with the respective concentrations of OPC and stimulated with IO or Mel, showed only a mild reduction of BTC-AP release indicating that the inhibitory effect on ADAM10-mediated BTC-AP shedding was OPS specific (Fig. 2 a&b). The inhibitory effect of OPS on the release of BTC-AP confirmed the importance of IO or Mel induced PS exposure for ADAM10 shedding activity. The inhibitory effect of OPS on the release of BTC-AP confirmed the PS dependency of ADAM10-mediated substrate shedding; opening the question whether this effect would be visible in the shedding of other substrates.

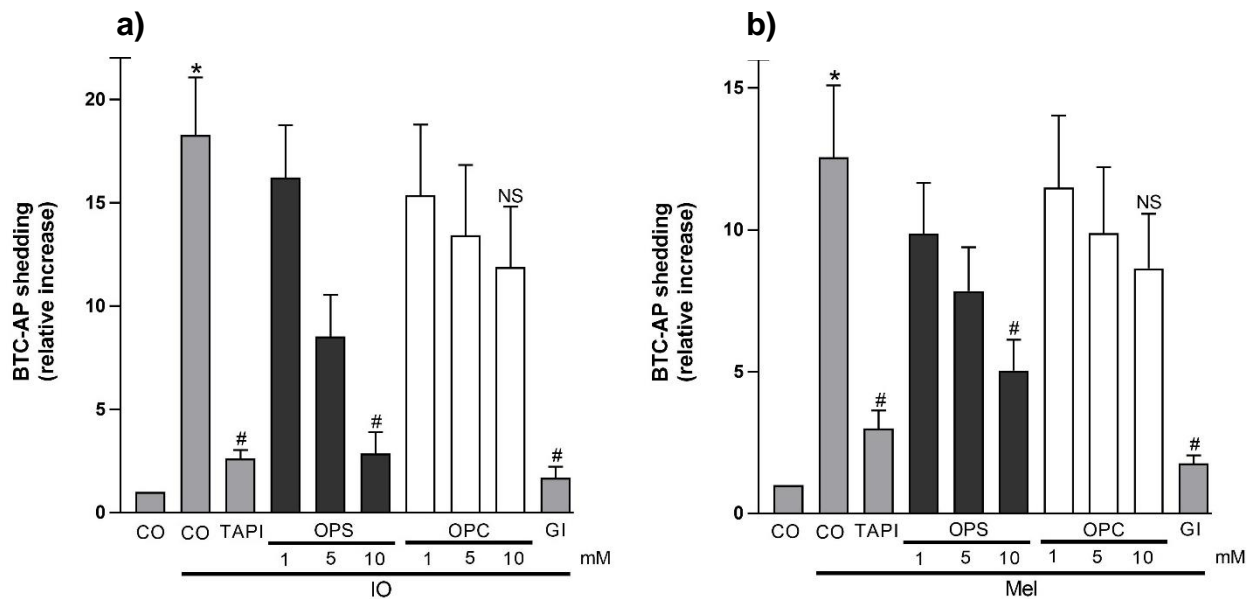


Figure 6. OPS inhibits ADAM10-mediated BTC-AP shedding.

COS7 cells were transfected with alkaline phosphatase betacellulin fusion protein (BTC-AP) and either stimulated with **a)** ionomycin (IO, 1 μ M) or **b)** melittin (Mel, 0.5 μ M) for 30 minutes. BTC-AP transfected cells were 15 minutes preincubated with broad-spectrum metalloproteinase inhibitor TAPI-1 (TAPI, 10 μ M), ADAM10 inhibitor GI254023X (GI, 3 μ M), OPS (1 mM, 5 mM, 10 mM) or OPC (1 mM, 5 mM, 10 mM), in addition to the respective stimuli. Differences among treatments were assessed with an ANOVA ($n=3$ for each treatment) and multi comparisons were carried out with the Bonferroni post-hoc test. Significant increase compared to unstimulated control (CO) is indicated by a * ($p<0.05$) and a significant decrease compared to IO or Mel stimulated substrate release is indicated by a # ($p<0.05$). NS=non-significant.

To answer this question, COS7 cells were transfected with the ADAM10 substrate vascular endothelial cadherin (VE-Cad), which was also fused to alkaline phosphatase (VE-Cad-AP). As in the experiments with BTC-AP, COS7 cells expressing VE-Cad-AP were stimulated with IO for 30 minutes. As expected, stimulation with IO led to the enhanced shedding of VE-Cad-AP (Fig. 7). To verify that the enhanced VE-Cad-AP release was a result of ADAM10 shedding activity, the VE-Cad AP expressing cells were incubated with TAPI-1 (TAPI) or GI254023X (GI) before the stimulation with IO. Both inhibitors showed a significant inhibitory effect on the release of VE-Cad-AP to the supernatant, confirming that VE-Cad-AP is shed by ADAM10 (Fig. 7). Additionally, to ascertain that PS also regulates VE-Cad-AP shedding, COS7 cells expressing the substrate were incubated with OPS (10 mM). The results confirmed that OPS reduced ADAM10-mediated shedding of VE-Cad AP (Fig. 7). Incubation with OPC (10mM) showed only a mild effect on the release of VE-Cad-AP (Fig. 7). The results indicated that ADAM10-mediated shedding of VE-Cad-AP is PS-dependent. Altogether, these results indicate that ADAM10 shedding activity is regulated by PS, irrespective of the nature of its activators or substrates.

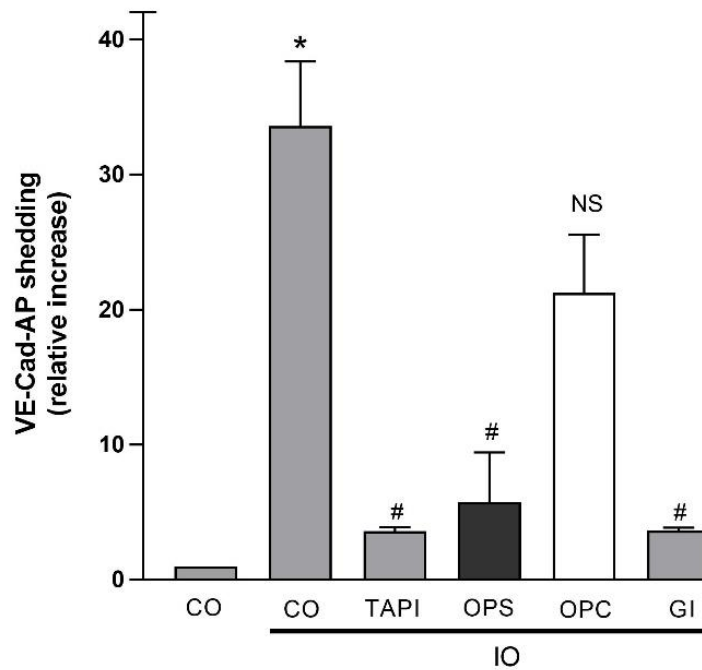


Figure 7. OPS inhibits ADAM10-mediated VE-Cad-AP shedding.

COS7 cells transfected with the alkaline phosphatase vascular endothelial fusion protein (VE-Cad-AP) and stimulated with IO for 30 minutes. Additionally, VE-Cad-AP transfected cells were incubated with TAPI-1 (TAPI, 10 μ M), GI254023X (GI, 3 μ M), OPS (10 mM) or OPC (10 mM) for 15 minutes before the IO stimulation. Differences among treatments were assessed with an ANOVA (n=3 for each treatment) and multi comparisons were carried out with the Bonferroni post-hoc test. Significant increase is indicated by a * ($p < 0.05$) compared to unstimulated control (CO), and a significant decrease is indicated by a # ($p < 0.05$) compared to IO stimulated control (CO-IO). NS=non-significant.

4.3 OPS inhibits ADAM10-mediated shedding of endogenously expressed substrates

The previous results showed that the headgroup of phosphatidylserine led to a dosage-dependent decrease of ADAM10-mediated shedding of overexpressed substrates. In this context the following question came up: Would OPS also show a competitive inhibitory effect on the ADAM10-mediated release of endogenous substrates? The release of two major substrates of ADAM10, neuronal cadherin (N-Cad), expressed by murine embryonic fibroblasts (Mef cells, Reiss et al., 2005) and epithelial cadherin (E-Cad), expressed by human keratinocytes (HaCaT cells, Maretzky et al., 2005), were therefore analyzed under stimulation with IO (1 μ M) and in the presence of OPS or OPC. As a proof of principle, Mef cells were stimulated with IO, and the shedding of endogenous N-Cad was determined with an antibody recognizing full-length N-Cad and the remaining C-terminal fragment (CTF) in Western Blot analysis. IO stimulation led to an enhanced N-Cad CTF band, indicating that the full-length protein was proteolytically degraded (Fig. 8a). Mef cells were further incubated with metalloproteinase inhibitor marimastat (MM), before the stimulation with IO, to ensure that proteolytic degradation was a result of enhanced metalloprotease activity. MM incubated cells, after IO stimulation, showed a reduced N-Cad CTF band in comparison to the CTF band shown by the cells only stimulated by IO, confirming that full-length protein is shed by a metalloproteinase, presumably ADAM10 (Fig.

8a). In addition to MM, Mef cells were incubated with different concentrations of OPS or OPC (either 1mM, 5mM, and 10mM) and stimulated with IO, to assess whether enhanced N-cad shedding is PS regulated. Dosage dependent OPS, but not OPC, blocked the shedding of full-length N-Cad, as indicated by the stepwise reduction of its CTF band in the Western Blot (Fig. 8a). The most substantial inhibitory effect on substrate shedding was shown by 10mM OPS, as this concentration led to a similar N-Cad CTF band to that of MM and IO CTF. The inhibitory effect of OPS on the shedding of full-length N-Cad confirmed that PS regulates the shedding of this substrate. Furthermore, to ensure that the inhibitory effect of OPS was not species specific, ADAM10-mediated E-Cad shedding was measured in human keratinocyte cells (HaCaT) endogenously expressing the substrate. The cells were stimulated with IO, to enhance ADAM10 shedding activity and the resulting proteolysis of E-Cad was analyzed via Western Blot. As in the N-Cad experiments, E-Cad shedding was analyzed with an antibody that recognises the full-length E-Cad protein and remaining CTF shedding product. The stimulation with IO led to the enhanced shedding of full-length E-Cad, indicated by the distinct E-Cad CTF band (Fig. 8b). Densitometric analysis of the IO stimulated cells showed a significant increase of E-Cad CTF compared to the unstimulated control (Fig. 8c). HaCaT cells were treated with TAPI-1 (TAPI) or GI254023X (GI), before stimulation, to confirm that ADAM10 was the responsible protease for the shedding of full-length E-Cad. Both inhibitors led to a significant reduction of E-Cad CTF corroborating ADAM10-mediated shedding of the full-length E-Cad (Fig. 8b). Even though cleavage of E-Cad was shown to be ADAM10 dependent, whether PS exposure triggered the protease activity remained unknown. Consequently, HaCaT cells were treated with OPS (10mM), before the stimulation with IO, which resulted in an apparent inhibitory effect on ADAM10-mediated E-Cad shedding, indicated by the significant reduction of E-Cad CTF (Fig. 8b). In contrast to OPS, OPC showed no effect on ADAM10-mediated E-Cad shedding (Fig. 8c). Thus, confirming that human ADAM10-mediated E-Cad shedding was PS regulated. These results indicate that PS-dependent ADAM10-mediated substrate release is generally regulating the protease activity.

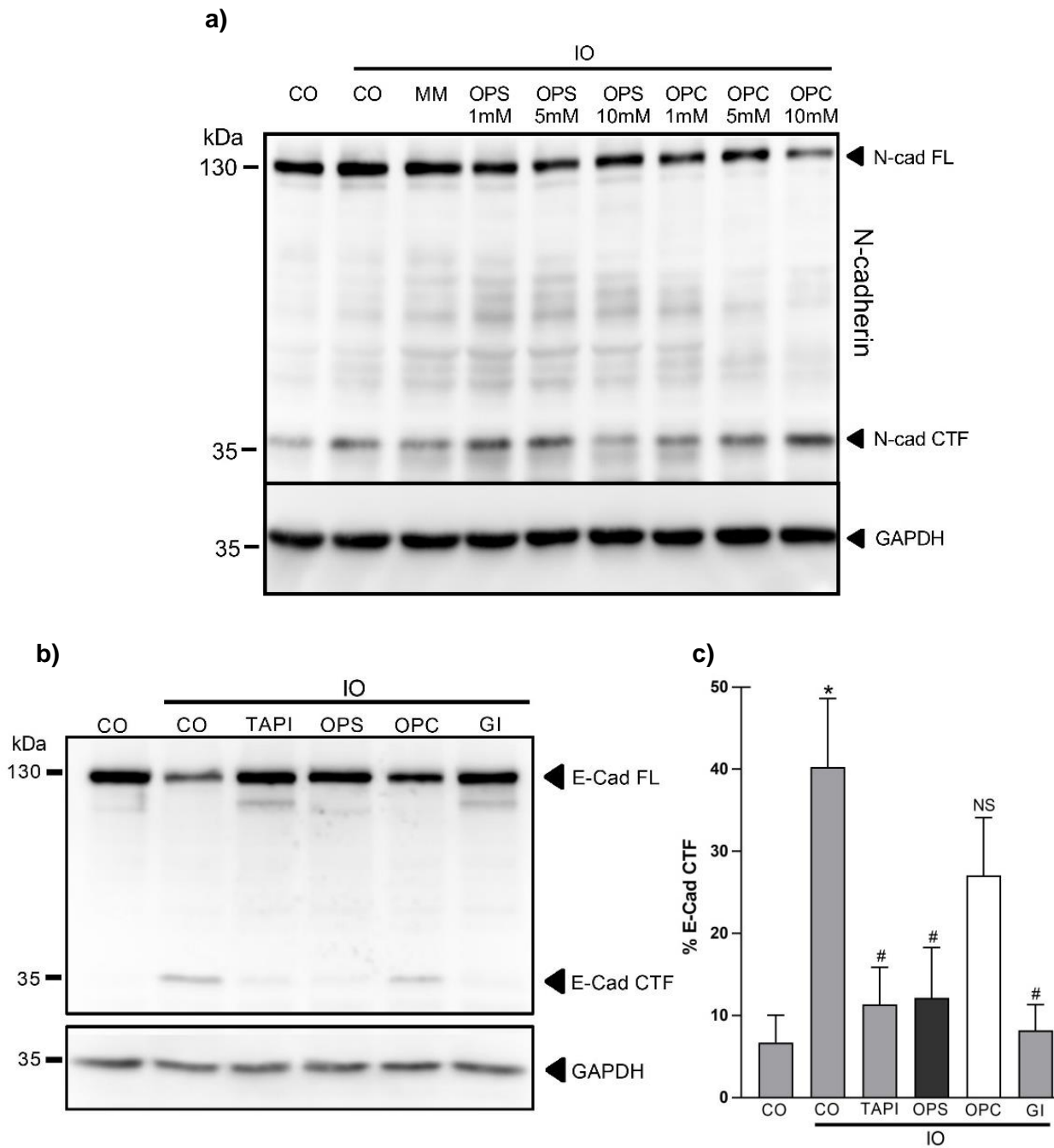


Figure 8. OPS inhibits ADAM10-mediated shedding of endogenous N-cadherin and E-cadherin.

a) Murine embryonic fibroblasts (Mefs) or **b)** human keratinocytes (HaCaT) were stimulated with IO for 30 minutes. Shedding of endogenously expressed neuronal cadherin (N-Cad) or epithelial cadherin (E-Cad) was visualised via Western blot analysis with respective antibodies recognising the full-length proteins (FL) and respective C-terminal cleavage products (CTF). Mef or HaCaT cells were incubated with TAPI-1 (TAPI, 10 μ M), ADAM10 inhibitor GI254023X (GI, 3 μ M), different concentration of OPS (a: 1mM, 5mM,10mM, b: 10mM) or OPC (a: 1mM, 5mM,10mM, b: 10mM) 15 minutes prior to the IO stimulation. All Western Blots were stripped and stained again with an antibody against GAPDH as a loading control. One representative Western Blot was shown for b. **c)** Densitometric quantification of the E-Cad Western Blot was performed using Bio1D software, depicting the percentage of E-Cad CTF to total E-Cad. Differences among treatments were assessed with an ANOVA (n=4) and multi comparisons were carried out with the Bonferroni post-hoc test. A significant increase compared to untreated cells (CO) is indicated by a * ($p<0.05$) and a significant decrease compared to IO treated cells is indicated by a # ($p<0.05$). NS=non-significant.

4.4 ADAM10 constitutive *bona fide* enzymatic activity remains functional under OPS

While OPS showed a competitive inhibitory effect on ADAM10-mediated substrate release, it remains unclear whether this was a result of OPS affecting the *bona fide* enzymatic activity of ADAM10 and thereby decreasing respective substrate release. To further analyse the effect of OPS on ADAM10 *bona fide* enzymatic activity, COS7 cells were incubated with a soluble ADAM10 fluorescent peptide substrate together with OPS. The fluorescent peptide substrate is quenched and only turns fluorescent when enzymatically cleaved.

Incubation of COS7 with the fluorescent peptide substrate led to an increase of the fluorescent signal in the supernatant of these samples. When compared to the respective buffer control, these results confirmed that the incubation of the ADAM10 fluorescent peptide substrate on COS7 cells led to its proteolytic processing (Fig. 9). The ADAM10 inhibitors TAPI-1 (TAPI) and GI254023X (GI) bind to the catalytic domain of the protease and thereby affect ADAM10 *bona fide* enzymatic activity and substrate release. To assess the effect of both inhibitors on ADAM10 *bona fide* enzymatic activity COS7 cells were incubated with TAPI-1 (TAPI) and GI254023X (GI) for 15 minutes before the fluorescent peptide substrate was added.

As expected, both inhibitors led to a reduction of the fluorescent signal in the supernatant of the respective samples compared to COS7 cells incubated only with the substrate (Fig. 9). These results indicated that blocking of ADAM10 catalytic domain led to a reduction of the proteases *bona fide* enzymatic activity. Additionally, COS7 were incubated with OPS and OPC (both 10mM) for 15 minutes before the fluorescent peptide substrate was added to the cells. The obtained results suggested that both OPS and OPC did not affect ADAM10 *bona fide* enzymatic activity. The signal of the fluorescent peptide substrate in the supernatant of these samples remained unaffected, and the respective fluorescent signal was similar to that of the control (Fig. 9). These results suggest that OPS inhibits ADAM10-mediated substrate release differently to TAPI-1 (TAPI) or GI254023X (GI), leaving ADAM10 *bona fide* enzymatic activity unaffected.

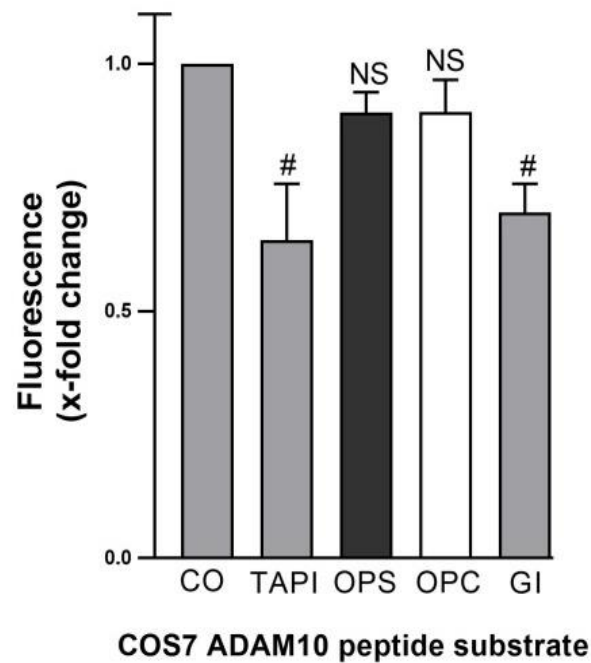


Figure 9. ADAM10 *bona fide* enzymatic activity remains functional under OPS.

ADAM10 enzymatic activity was analyzed with a protease specific fluorescent peptide substrate. Metalloproteinase inhibitor TAPI-1 (TAPI, 10 μ M), ADAM10 inhibitor GI254023X (GI, 3 μ M), OPS (10 mM) or OPC (10 mM) was added 15 minutes prior to the ADAM10 fluorescent peptide substrate (15 μ M). Buffer control with the ADAM10 fluorescent peptide substrate without cells was subtracted from all samples. Differences among treatments were assessed with an ANOVA (n=3 for each treatment) and multi comparisons were carried out with the Bonferroni post-hoc test. A significant decrease is indicated by a # ($p < 0.05$) compared to control treated cells (CO). NS=non-significant.

4.5 PS exposure regulates ADAM10 shedding activity

Previous results from cell-based systems highlighted the importance of PS exposure for ADAM10-mediated substrate release. However, whether PS is the primary trigger of ADAM10 shedding activity required further examination. On the one hand, cell-based systems might be too complex to accurately pinpoint PS as the primary trigger for ADAM10 shedding activity. On the other hand, data from liposomal systems are inconclusive, since the protease and its substrate need to be artificially implanted and correctly aligned in the liposomes. Therefore, an erythrocyte-based model together with the pro-form of the *Vibrio cholerae* cytotoxin (pVCC) as a substrate was developed (Fig. 10). This model combines the simplicity of a liposomal model with the physiological advantages of a cellular system. VCC-mediated rabbit erythrocytes hemolysis and Western Blot analysis were used as readout systems of ADAM10 activity.

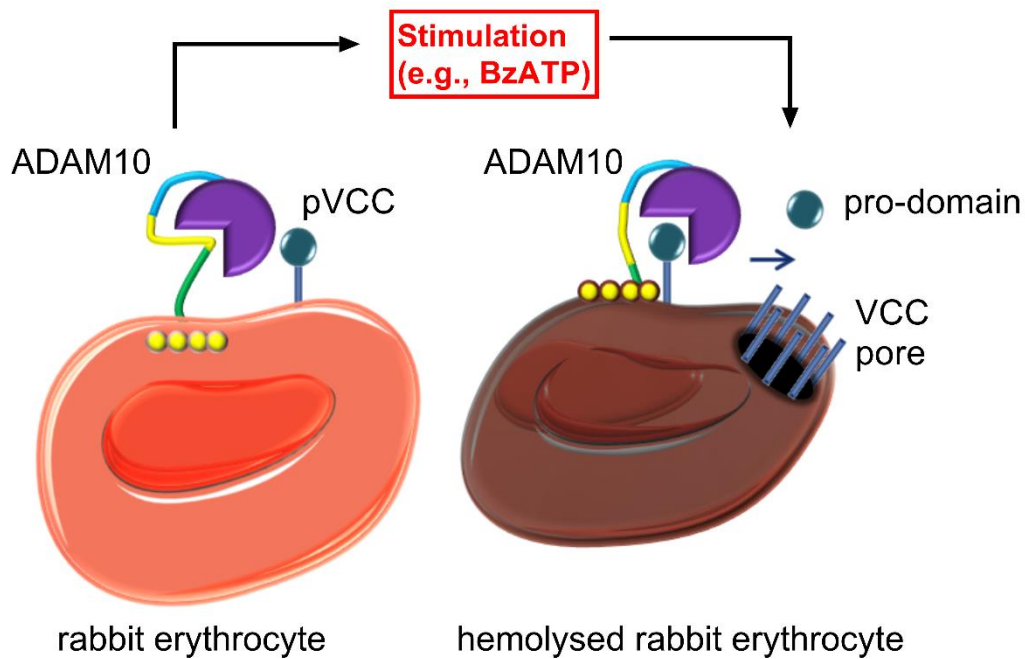


Figure 10. Rabbit erythrocyte – pVCC model

Schematic overview of ADAM10-mediated cleavage of pVCC and related hemolysis. The stimulation of rabbit erythrocytes with P2 receptor activators (e.g., BzATP) led to PS exposure. After stimulus removal the rabbit erythrocytes remained PS-positive, thus driving ADAM10-mediated cleavage of pro-VCC (pVCC, left) and respective heptamerization of the mature VCC (VCC). Heptameric VCC accumulated membrane pore (right) leads to rabbit erythrocytes hemolysis. The ADAM10-mediated cleavage of pVCC and related hemolysis were then used as readout systems.

To evaluate the capability of rabbit erythrocytes to expose PS, the cells were stimulated for 15 minutes with the P2X7 receptor activator BzATP (0.5 mM). The cells were stained with Annexin-V FITC, to determine PS exposure, and analysed via flow cytometry. Noticeably, stimulation with BzATP led to a positive Annexin-V FITC signal in about one-third of the rabbit erythrocytes (Fig. 11), indicating that this population reacted to the stimuli and exposed PS. To confirm PS exposure was a result of BzATP induced activation of P2 receptors, rabbit erythrocytes were incubated with the P2 receptor inhibitor PPADS (100 μ M) before the stimulation. The incubation with the P2 receptor inhibitor PPADS abolished the ability of rabbit erythrocytes to expose PS. Moreover, the P2 receptor inhibitor PPADS prevented PS exposure only when added before the stimulation but not after (Fig. 11). These results confirmed that rabbit erythrocytes expose PS through P2 receptor activation.

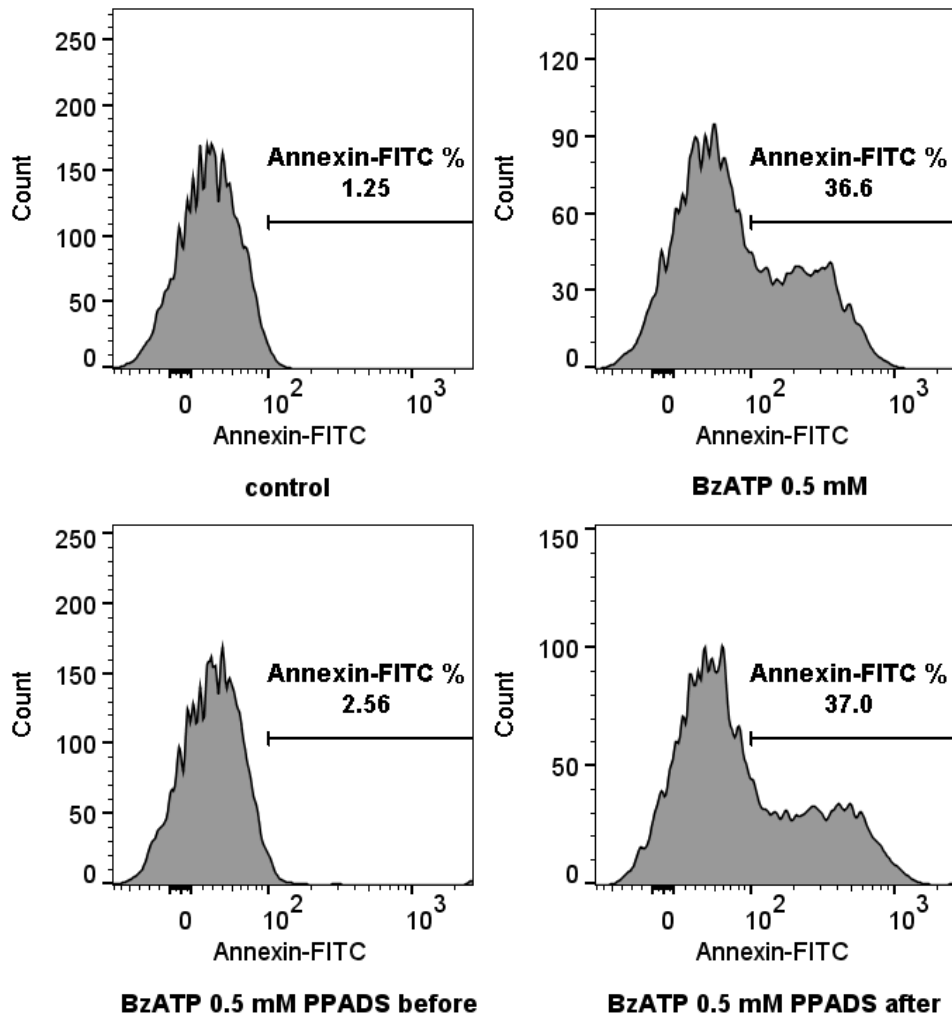


Figure 11. P2 receptor activation leads to PS exposure on rabbit erythrocytes.

Rabbit erythrocytes PS exposure was visualised with Annexin-V FITC and analysed via flow cytometry. Erythrocytes were stimulated with BzATP (0.5 mM) for 15 minutes and incubated with P2 receptor inhibitor PPADS (100 μ M) before or after the stimulation. Percentage of Annexin-V FITC positive rabbit erythrocytes for each sample is shown in %.

The previous experimental setup was used to further investigate the role of PS in ADAM10-mediated cleavage of pVCC. Firstly, to determine cleavage of pVCC as a trigger, respective hemolysis assays were carried out. The cleavage of pVCC should result in increasing levels of mature VCC (VCC) formed membrane pores thus enhancing hemolysis (Fig. 10). Secondly, to assert whether cleavage of pVCC was a trigger for hemolysis, pVCC incubated rabbit erythrocytes were assessed by Western Blot with an antibody recognizing the pro (pVCC) and mature form (VCC) of the protein. The rabbit erythrocytes were then stimulated with BzATP for 15 minutes in the presence of broad spectrum metalloprotease inhibitor marimastat (MM, 10 μ M) and AEBSF (100 μ M) to enhance PS externalisation but to avoid metalloproteases or serine proteases cleavage of pVCC. Additionally, samples were incubated with PPADS before or after stimulation respectively, to confirm P2 receptor dependency of the PS exposure and related ADAM10 cleavage of pVCC. Subsequently, after 15 minutes stimulation with BzATP, the

metalloproteinase inhibitor MM was removed, and only PPADS in the respective samples was replaced. The samples were then further incubated at 37 °C, and erythrocyte hemolysis was determined after 5 and 40 minutes. The comparatively low levels of hemolysis between the stimulated and unstimulated samples after 5 minutes confirmed that hemolysis did not occur during the stimulation (Fig. 12a). However, increasing incubation time showed increasing degree of hemolysis between the stimulated and unstimulated control samples, which reached its maximum after 40 minutes (Fig. 12a). Analysis of the stimulated and unstimulated control erythrocytes after 40 minutes showed a significant difference in the percentage of hemolyzed rabbit erythrocytes (Fig. 12a). Western Blot analysis was carried out to confirm that the increase in the percentage of hemolyzed rabbit erythrocytes was a result of enhanced cleavage of pVCC. The Western Blot analysis indeed confirmed a stronger VCC band for the stimulated and PS-positive rabbit erythrocytes compared to the VCC band of the unstimulated and PS-negative cells (Fig. 12a). However, incubation of the pVCC containing erythrocytes with the P2 receptor inhibitor PPADS, before the stimulation with BzATP, led to significant reduction of the percentage of hemolyzed rabbit erythrocyte. Analysis of the respective sample via Western Blot confirmed a reduced cleavage of pVCC (Fig. 12a). This inhibitory effect of PPADS on erythrocytes hemolysis and pVCC cleavage only occurred in cells incubated with the inhibitor before the stimulation but not after (Fig. 12a). These results confirmed that the cleavage of pVCC is driven by P2 receptor activation which in turn causes PS externalisation and thereby rabbit erythrocytes hemolysis.

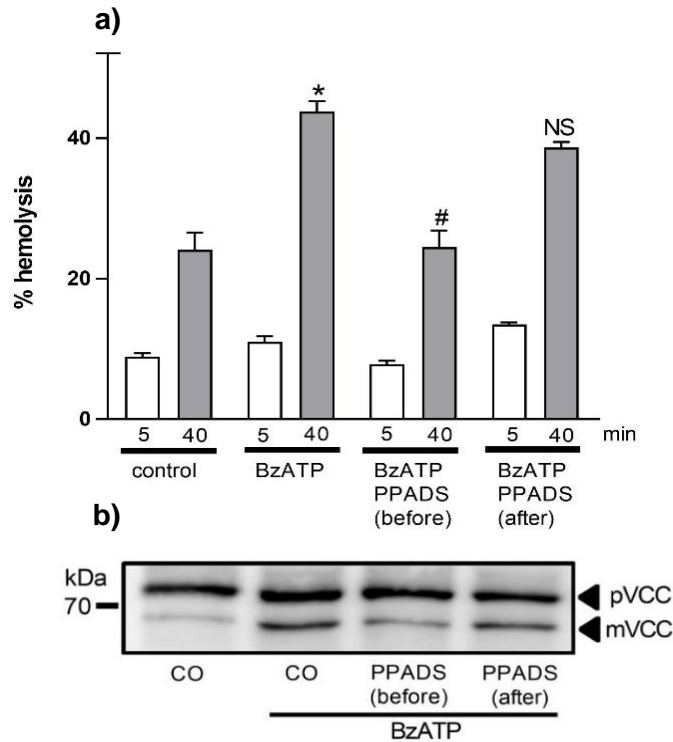


Figure 12. P2 receptor activation leads to VCC driven hemolysis.

a) Rabbit erythrocytes with pVCC were incubated with BzATP (0.5 mM) for 15 minutes in the presence of metalloproteinase inhibitor marimastat (MM, 10 μ M) and serine proteases inhibitor AEBSF (100 μ M). Control cells were treated with PPADS (100 μ M) before or after the stimulation. The BzATP stimulus was removed from rabbit erythrocytes, and respective cell hemolysis (a) and pVCC cleavage (b) was analyzed after 5 and 40 minutes of incubation. **b)** The picture represents on exemplary Western Blot (n=3). Differences among treatments were assessed with an ANOVA (n=3 for each treatment) and multi comparisons were carried out with the Bonferroni post-hoc test. Significant increase is indicated by a * ($p < 0.05$) compared to unstimulated control, and a significant decrease is indicated by a # ($p < 0.05$) compared to stimulated cells. NS=non-significant

In the next approach, the rabbit erythrocyte-pVCC model was used to determine whether PS-related cleavage of pVCC and respective erythrocyte hemolysis was ADAM10-dependent. As with the previous setup, the pVCC carrying erythrocytes were stimulated with BzATP for 15 minutes in the presence of the metalloproteinase inhibitor marimastat and the serine proteinase inhibitor AEBSF. Additionally, ADAM10 inhibitors TAPI-1 (TAPI, 10 μ M), GI254023X (GI, 3 μ M) and different concentrations of OPS (20 or 40 mM) or OPC (20 or 40 mM) were added to the samples, respectively. After 15 minutes of BzATP stimulation, the inhibitors and the stimulus were removed, and all samples were additionally incubated for 5 and 40 minutes. As seen in the previous approach, there was no significant difference among the different samples after 5 minutes of incubation (Fig. 13a), confirming that cleavage of pVCC and related hemolysis did not occur during the stimulation with BzATP. After 40 minutes of incubation, stimulated and unstimulated cells showed a significant difference in their degree of hemolysis, confirming that the stimulation and related PS exposure led to increased hemolysis through the enhanced cleavage of pVCC (Fig. 13a). Confirming this, Western Blot analysis showed an enhanced VCC band in the stimulated and PS-positive erythrocytes but not in the unstimulated and PS-negative control cells.

These results indicate that more pVCC was cleaved due to PS exposure but after the stimulus was removed (Fig. 13b). As expected, TAPI-1 (TAPI) and GI254023X (GI) led to a significant reduction of erythrocytes hemolysis (Fig. 13a), indicating that ADAM10-mediated cleavage of pVCC led to VCC driven hemolysis (Fig. 13b). Incubation with different concentrations of OPS showed a dosage-dependent reduction of erythrocyte hemolysis, with the most substantial effect at 40 mM OPS (Fig. 13a). Noticeable, OPC, showed no inhibitory effect on rabbit erythrocytes hemolysis or pVCC cleavage, confirming that the ADAM10-mediated cleavage of pVCC is PS-driven (Fig. 13b). The results of the rabbit erythrocyte pVCC model allowed to corroborate PS as the primary trigger of ADAM10-mediated cleavage of pVCC.

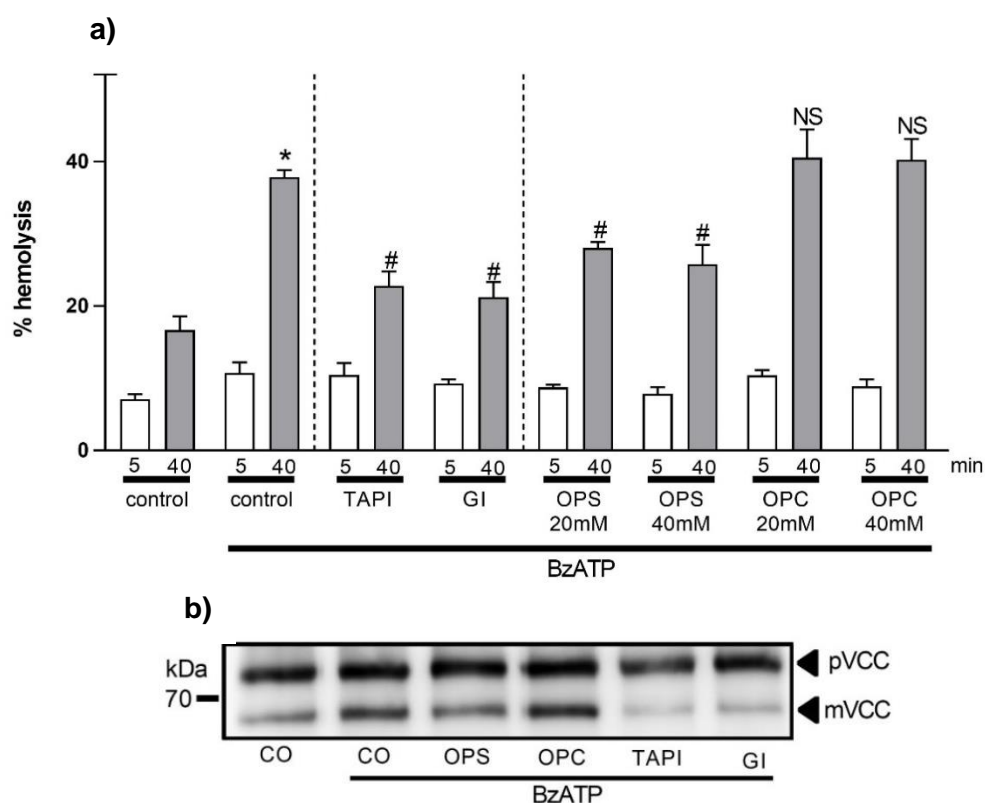


Figure 13. PS regulates ADAM10-mediated cleavage of pVCC and rabbit erythrocytes hemolysis.

a) Rabbit erythrocytes with pVCC were incubated with BzATP (0.5 mM) for 15 minutes in the presence of metalloproteinase inhibitor marimastat (MM, 10 μ M) and serine proteases inhibitor AEBSF (100 μ M). a) Rabbit erythrocytes were incubated with TAPI-1 (TAPI, 10 μ M), GI254023X (GI, 3 μ M), different concentrations of OPS (20 mM and 40 mM) or OPC (20 mM and 40 mM) prior and after incubation with BzATP. Rabbit erythrocyte hemolysis (a) and pVCC cleavage (b) was analyzed after 5 and 40 minutes incubation. **b)** The picture represents on exemplary Western Blot (n=3). Differences among treatments were assessed with an ANOVA (n=3 for each treatment) and multi comparisons were carried out with the Bonferroni post-hoc test. Significant increase is indicated by a * ($p < 0.05$) compared to unstimulated control, and a significant decrease is indicated by a # ($p < 0.05$) compared to stimulated cells. NS=non-significant.

4.6 TMEM16F/ANO6-related activity supports the functional role of PS in ADAM10-mediated shedding activity

A variety of proteins are involved in maintaining plasma membrane phospholipid asymmetry. One is the calcium-activated phospholipid scramblase TMEM16F/ANO6. Calcium influx has been shown to activate TMEM16F/ANO6 scrambling activity which enhances PS externalisation. Consequently, ionomycin-induced calcium influx in TMEM16F/ANO6 overexpressing cells should lead to enhanced PS externalisation which possibly affects ADAM10-mediated substrate release. In a first approach, COS7 cells were seeded on glass coverslips and transfected with either GFP control vector or TMEM16F/ANO6GFP. The transfected cells were then stimulated with IO (1 μ M) for 30 minutes and together with unstimulated control cells stained with Annexin-V Alexa 568 to visualise PS exposure. As observed before, COS7 cells showed a clear enhanced Annexin-V Alexa 568 signal compared to unstimulated control cells after the stimulation with IO (Fig. 14, upper panel). The analysis of the TMEM16F/ANO6GFP transfected COS7 cells also revealed an increased Annexin-V Alexa 568 signal after 30 minutes under IO stimulation compared to unstimulated TMEM16F/ANO6GFP overexpressing control cells (Fig. 14, lower panel). The overlay of the TMEM16F/ANO6GFP signal (green) and the Annexin-V Alexa 568 signal suggested a stronger PS pattern on cells overexpressing TMEM16F/ANO6GFP.

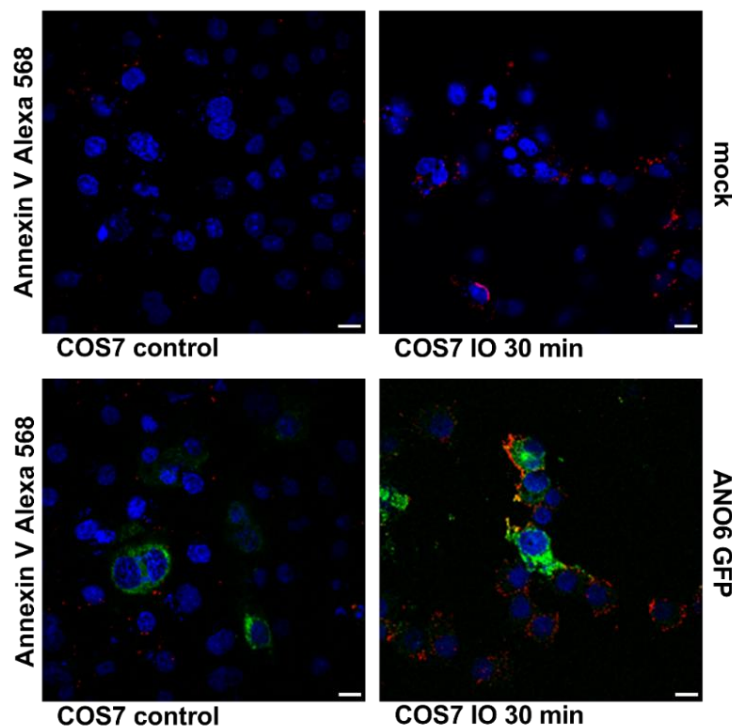


Figure 14. Overexpression of TMEM16F/ANO6GFP increases PS exposure in COS7 cells.

COS7 cells were transfected with either GFP control vector (upper panel, GFP signal not shown) or TMEM16F/ANO6GFP (lower panel, green) and labelled with DAPI (blue) Annexin-V Alexa 568 (red) to visualise cellular DNA and PS exposure respectively. Transfected COS7 cells were incubated for 30 minutes with or without IO (1 μ M). Displayed is one exemplary picture (n=3). Scale bar (white) shows 10 μ m.

However, quantification of these signals was not sensitive enough to show a definite increase in the Annexin-V Alexa 568 signal of control transfected and IO stimulated cells when compared to the corresponding cells overexpressing TMEM16F/ANO6GFP. To increase the sensitivity of the analysis of the Annexin-V signal, COS7 transfected with either GFP control vector, TMEM16F/ANO6GFP or TMEM16A/ANO1GFP were analyzed via flow cytometry. All samples were incubated for 10 minutes with or without IO (1 μ M) and stained with Annexin-V APC to describe the levels of PS on the outer plasma membrane leaflet. TMEM16A/ANO1 was additionally added to the group as a negative control, since it is described as a calcium-activated chloride channel with no scrambling activity. The flow cytometry analysis of the Annexin-V APC signal was only performed on GFP signal positive cells. The stimulation with IO lead to an increased Annexin-V APC signal on IO stimulated GFP transfected cells in comparison to unstimulated GFP expressing control cells (Fig. 15). The obtained increase in Annexin-V APC was in line with previous results where IO stimulation led to PS exposure. The analysis of IO stimulated COS7 cells overexpressing TMEM16F/ANO6GFP showed an increase in the total number of Annexin-V APC positive cells compared to the Annexin-V APC signal for respective transfected and stained but unstimulated control cells (Fig. 15). Quantification of the Annexin-V APC signal from IO stimulated GFP control cells compared to the Annexin-V APC signal of TMEM16F/ANO6GFP transfected, and IO stimulated cells showed a significant increase of the Annexin-V signal for the TMEM16F/ANO6GFP expressing cells (Fig. 16). These results show that indeed with the overexpression of TMEM16F/ANO6GFP more PS is exposed following IO stimulation. The analysis of the TMEM16A/ANO1GFP overexpressing cells also showed an enhanced Annexin-V APC signal after IO stimulation compared to the respective control. Interestingly, the quantification of the Annexin-V APC signal for IO stimulated TMEM16A/ANO1GFP overexpressing cells revealed an enhanced PS exposure located between the signals for the IO stimulated GFP control and TMEM16F/ANO6GFP overexpressing cells (Fig. 16).

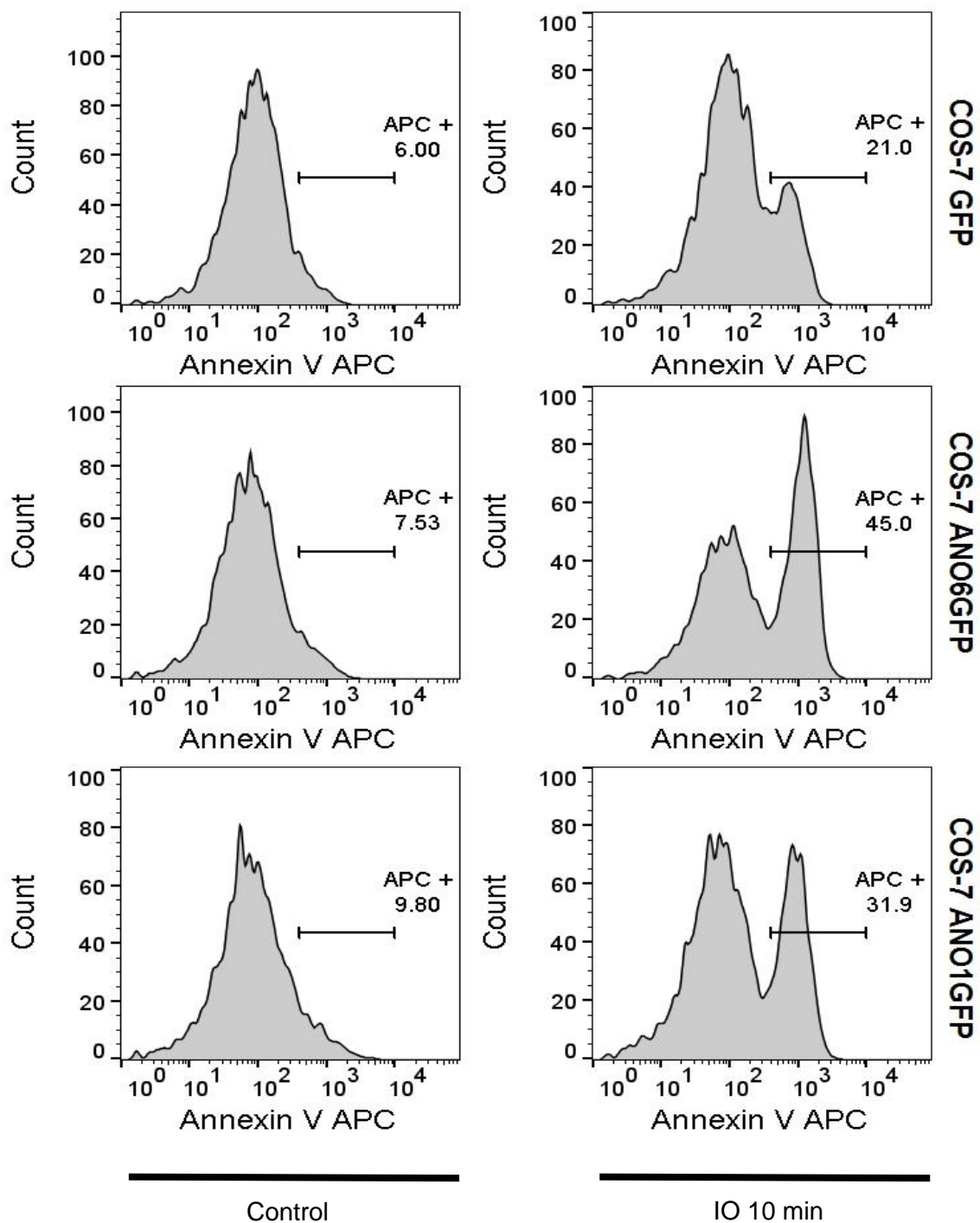


Figure 15. Stimulation of TMEM16F/ANO6GFP and TMEM16A/ANO1GFP overexpressing COS7 cells leads to enhanced PS exposure.

COS7 cells were transfected either with GFP control vector, TMEM16F/ANO6GFP or TMEM16A/ANO1GFP. Transfected cells were incubated for 10 minutes with or without IO (1 μ M) and stained with Annexin-V APC to label PS. All samples were analyzed via Flow cytometry under identical settings. Displayed is the Annexin-V APC signal of GFP positive cells in %, one exemplary picture per treatment (n=3).

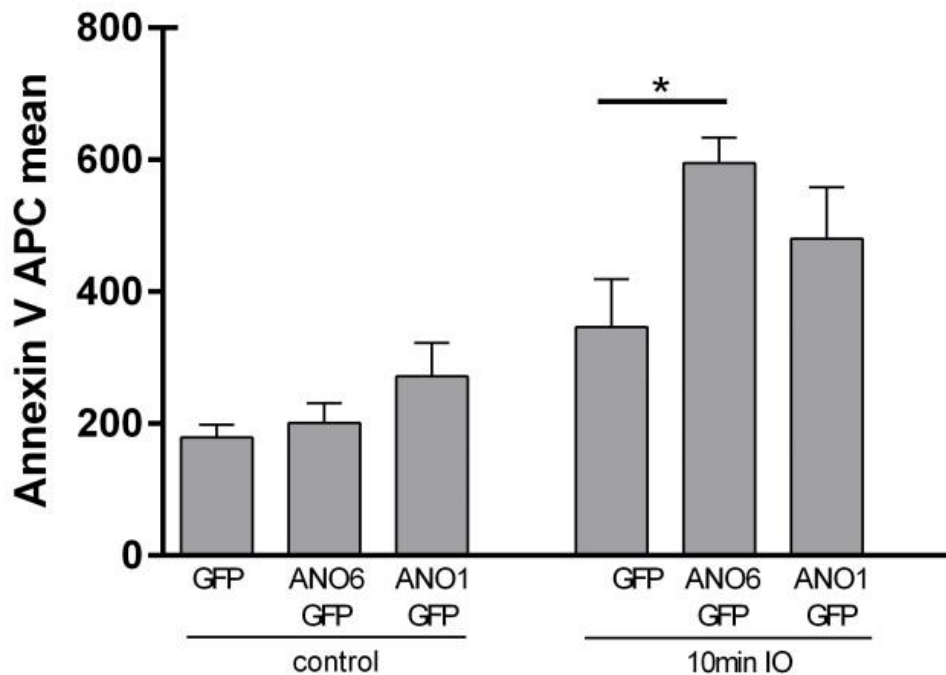


Figure 16. Overexpression of TMEM16F/ANO6GFP leads to a significant increase in PS exposure.

Quantification of the Annexin-V APC signal of unstimulated and IO (1 μ M) stimulated GFP control, TMEM16F/ANO6GFP and TMEM16A/ANO1GFP transfected COS7 cells. Differences among treatments were assessed with an ANOVA (n=3 for each treatment) and multi comparisons were carried out with the Bonferroni post-hoc test. Significant increase is indicated by a * (p<0.05) compared to IO stimulated GFP control.

The obtained results showed that TMEM16F/ANO6GFP and TMEM16A/ANO1GFP led to enhanced PS exposure although with differing strength in PS levels. It was, therefore, asked, whether the differently enhanced PS levels, for TMEM16F/ANO6 and TMEM16A/ANO1, would lead to consequently similar output on ADAM10-mediated substrate release. To assess this question, COS7 cells were transfected with GFP control, TMEM16F/ANO6GFP or TMEM16A/ANO1GFP together with the ADAM10 substrates BTC-AP or VE-Cad-AP. In this approach the time for the stimulation with IO (1 μ M) was set to 30 minutes, to ensure PS exposure and substrate shedding. The analysis of the shedding assays confirmed that TMEM16F/ANO6GFP overexpression, when compared to control GFP cells, led to a significantly enhanced shedding of BTC-AP and VE-Cad-AP (Fig. 17 a&b). Overexpression of TMEM16A/ANO1GFP also led to an increased ADAM10-mediated shedding of BTC-AP and VE-Cad-AP, compared to the increase in the cells that only express the GFP control (Fig. 17 a&b). These results go along with the PS signals obtained for the different ANOs and confirmed that TMEM16F/ANO6GFP and TMEM16A/ANO1GFP overexpressing cells led to an increased ADAM10-mediated substrate shedding, according to their PS signal. Western Blot analysis of COS7 cells with an antibody against GFP further confirmed the successful overexpression of TMEM16F/ANO6GFP and TMEM16A/ANO1GFP fusion proteins (Fig. 17 a&b). Although TMEM16A/ANO1 has not been shown to be involved in phospholipid scrambling, the observed increase of Annexin-V-APC signal and the corresponding increase in the ADAM10-mediated shedding of BTC-AP and VE-Cad-AP in TMEM16A/ANO1 overexpressing cells suggests its indirect involvement in PS exposure.

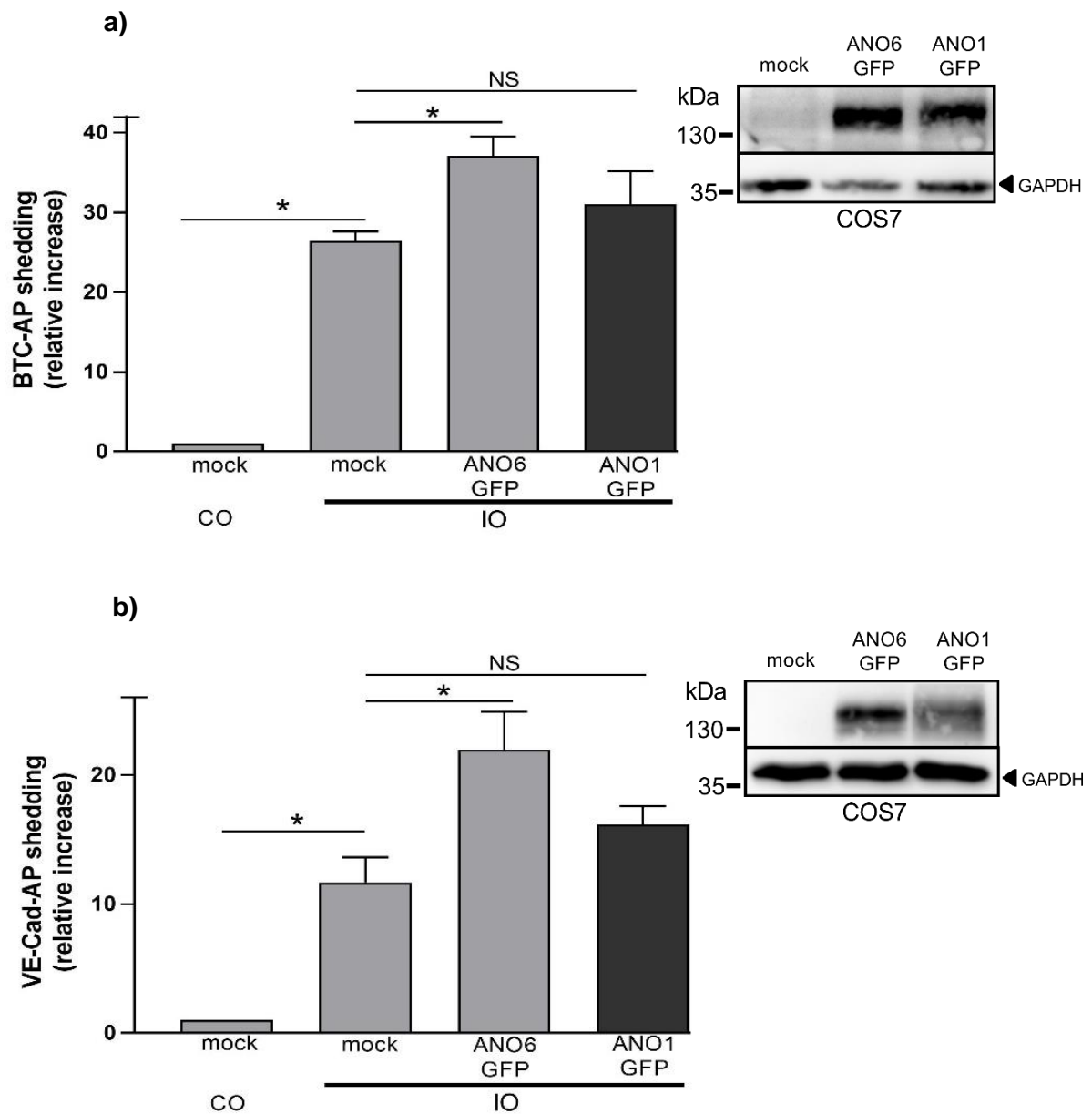


Figure 17. TMEM16F/ANO6 and TMEM16A/ANO1 overexpression enhance ADAM10-mediated substrate release.

a) COS7 cells were transfected with GFP, TMEM16F/ANO6GFP or TMEM16A/ANO1GFP and BTC-AP or b) COS7 cells were transfected with GFP, TMEM16F/ANO6GFP or TMEM16A/ANO1GFP and VE-Cad-AP: Transfected COS7 cells were then stimulated with IO for 30 minutes. Western Blot analysis of transfected COS7 with an antibody against GFP indicated the overexpression of TMEM16F/ANO6GFP and TMEM16A/ANO1GFP fusion proteins. Differences among treatments were assessed with an ANOVA (n=3 for each treatment) and multi comparisons were carried out with the Bonferroni post-hoc test. A significant increase is indicated by a * (p<0.05), and a significant decrease is indicated by a # (p<0.05). NS=non-significant.

The different Annexin-V APC signals and the results from the shedding assays suggested a general correlation between PS levels and ADAM10 activity on these cells. This correlation was assessed by means of a linear regression model, where PS levels determined ADAM10 activity. Substrate release was represented by the pooled data for BTC-AP and VE-Cad-AP from the IO (1 μ M) stimulated GFP

control, TMEM16A/ANO1GFP and TMEM16F/ANO6GFP overexpressing cells, and Annexin-V APC signals were represented by the pooled data from IO (1 μ M) stimulated GFP control, TMEM16A/ANO1GFP and TMEM16F/ANO6GFP cell. The significant regression model showed that indeed PS surface levels on COS7 cells have a positive effect in ADAM10-mediated substrate release in these cells (Fig. 18, $p < 0.05$). Although these data came from a small number of replicates, the model confirms that with more PS on the cell surface, more ADAM10-mediated substrate release occurred. Taken together these results indicate that the levels of PS on the outer leaflet directly determine ADAM10-mediated shedding activity.

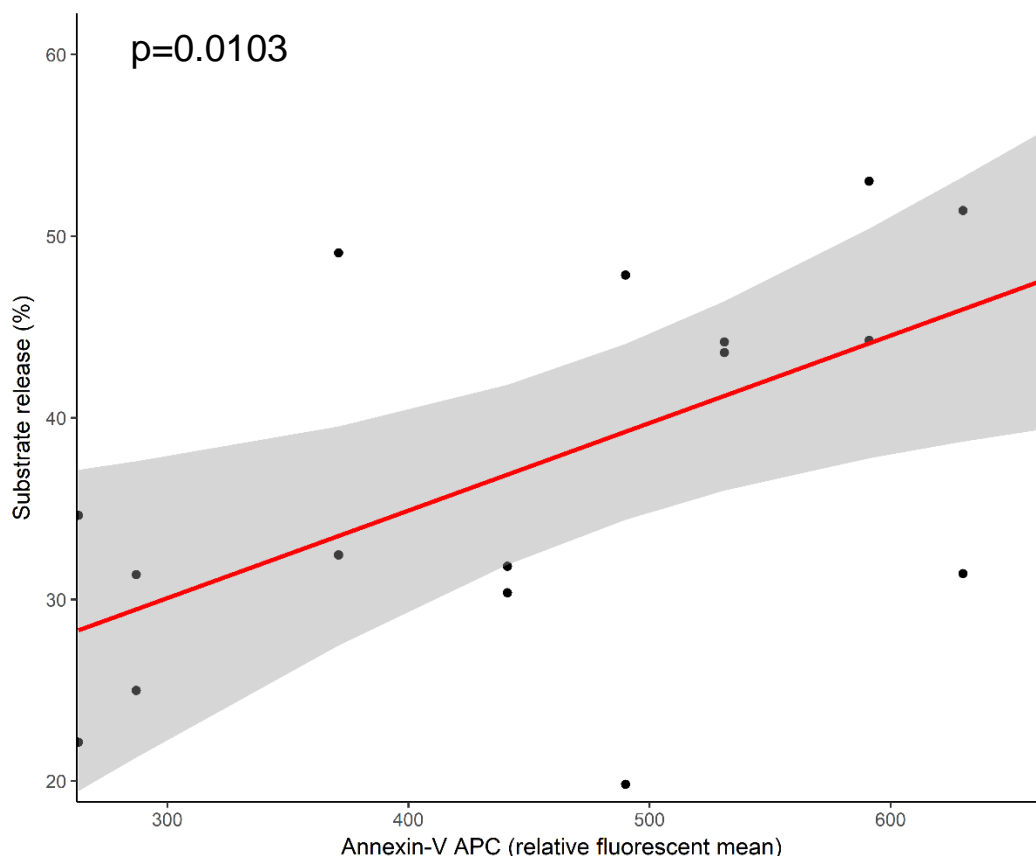


Figure 18. PS levels determined ADAM10-mediated shedding activity.

Data for the Annexin-V APC signal from COS7 cells with overexpressed control GFP, TMEM16F/ANO6GFP, and TMEM16A/ANO1GFP were related to those from respective samples from AP-shedding assays for the ADAM10-mediated release of BTC-AP and VE-Cad-AP. Individual points indicate the Annexin-V APC signal for the GFP control, TMEM16F/ANO6GFP or TMEM16A/ANO1GFP in relation to the % values of BTC-AP and VE-Cad-AP released from AP assays from COS7 cells transfected with the GFP control, TMEM16A/ANO1GFP or TMEM16F/ANO6GFP. The linear regression model was performed using R statistical software. The p-value ($p=0.0103$) indicates a significant correlation between the levels of Annexin-V APC and the % of released substrates; the direction of the slope indicates that the relationship is positive.

4.7 Gain of function in TMEM16F/ANO6 PS scrambling activity drives ADAM10-mediated substrate release

Elevation of cytosolic calcium activates a variety of signalling pathways additionally to TMEM16F/ANO6. To analyse whether enhanced PS exposure and consequently ADAM10 shedding activity were indeed a result of TMEM16F/ANO6 scrambling activity, COS7 cells were transfected with a functionally hyperactive mutant of TMEM16F/ANO6. The TMEM16F/ANO6 mutant (human TMEM16F/ANO6 D408G GFP) carries a single point mutation in its calcium binding domain (Fig. 19a) and represents the human equivalent to the mouse TMEM16F/ANO6 D409G, which leads to constitutively high PS scrambling under physiological calcium levels without requiring any stimulation. As in the previous setup, the experiments with human TMEM16F/ANO6 D408G GFP were divided into two experimental setups. In the first, COS7 cells were seeded on glass coverslips and transfected with either human TMEM16F/ANO6 D408G GFP and respective GFP control. The transfected COS7 cells were subsequently stained with Annexin-V Alexa 568 24 hours after transfection and analysed with a confocal microscope. The cells overexpressing the human TMEM16F/ANO6 D408G GFP mutant showed an enhanced Annexin-V Alexa 568 signal in comparison to GFP transfected control cells in the absence of any stimuli (Fig. 19b). Although the increase in Annexin-V Alexa 568 in the human TMEM16F/ANO6 D408G GFP transfected COS7 cells was visibly more pronounced, a second approach was performed where the GFP and human TMEM16F/ANO6 D408G GFP cells were analysed via flow cytometry. Human TMEM16F/ANO6 D408G GFP and GFP control transfected cells were therefore stained with Annexin-V APC 24 hours after the transfection and the Annexin-V APC signals were only obtained from GFP positive cells. Indeed, the flow cytometry analysis revealed that human TMEM16F/ANO6 D408GFP positive cells showed a clear Annexin-V APC signal (Fig. 19c) that was significantly higher compared to the Annexin-V APC signal of GFP control cells (Fig. 19d).

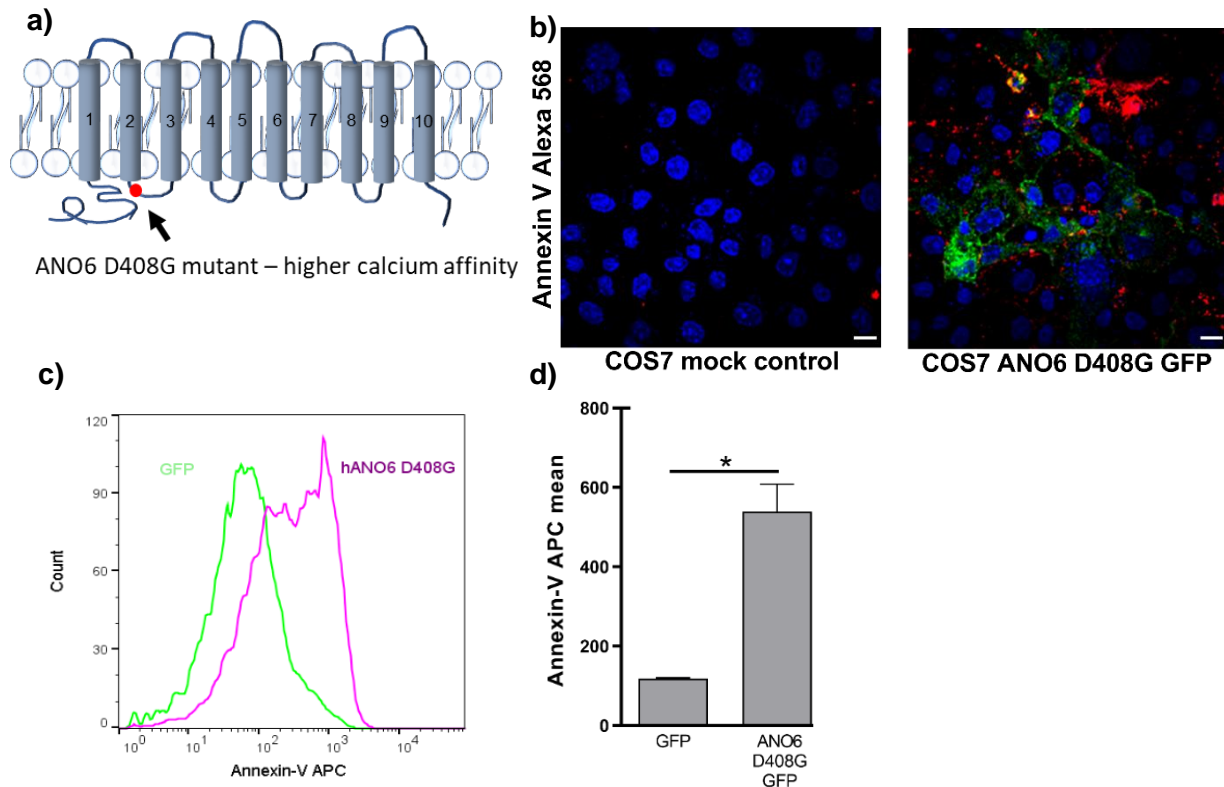


Figure 19. Hyperactive TMEM16F/ANO6 D408G leads to constitutive high PS exposure.

a) Schematic depiction of TMEM16F/ANO6 D408G. A single amino acid exchange at the position 408 from aspartic acid to glycine (red dot) led to a constitutively high PS scrambling activity of human TMEM16F/ANO6 mutant. **b)** Confocal microscopic analysis of overexpressed control GFP or human TMEM16F/ANO6 D408G GFP in COS7 cells. PS exposure was visualised with Annexin-V Alexa 568. One exemplary picture out of n=3. **c)** Flow cytometry analysis of control GFP (green histogram) or TMEM16F/ANO6 D408G GFP (magenta histogram) in COS7 cells. PS exposure was visualised with Annexin-V APC. One exemplary experiment out of n=3. **d)** Quantification of the flow cytometry data for the Annexin-V APC signal of control GFP or TMEM16F/ANO6 D408G GFP overexpressing COS7 cells (n=3). A significant increase is indicated by a * ($p < 0.05$) compared to control GFP. Scale bar (white) shows 10 μm .

A follow up question to whether the human TMEM16F/ANO6 D408G mutant leads to constant PS exposure was, whether this constant PS exposure would also lead to a constant ADAM10-mediated substrate release. Therefore, the effect of human TMEM16F/ANO6 D408G on ADAM10-mediated substrate release was further assessed. COS7 cells were transfected with ANO6 D408G GFP, and either BTC-AP or VE-Cad-AP and shedding activity was measured over time. After 30 minutes of incubation, BTC-AP and VE-Cad-AP release was significantly elevated in the COS7 cells overexpressing the constitutively hyperactive human TMEM16F/ANO6 D408G GFP mutant, in comparison to TMEM16F/ANO6GFP transfected cells (Fig. 20 a&b). The elevated levels of BTC-AP and VE-Cad-AP were maintained after 60 and 90 minutes of incubation (Fig. 20 a&b).

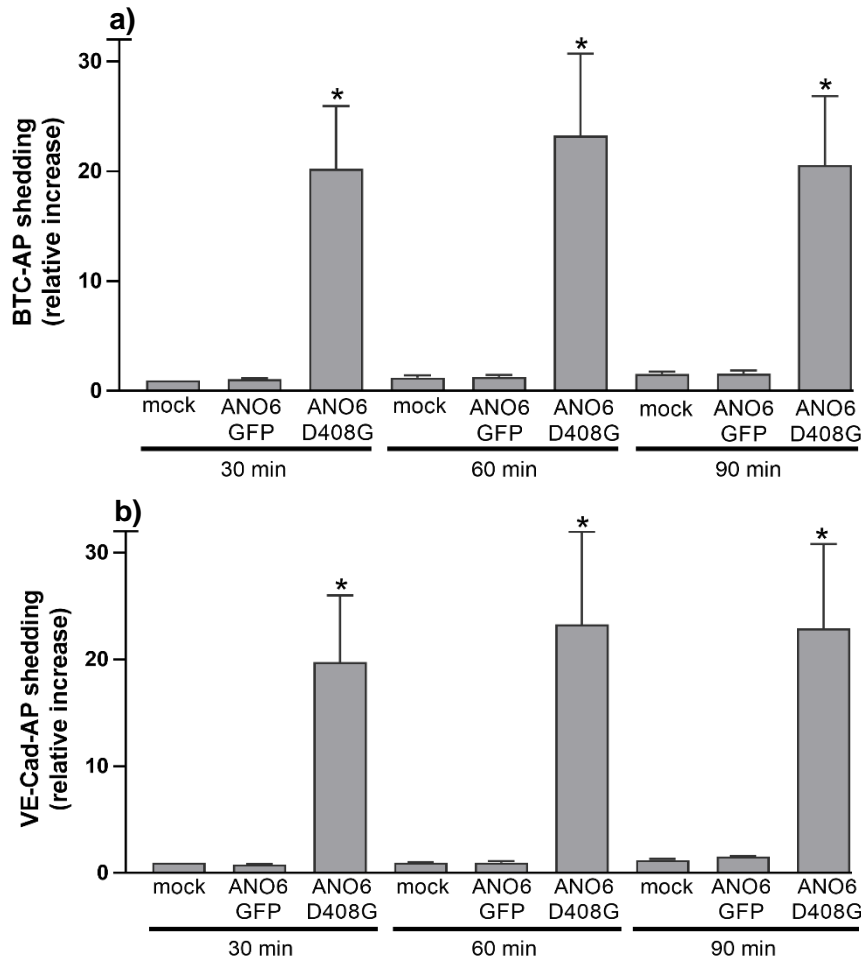


Figure 20. TMEM16F/ANO6 D408G overexpression led to constantly enhanced substrate shedding.

COS7 cells were transfected with GFP, TMEM16F/ANO6GFP or human TMEM16F/ANO6 D408G and either BTC-AP or VE-Cad-AP. **a)** BTC-AP and **b)** VE-Cad-AP shedding were analysed over indicated time. Differences among treatments were assessed with an ANOVA (n=3 for each treatment) and multi comparisons were carried out with the Bonferroni post-hoc test. A significant increase is indicated by a * ($p < 0.05$) compared to TMEM16F/ANO6GFP for the respective time.

Although these results showed that overexpression of human TMEM16F/ANO6 D408G GFP led to the enhanced release of BTC-AP and VE-Cad-AP, it remained to be shown whether the release of both substrates was a result of ADAM10 shedding activity. Therefore, COS7 cells overexpressing human TMEM16F/ANO6 D408G GFP and either BTC-AP or VE-Cad AP were incubated with either broad-spectrum metalloproteinase inhibitor TAPI-1 (TAPI) or GI254023X (GI). Incubation with TAPI-1 (TAPI) or GI254023X (GI) reduced the release of BTC-AP and VE-Cad-AP significantly, confirming the role of ADAM10 in the release of both substrates (Fig. 21 a&b). To further analyse whether PS triggers ADAM10-mediated shedding of both substrates, the human TMEM16F/ANO6 D408G GFP and either BTC-AP or VE-Cad-AP expressing COS7 cells were incubated with either OPS (10mM) or OPC (10mM). OPS, but not OPC, significantly reduced the shedding of BTC-AP and VE-Cad-AP, confirming that PS regulates ADAM10-mediated shedding of both substrates (Fig. 21 a&b). In summary, human TMEM16F/ANO6 D408G GFP overexpression upregulates the levels of external PS under physiological conditions, consequently leading to enhanced ADAM10-mediated substrate release.

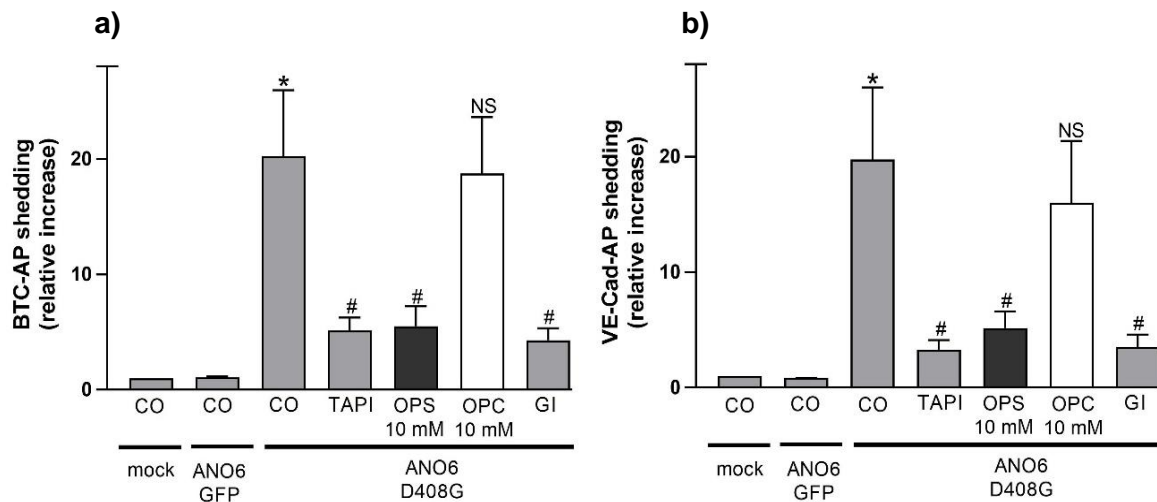


Figure 21. TMEM16F/ANO6 D408G overexpression drives ADAM10-mediated substrate shedding.

COS7 cells were transfected with GFP, TMEM16F/ANO6GFP and human TMEM16F/ANO6 D408G and either BTC-AP or VE-Cad-AP. Transfected cells were incubated with TAPI-1 (TAPI, 10 μ M), GI254023X (GI, 3 μ M), OPS (10 mM) or OPC (10 mM) and shedding of **a)** BTC-AP or **b)** VE-Cad-AP was analysed for the respective treatments after 30 minutes of incubation. Differences among treatments were assessed with an ANOVA (n=3 for each treatment) and multi comparisons were carried out with the Bonferroni post-hoc test. Significant increase is indicated by a * ($p < 0.05$) compared to TMEM16F/ANO6GFP, and a significant decrease is indicated by a # ($p < 0.05$) compared to human TMEM16F/ANO6 D408G.

4.8 Loss of function of TMEM16F/ANO6 PS scrambling impairs ADAM10 shedding activity

Blood cells in patients with the Scott syndrome show an impaired ability to scramble PS (Toti et al., 1996) due to a mutation in TMEM16F/ANO6, which causes loss of function in its ability to scramble PS (Lhermusier et al., 2011). An interesting question in this context is whether the impaired PS scrambling ability of TMEM16F/ANO6 in B-cells, from a Scott patient, would have a direct impact on ADAM10 shedding activity. To that end, B-cells from a Scott syndrome patient (Scott UK B-cells) were compared to control B-cells in their ability to externalise PS and the capacity of ADAM10 to shed CD23. Lactadherine-FITC and CD23-APC antibody staining were used as read-out system to analyse PS externalisation and ADAM10-mediated release of CD23. Flow cytometry analyses showed comparable high surface levels of CD23 and low levels of PS in both control B-cells and Scott UK B-cells (Fig. 22a, upper panel). Both samples were then stimulated with BzATP (0.5 mM) for 30 minutes and afterwards, as with the previous experimental setup, stained to compare PS externalisation and CD23 expression. As expected, the stimulated control B-cells showed an enhanced lactadherin-FITC signal, indicating that PS was externalised upon stimulation (Fig. 22a, upper panel). Moreover, these lactadherin-FITC positive cells showed a reduced CD23-APC signal upon stimulation with BzATP, suggesting that the protein was released from the cell surface (Fig. 22a, upper panel). Incubation of control B-cells with GI254023X (GI), before the stimulation, stabilised the CD23-APC signal on these cells, confirming that the loss of CD23-APC signal was a result of ADAM10-mediated shedding of the substrate (Fig. 22a, upper panel). In comparison to the control B-cells, Scott UK B-cells showed neither an increase of

lactadherin-FITC nor a decrease of CD23-APC signals. Indicating that the stimulation of the cells did not result in PS externalisation or activation of ADAM10-mediated release of CD23 (Fig. 22a, lower panel).

To ensure that this was not caused by an impaired reaction of the Scott UK B-cells to BzATP, the expression of the P2X7 receptor (P2X7R) was further investigated. Impaired expression of the receptor might lead to a weaker response of the Scott UK B-cells to BzATP. Comparison of Scott UK B-cells and control B-cells via Western Blot with an antibody against P2X7R revealed comparable levels of the receptor in both B-cells types (Fig. 23a). Alongside P2X7R expression, ADAM10 expression of Scott UK B-cells and control B-cells was compared since different surface levels of the protease would affect the shedding of CD23. Flow cytometry revealed equal surface levels of ADAM10 on surface cells of both Scott UK B-cells and control B-cells (Fig. 23b). These results confirmed that Scott UK B-cells possessed the phenotypical prerequisites to react to BzATP and to shed CD23.

Nonetheless, to ensure that Scott UK B-cells were general capable to react to an external stimulus, the cells were incubated with an antibody against the Fas receptor (0.5 µg/ml) for 6 hours and stained with lactadherin-FITC and CD23-AP. Incubation with the Fas receptor antibody led to caspase-dependent induction of apoptosis. After 6 hours, untreated control Scott UK B-cells showed neither enhanced lactadherin-FITC levels nor a decreased CD23-APC signal, indicating that the incubation itself did not result in PS exposure or CD23 shedding (Fig. 22b). However, incubation of Scott UK B-cells with the Fas receptor antibody led to an enhanced lactadherin-FITC signal and a reduced CD23-APC signal, confirming that the Scott UK cells exposed PS and released CD23 upon the induction of apoptosis (Fig. 22b). Co-incubation of the Scott UK B-cells with GI254023X (GI) and the Fas receptor antibody led to an enhanced lactadherin-FITC signal but did not affect the CD23-APC signal, confirming that ADAM10 is also responsible for the shedding of CD23 under apoptosis (Fig. 22b). The results for the Scott UK cells showed that on the one hand, impaired TMEM16F/ANO6 scrambling function affects ADAM10-mediated shedding of CD23 under BzATP stimulation; while on the other hand, TMEM16F/ANO6 independent apoptosis-related PS externalization activates ADAM10-mediated shedding of CD23.

These results provide substantial evidence that ADAM10 shedding activity is tightly controlled by PS. These results provide substantial evidence that ADAM10 shedding activity is tightly controlled by PS. independent apoptosis-related PS externalization activates ADAM10-mediated shedding of CD23. These results provide substantial evidence that ADAM10 shedding activity is tightly controlled by PS.

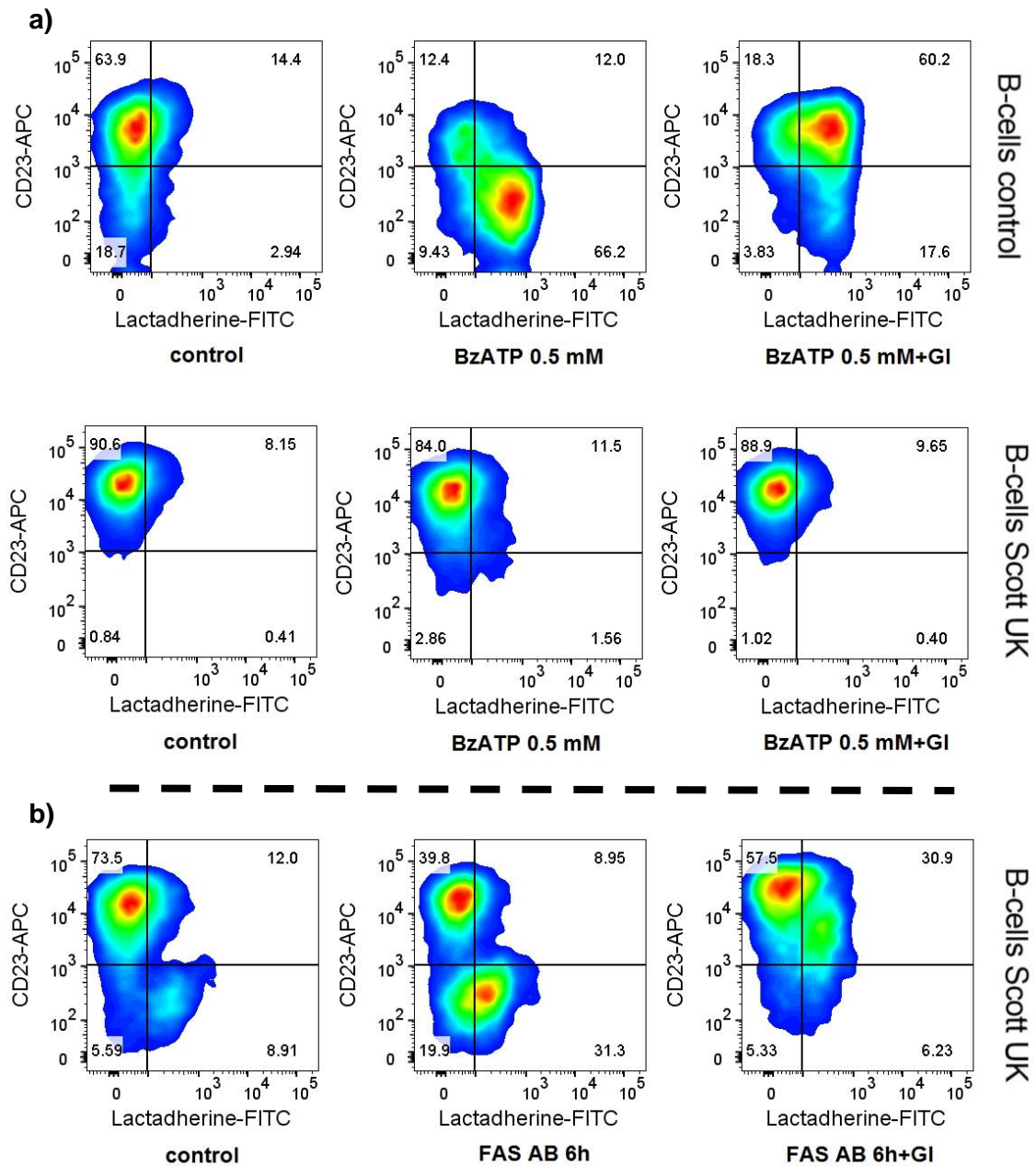


Figure 22. Loss of function of TMEM16F/ANO6 abolishes ADAM10-mediated shedding of CD23.

a) Control B-cells and Scott UK B-cells were incubated with BzATP (0.5mM) for 30 minutes, and cells were stained with lactadherin-FITC and CD23-APC and analyzed via flow cytometry. Additionally, both cell types were incubated with GI254023X (GI, 3 μ M) before the stimulation with BzATP. **b)** Scott UK B-cells were incubated with the FAS-receptor antibody (0.5 μ g/ml) and stained with lactadherin-FITC and CD23-APC and analyzed via flow cytometry. ADAM10 mediated shedding of CD23 under FAS receptor antibody treatment was analyzed by incubation of the Scott UK B-cells with ADAM10 inhibitor GI254023X. Displayed are one exemplary picture per treatment (n=3).

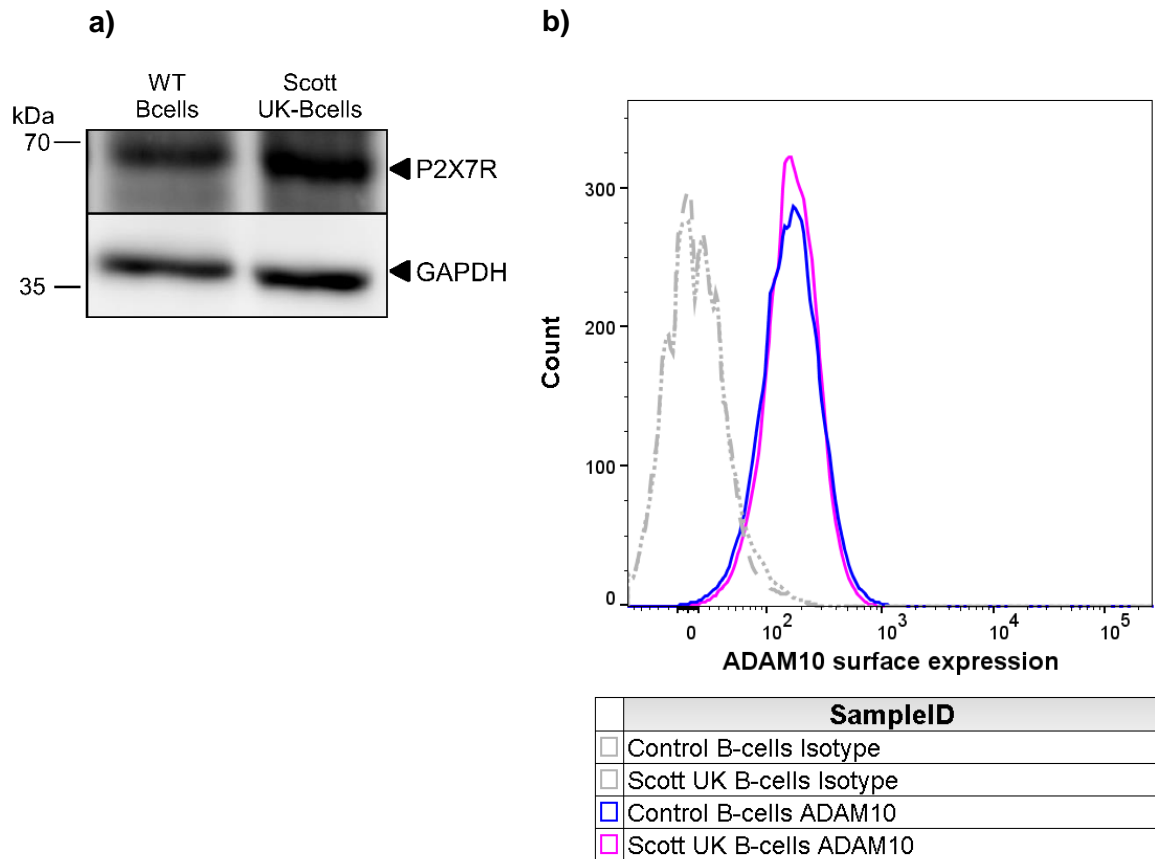


Figure 23. Impaired shedding of CD23 from Scott B-cells is unrelated to ADAM10 or P2X7R expression.
a) Control B-cells and Scott UK B-cells were compared for P2X7R expression via Western Blot analysis. GAPDH was stained as a loading control (n=1). **b)** Flow cytometry analysis of ADAM10 expression on control B-cells and Scott UK B-cells. Control B-cells and Scott UK B-cells were stained with either Isotype control (dashed grey lines) or ADAM10 antibody coupled to IgG Alexa 488 (blue, control B-cells, magenta, Scott UK B-cells), to compare ADAM10 expression. One representative picture for flow cytometry analysis of ADAM10 is shown (n=2).

4.9 ADAM10 stalk domain interacts with PS, based on sequence and structural data analyses

The interaction of ADAM17 with PS has been demonstrated, and a respective cationic motif within its membrane-proximal domain (MPD) enabling this interaction has been described (Sommer et al., 2016). In order to identify common structural highlights and sequence similarities between ADAM10 and ADAM17, the amino acid sequence of ADAM17 MPD and CANDIS domain was compared to the respective amino acid sequence of ADAM10 (Cysteine-rich domain and stalk domain). Indeed, the sequence alignment between the amino acid sequence of ADAM17 and ADAM10 revealed various clusters of amino acids shared by both proteases (Fig. 24a). However, only ADAM17 contains a cationic triplet motif within its MPD (Fig. 24a). A similar motif in ADAM10 cysteine-rich domain could not be identified (Fig. 24a). Interestingly, a motif like the one described for ADAM17 was identified in the stalk domain of ADAM10 (Fig. 24a). This motif comprises three cationic amino acids (R656, K658, and K659). To assess to which extent the cationic motif in the ADAM10 stalk domain might be essential for the interaction with PS, the capacity of the ADAM10 PDB structure (PDB: 6BE6, contains all extracellular domains of ADAM10) to interact with PS was analyzed. Although the ADAM10 PDB structure contains all extracellular domains of ADAM10, it lacks the relevant cationic amino acids identified in the sequence alignment (Fig. 24a). The missing amino acids were added to the ADAM10 PDB structure with the Chimera program, based on their predicted secondary structure. The modified ADAM10 PDB structure and the ADAM17 PDB (PDB: 2M2F) of the MPD as control were then docked with OPS, and not with PS, to avoid interference of the phospholipid backbone for the docking prediction. As expected, the docking of the ADAM17 MPD structure to OPS confirmed the cationic triplet motif as the motif with the highest affinity to OPS (Fig. 24b). The docking of OPS to the modified ADAM10 PDB structure showed that the added cationic triplet motif in the stalk domain is the docking side with the highest affinity to OPS (Fig. 24b). These results suggest that the cationic triplet motif in the ADAM10 stalk domain might be of similar importance for the interaction with PS as the cationic triplet motif in ADAM17 MPD.

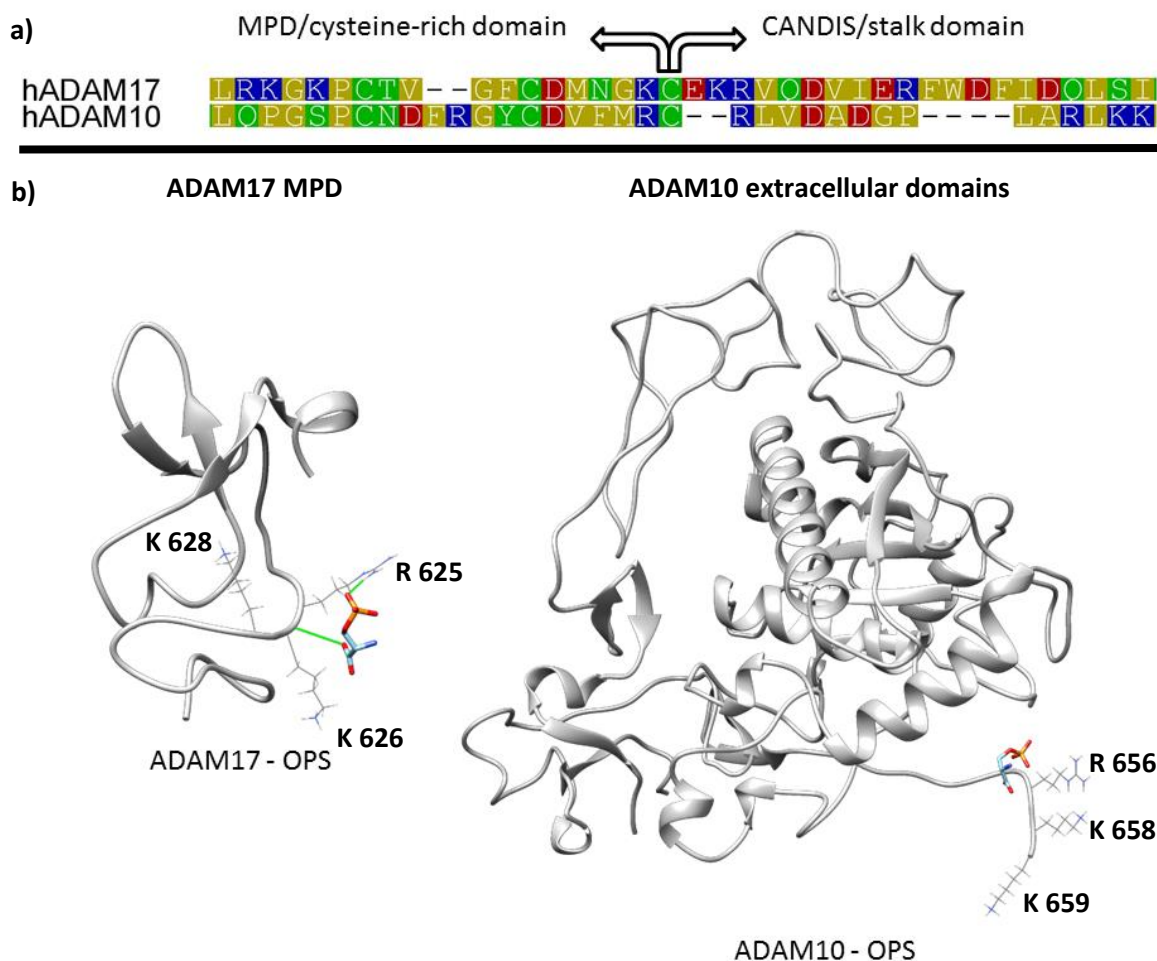


Figure 24. ADAM10 stalk domain is predestined for the interaction with PS.

a) A sequence alignment between the amino acid sequence of human ADAM17 (hADAM17) MPD and CANDIS domain and human ADAM10 (hADAM10) cysteine-rich domain and stalk domain highlights the ADAM17 cationic triplet motif (R625, K626, K628) in the protease MPD. ADAM10 contains a similar motif (R656, K658, K659) in its stalk domain. **b)** Ribbon structure of human ADAM17 (left, grey, PDB: 2M2F) and the ribbon structure of human ADAM10 (right, grey, PDB: 6BE6) were paired with OPS (coloured structure). ADAM17 cationic triplet motif (highlighted side chains) was predicted as the primary site for the docking with OPS. The respective cationic triplet motif in ADAM10 was added to the 6BE6 file with the Chimera program. ADAM10 cationic triplet motif (highlighted side chains) was predicted as the primary site for the docking with OPS. Colours in a indicate the different amino acids polarity (blue: positively charged side chains, red: negatively charged side chains, green: polar uncharged side chains, yellow: non-polar side chains).

4.10 ADAM10 stalk domain intercalates into PS liposomes via a biphasic mechanism of interaction

The results from OPS docking experiments suggested that the ADAM10 stalk domain might be essential for the protease interaction with PS. Since cationic motifs are predestined for electrostatic interactions, it was suggested that the stalk domain of ADAM10 interacts with PS via electrostatic interaction, as in ADAM17. To analyse the binding affinity of the ADAM10 stalk domain to PS, a peptide version of this domain was produced (amino acid sequence: CRLVDADGPLARLKKAI FSGSGSGK-OH) to be

analysed with a liposomal model. The respective experiments were carried out by Christian Nehls and Wilmar-Alexander Correa-Vargas from the AG Gutschmann (Research Center Borstel). Protein-PS interaction is facilitated in multiple ways. Two prominent ways are the direct interaction with negatively charged PS via multi cationic motifs or through calcium bridges that connect anionic amino acids to the negatively charged PS. Since the stalk domain of ADAM10 contains clusters of both groups of amino acids, it was first tested whether calcium might enhance the interaction of the ADAM10 stalk domain with PS. To analyse the binding capacity of the ADAM10 stalk peptide to PS-liposomes (PS:PC-9:1), with or without calcium, research colleagues in Borstel performed isothermal calorimetry analysis to determine the energy release as a direct indicator for the binding of ADAM10 stalk domain peptide. The ADAM10 stalk peptide was titrated to the different buffered PS-liposomes and the energy released from the interaction was recorded over time. The presence of calcium impeded the interaction between ADAM10 and the PS-liposomes, as no energy release was detected over time (Fig. 25a, black titration curve). In the absence of calcium, however, the ADAM10 stalk domain peptide bound to the PS-liposomes at a moderate level (K_d : 1,26 μ M, Fig. 25a, green titration curve). These results suggest that calcium has a somewhat inhibitory effect on the interaction of the ADAM10 stalk domain with PS and that ADAM10 binds directly to PS through its cationic amino acids rather than its anionic amino acids. Moreover, the released energy slowly decreased over time, indicating that the fixed concentration of PS-liposomes in the solution, reached saturation with increasing concentration of the ADAM10 stalk peptide.

To further analyse the specificity between the ADAM10 stalk domain peptide and PS, the peptide was also titrated onto PC-liposomes (Fig. 25b). The titration of the ADAM10 stalk peptide to PC-liposomes led to no measurable energy release over time, indicating a specific interaction of the ADAM10 stalk domain peptide to PS (Fig. 25b). For a further analysis of the binding characteristics, the ADAM10 stalk peptide was titrated onto a fix arrested PS-liposome layer (PS:PC-9:1), PC-liposome layer or buffer control. The surface acoustic wave (SAW) experiments indicated that the ADAM10 stalk peptide first: interacted with the PS-liposomes and second: intercalated into the PS-liposome layer with increasing concentration of the peptide (Fig. 25c). Similar experiments with the ADAM10 stalk peptide titrated onto a PC-liposome layer and buffer control showed no interaction, irrespective of increasing concentration of the peptide (Fig. 25c). These results made clear that ADAM10 peptide interacted explicitly with PS in a biphasic manner. The intercalation of the peptide into the PS-liposome layer was further analysed with a FRET-based assay. PS liposomes were modified with either NBD-PE as donor or Rhodamine-DHPE as an acceptor molecule, and the peptide was then titrated onto these differently labelled PS-liposomes (PS:PC-9:1). Positive intercalation of the ADAM10 stalk peptide into either PS or PC liposomes should, therefore, lead to a separation of donor and acceptor, thus resulting in a reduced electron transfer between them. Spatial distance between donor and acceptor increased, with accumulating concentration of ADAM10 stalk peptide in the solution (Fig. 25d). Incubation of the ADAM10 stalk peptide to PC-liposomes showed now increase in the spatial distance between donor and

acceptor, indicating that the peptide exclusively intercalates into PS membranes (Fig. 25d). The interaction and intercalation experiments confirmed the specificity of the interaction between the ADAM10 stalk peptide and PS liposomes, supporting the assumption that the proteases stalk domain is a viable part of the PS interaction mechanism of ADAM10.

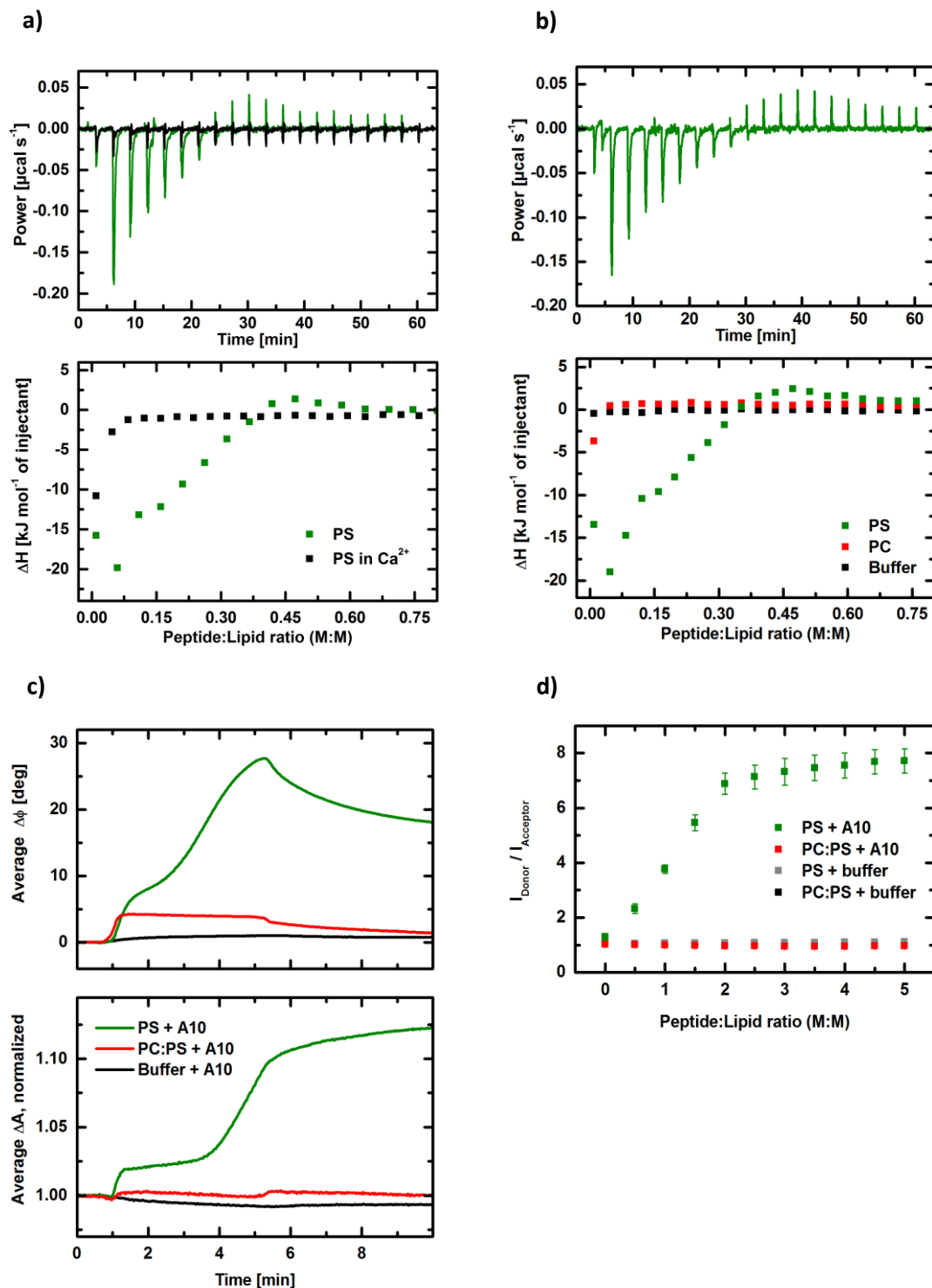


Figure 25. ADAM10 stalk domain interacts with PS.

a) Isothermal titration calorimetry (ITC) measurements of ADAM10 stalk peptide with PS-liposomes (PS: 9 PC: 1) with calcium (black) or without calcium (green). **b)** Isothermal titration calorimetry (ITC) measurements of ADAM10 stalk peptide with PS-liposomes (PS: 9 PC: 1, green), PC-liposomes (red) and buffer control (black). The heating power corresponds to the interaction of the ADAM10 peptide with PS liposomes in 20 titration steps

and is plotted as a function of time (a and b, upper panel) and the interaction enthalpy for both lipid systems in relation to peptide:lipid ratio (a and b, lower panel). **c**) SAW measurements showed the interaction of the ADAM10 stalk domain peptide with PS membranes (green) or PC:PS (9:1) membranes (red) immobilised on the CM-dextran/poly-L-lysine (PLL) functionalization of the sensor chip surface. The binding of the peptide to the functionalization (black) was used as a control. The increased of the phase signal $\Delta\Phi$ indicated an additional mass loading on the chip surface which was more pronounced for PS than for PC:PS (b, upper panel); the increase of the amplitude signal ΔA corresponds to an increased viscosity on the surface (b, lower panel). Shown are average curves of five individual sensor channels. **d**) FRET spectroscopy. Intercalation of the ADAM10 peptide into PS liposomes (green) and PC:PS (9:1) liposomes (red). The liposomes were double labelled with NBD-PE (donor) and Rhodamine-DHPE (receptor). An increased ratio between donor and receptor fluorescence intensities indicates insertion of peptides between the lipid molecules. This effect is only visible for PS liposomes but not for PC:PS liposomes, controls (grey and black) showed no effect. Error bars indicate the standard deviations of three independent measurements.

4.11 ADAM10 enhanced shedding activity depends on a positively charged stalk domain

The ADAM10 stalk peptide contained several positively charged amino acids representing a multi cationic motif and showed an overall positive net charge, indicating that the interaction between ADAM10 and PS might be regulated through electrostatic interaction. Raising the question whether the multi cationic motif or the positively charged amino acids in the stalk domain of ADAM10 are essential for the interaction with PS and the protease ability to shed its substrates. Several ADAM10 mutants (Fig. 26a) were generated, containing an increasing number of mutations of one amino acid (R647N), the cationic triplet motif (R656N, K658N, K659N) or a combination of both (R647K, R656.K, K658N, K659N). The ADAM10 mutants (Stalk 1 -3), inactive mADAM10 E/A and mADAM10wt were transfected with BTC-AP into ADAM10/ADAM17-deficient HEK293-T cells to evaluate the shedding ability of each mutant in comparison to mADAM10wt under constitutive and IO (1 μ M), or Mel (0.5 μ M) enhanced shedding. The constitutive and IO or Mel stimulated shedding of BTC-AP for each ADAM10 was then analysed after 30 minutes. The shedding of BTC-AP was significantly enhanced in the IO and Mel stimulated mADAM10wt sample compared to respectively treated inactive ADAM10 E/A (Fig. 26b), confirming that both stimuli led to an enhanced shedding activity of mADAM10wt. The comparison of the shedding activity between mADAM10wt and mADAM10 Stalk1, both stimulated with IO and Mel, revealed a significant reduction in the ability of ADAM10 Stalk1 to release BTC-AP (Fig. 26b). This result showed that the exchange of a single positively charged amino acid in the stalk domain of ADAM10 affected the proteases shedding activity. Further analysis of the shedding ability of the remaining two ADAM10 mutants under IO or Mel stimulation showed that an increase in the number of mutations and a corresponding decrease of the net charge of the stalk domain led to a continuous reduction of BTC-AP shedding (Fig 26b). Interestingly, the constitutive shedding activity of the different ADAM10 mutants showed an enhanced activity with each amino acid exchange (Fig. 26b). The release of BTC-AP increased with each mutation when compared to the constitutive activity of mADAM10wt (Fig. 26b).

a)

		ADAM10 stalk domain			
		646	655	665	
mADAM10wt	C-domain*	C	R	L	TMD [§]
mADAM10 Stalk 1		C	N	L	
mADAM10 Stalk 2		C	R	L	
mADAM10 Stalk 3		C	N	L	

* C-domain=cysteine-rich domain, § TMD=transmembrane domain

b)

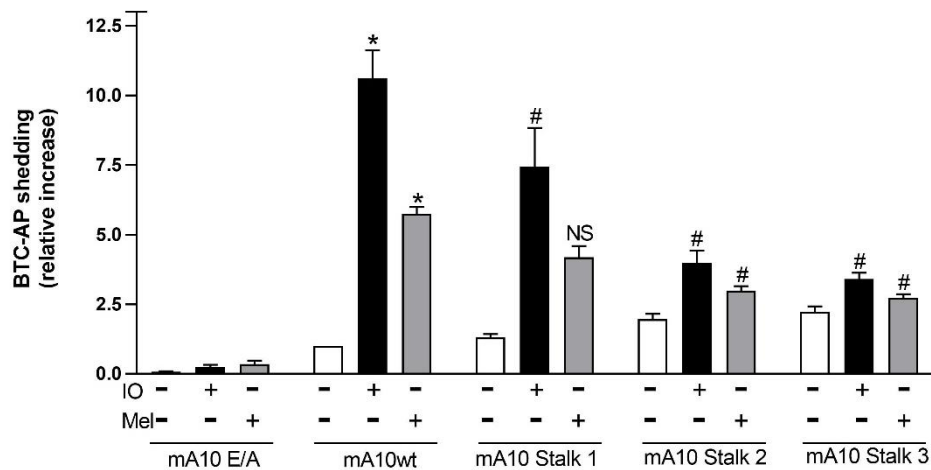


Figure 26. ADAM10 shedding activity requires a positively charged stalk domain.

a) Overview of the different mADAM10 stalk mutants (mADAM Stalk 1 -3) and the respective mutated amino acids compared to mADAM10wt. b) ADAM10/ADAM17-deficient HEK-293T cells were transfected with either mock control vector, inactive mADAM10 E/A, mADAM10wt, mADAM10 Stalk 1, mADAM10 Stalk 2 or mADAM10 Stalk 3 and BTC-AP. Constitutive, IO (1 μ M) or Mel (0.5 μ M) stimulated BTC-AP shedding was measured after 30 minutes. Values from mock-transfected control samples were subtracted from all other sample values. Differences among treatments were assessed with an ANOVA (n=3 for each treatment) and multi comparisons were carried out with the Bonferroni post-hoc test. Significant increase is indicated by a * (p<0.05) compared to respective stimulated inactive mADAM10 E/A and a significant decrease is indicated by a # (p<0.05) compared to respective stimulated mADAM10wt. NS=non-significant.

Since the mADAM10 Stalk 2 mutant showed a significant reduction in the release of BTC-AP from IO or Mel stimulated retransfected ADAM10/ADAM17-deficient HEK-293T cells, only the expression of this mutant was further analysed. The analysis of the expression of mADAM10wt and the mADAM10 Stalk 2 mutant via Western Blot, with an ADAM10 antibody which recognises the pro and mature form of the protease, showed an unequal expression of the pro and mature forms for the wild-type ADAM10 in comparison to the ADAM10 Stalk 2 mutant. The mADAM10 Stalk 2 mutant showed enhanced levels of the mature form of the protease in comparison to mADAM10wt (Fig. 27a). Since the mature form of ADAM10 is mainly localised at the cell surface, it was further assessed whether the increase of mature

mADAM10 Stalk 2 would lead to respective enhanced surface levels of this ADAM10 mutant. The flow cytometry analysis of the mADAM10wt and the mADAM10 Stalk 2 mutant with an N-terminal antibody against the extracellular domain of ADAM10 showed enhancement in the surface levels for the mADAM10 Stalk 2 mutant in comparison to the mADAM10wt. This result indicates that the mutation of the amino acids representing the cationic triplet motif to asparagine (N) resulted in increased surface expression of ADAM10 (Fig. 27b). However, these enhanced surface levels of the mADAM10 Stalk 2 mutant showed no positive effect on substrate shedding because IO or MeI stimulation was not able to enhance the ability of mADAM10 Stalk 2 to release BTC-AP. These results confirm that although the mutation of the stalk domains cationic triplet motif leads to higher surface levels of ADAM10, the cationic triplet motif is also involved in ADAM10 enhanced shedding activity, as the mutations also lead to an impaired ADAM10-mediated shedding of BTC-AP.

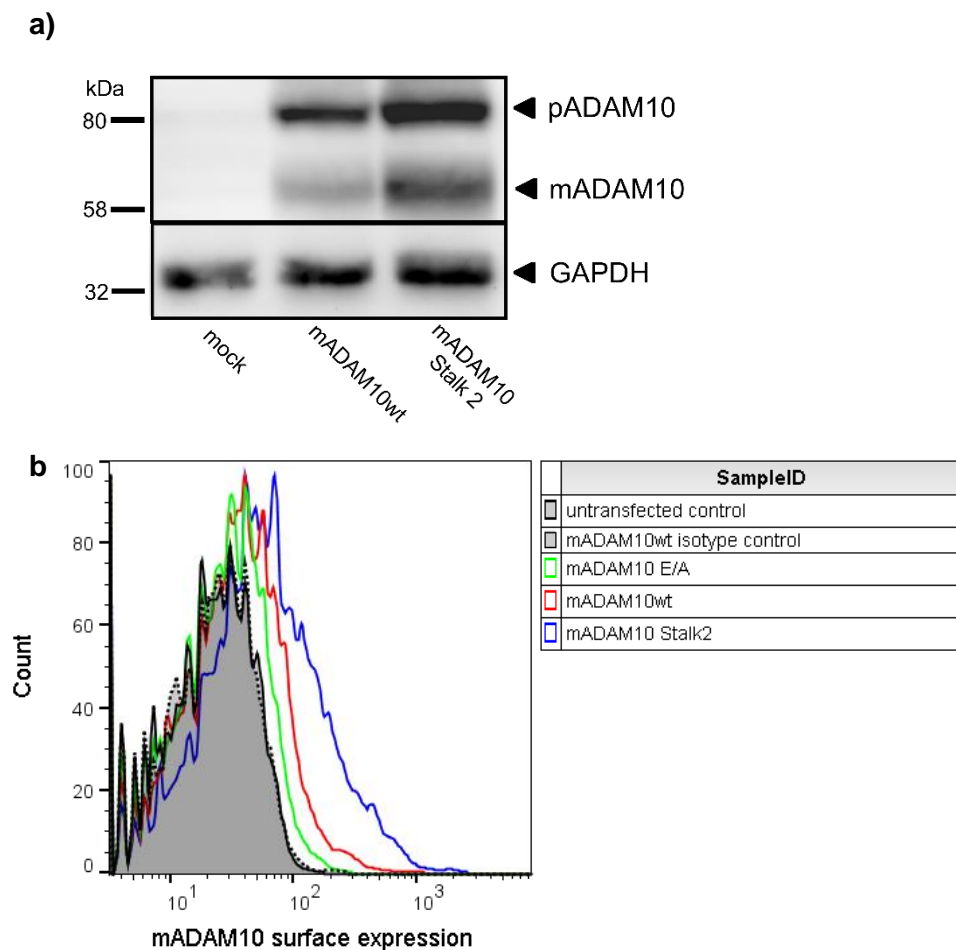


Figure 27. The mADAM10 Stalk 2 mutant is expressed and transported to the cell surface.

a) Western Blot analysis of the pro and mature form of ADAM10 with an antibody recognising both forms. ADAM10/ADAM17 deficient HEK-293T were transfected with mock control vector, mADAM10wt or mADAM10 Stalk2. **b)** Surface expression of ADAM10 was analysed with flow cytometry analysis. ADAM10/ADAM17-deficient HEK-293T cells were transfected with either mADAM10 E/A, mADAM10wt or mADAM10 Stalk 2. Transfected ADAM10/ADAM17-deficient HEK-293T cells were either stained with an antibody that recognised the extracellular site of ADAM10 or respective isotype control antibody and coupled with a secondary IgG Alexa 488 labelled antibody. Displayed pictures in a and b represent one exemplary result (n=3).

4.12 ADAM10 enhanced *bona fide* enzymatic activity depends on a positively charged stalk domain

Based on the results from the AP shedding assays for the different ADAM10 stalk mutants, the following question came up: would the mutation of the stalk domain affect the ADAM10 *bona fide* enzymatic activity? To assess the importance of the stalk domain for ADAM10 *bona fide* enzymatic activity, ADAM10/ADAM17-deficient HEK-293T cells were transfected with either mock control vector, inactive mADAM10 E/A, mADAM10wt or mADAM10 Stalk 2 and incubated with the previously introduced soluble ADAM10 fluorescent peptide substrate (Chapter 4.4). The cells were incubated with the soluble fluorescent peptide substrate, and the fluorescent signal in the supernatant was measured after 30 minutes. As expected, inactive mADAM10 E/A showed a reduced ability to cleave the soluble fluorescent peptide substrate (Fig. 28a). When compared to the fluorescent signal of the inactive mADAM10 E/A, mADAM10wt showed an enhanced ability to cleave the soluble fluorescent peptide substrate, as indicated by the significant increase of the fluorescent signal from mADAM10wt transfected cells (Fig. 28a). Interestingly, the *bona fide* enzymatic activity of the mADAM10 Stalk 2 mutant was comparable to that of mADAM10wt, as both led to a significant increase in fluorescent signal compared to inactive mADAM10 E/A (Fig. 28a). These results indicate that there is no difference in the *bona fide* enzymatic activity among mADAM10wt or the mADAM10 Stalk 2 mutant. To further confirm that the enhanced activity was indeed due to ADAM10 cleavage of the peptide substrate, each transfected ADAM10 was also additionally incubated with GI254023X (GI, 3 μ M). The preincubation with GI254023X (GI) led to a significant reduction of the fluorescent signal in all samples besides the one from inactive mADAM10 E/A (Fig. 28a). These results confirmed that cleavage of the soluble fluorescent peptide substrate in mADAM10wt and mADAM10 Stalk 2 mutant transfected samples was indeed a result of ADAM10 *bona fide* enzymatic activity.

Although the enzymatic activity seemed to be comparable between the mADAM10wt and the mADAM10 Stalk 2 mutant, whether their *bona fide* enzymatic activity is altered under enhanced PS exposure was not yet resolved. As shown before (Chapter 4.7), the hyperactive human TMEM16F/ANO6 D408G mutant led to an increase of PS on the outer plasma membrane in the absence of any stimuli. Therefore, overexpression of the human TMEM16F/ANO6 D408G hyperactive mutant could provide further insights on the *bona fide* enzymatic activity of ADAM10 under enhanced PS exposure. Consequently, ADAM10 and ADAM17-deficient HEK-293T cells were transfected with either inactive mADAM10 E/A mutant, mADAM10wt or mADAM10 Stalk2 mutant and either empty control vector or the human TMEM16F/ANO6 D408G hyperactive mutant. The transfected cells were then incubated for 30 minutes with the soluble ADAM10 fluorescent peptide substrate with or without GI254023X (GI). The supernatants from each sample were analyzed with a fluorescent plate reader for detecting cleaved soluble ADAM10 fluorescent peptide substrate.

Indeed, the fluorescent signal from the cells transfected with inactive mADAM10 E/A mutant, mADAM10wt or mADAM10 Stalk2 together with hyperactive human TMEM16F/ANO6 D408G showed an increased fluorescent signal when compared to the respective incubated control cells (Fig. 28b). Interestingly, the fluorescent signal in the supernatant from cells transfected with the inactive mADAM10 E/A mutant together with human TMEM16F/ANO6 D408G also showed an increased fluorescent signal compared to respective controls. The increase of the fluorescent signal, however, was significantly lower than the increase in the supernatant from cells transfected with mADAM10wt together with human TMEM16F/ANO6 D408G (Fig. 28b). Showing that with active ADAM10 more soluble fluorescent peptide substrate was cleaved. A similar but again weaker increase of fluorescent signal was also detected in the supernatants from cells transfected with mADAM10 Stalk2 together with TMEM16F/ANO6D408G. Nevertheless, the fluorescent signal in the supernatant from these cells was significantly lower compared to the fluorescent signal in the supernatant from mADAM10wt together with human TMEM16F/ANO6 D408G (Fig. 28b). To precisely determine the increase due to ADAM10 activity, each control and human TMEM16F/ANO6 D408G with the receptive ADAM10 transfected cells were incubated with specific ADAM10 inhibitor GI254023X (GI). The incubation with GI254023X (GI) led to a significant reduction of the fluorescent signal in the supernatant from cells transfected with mADAM10wt and human TMEM16F/ANO6 D408G (Fig. 28b). Noticeably, GI254023X (GI) had no reducing effect on the fluorescent signal in the supernatants from mADAM10 E/A and only mild effects on mADAM10 Stalk2 together with human TMEM16F/ANO6 D408G. These results suggest that mADAM10 Stalk 2 enzymatic activity could not be further enhanced when compared to the ADAM10 E/A background level. It is therefore plausible to claim that the ADAM10 Stalk2 mutant, which showed a decreased ability to shed BTC-AP under IO (1 μ M) or Mel (0.5 μ M) stimulation, is also reduced in its *bona fide* enzymatic activity. Taken together, TMEM16F/ANO6 D408G seems to upregulate ADAM10 shedding and *bona fide* enzymatic activity. Although these results suggest that both processes are regulated through PS exposure, it was found that 2/3 of the fluorescent signal in the TMEM16F/ANO6 D408G transfected cells was unrelated to ADAM10 *bona fide* enzymatic activity. This ADAM10-independent increase in the fluorescent signal might, therefore, hint that other, yet unknown proteases, could cleave the fluorescent peptide substrate and also be regulated by PS exposure.

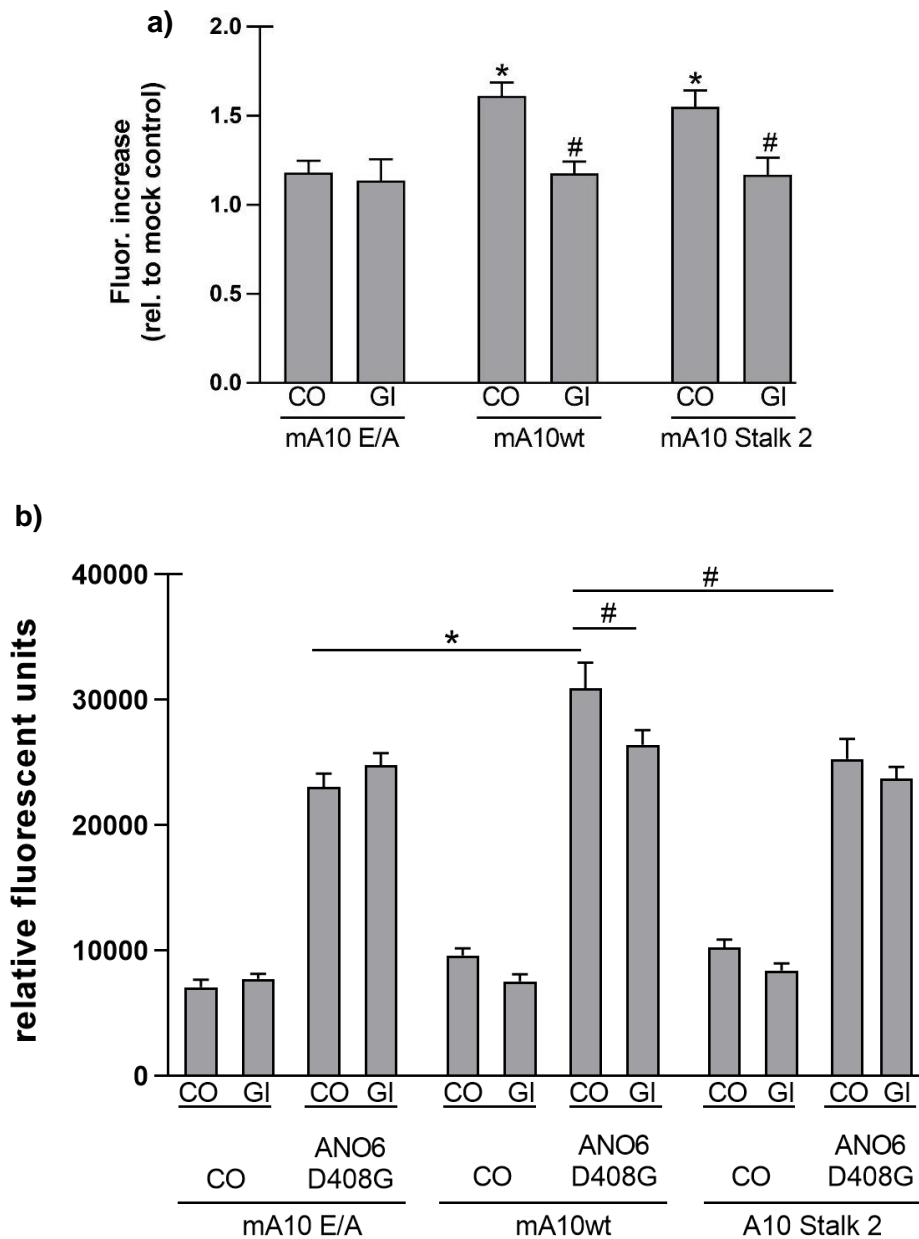


Figure 28. ADAM10 enzymatic activity alters under enhanced PS exposure.

a) ADAM10/ADAM17-deficient HEK-293T cells were transfected with either mock control vector, inactive mADAM10 E/A, mADAM10wt or mADAM10 Stalk 2 and preincubated with or without GI254023X (GI, 3 μ M) for 15 minutes. Transfected cells were incubated with a soluble ADAM10 fluorescent peptide substrate (15 μ M) for 30 minutes, and the fluorescent signal in the supernatant was measured with the fluorescent plate reader FLx800 (BioTek). **b)** ADAM10/ADAM17 deficient HEK-293T were transfected with inactive mADAM10 E/A, mADAM10wt or mADAM10 Stalk2 together with either mock control vector or TMEM16F/ANO6 D408G and preincubated with or without GI254023X (3 μ M) for 15 minutes. Transfected cells were incubated with a soluble ADAM10 fluorescent peptide substrate (15 μ M) for 30 minutes, and the fluorescent signal in the supernatant was measured with the fluorescent plate reader Infinite® 200 PRO (Tecan). Differences among treatments were assessed with an ANOVA (n=3 for each treatment) and multi comparisons were carried out with the Bonferroni post-hoc test. Significant increase is indicated by a * ($p < 0.05$) compared either to inactive mADAM10 E/A (a) or human TMEM16F/ANO6 D408G with inactive mADAM10 E/A (b) and a significant decrease is indicated by a # ($p < 0.05$) compared to mADAM10wt or the respective mADAM10 stalk mutants (a) or to mADAM10wt together with human TMEM16F/ANO6 D408G (b).

5. Discussion

The prominent significance of ADAM10 shedding activity, in a physiological and pathophysiological context, has been highlighted numerous times (Crawford et al., 2009, Marezky et al., 2009, Duffy et al., 2011, Saftig and Reiss, 2011, Saftig and Lichtenthaler, 2015). For instance, the deletion of ADAM10 leads to impaired Notch processing in mice, directly affecting prenatal development and viability (Hartmann et al., 2002). In contrast, overexpression of ADAM10 is presumed to enhance APP alpha cleavage, which supposedly stimulates the expression of various neuroprotective proteins (Stein et al., 2004). On the other hand, overexpression of ADAM10 has also been described as a hallmark of several cancer types, suggesting an ambivalent nature of ADAM10 (Crawford et al., 2009, Wentz, 2010, Guo et al., 2012). Although a vast majority of studies have described ADAM10-mediated substrate release, little is known about the mechanisms regulating the protease shedding activity. Recently, it has been established that plasma membrane phospholipid phosphatidylserine (PS) regulates ADAM17 shedding activity (Sommer et al., 2016), which raises the question whether PS exposure is of equal importance for ADAM10. This thesis aimed to find out whether PS also regulates ADAM10-mediated substrate release. Several lines of evidence showed that enhanced PS exposure drives ADAM10-mediated substrate shedding. Phospholipid scrambling proteins (e.g., TMEM16F/ANO6) contribute via enhanced PS exposure to ADAM10-mediated substrate release. Moreover, a gain or loss of TMEM16F/ANO6-mediated substrate shedding is accompanied by a direct increase or absence of ADAM10 shedding activity. Furthermore, the ADAM10 stalk domain directly interacted with PS via electrostatic interactions and the mutation of the positively charged amino acids in the ADAM10 stalk domain led to reduced substrate shedding.

5.1 PS exposure regulates ADAM10 shedding activity

Under physiological conditions, the phospholipids composing the plasma membrane are asymmetrically organized, with PS and PE located mainly at the inner membrane leaflet and PC and SM mainly at the extracellular leaflet. Abrogation of this asymmetry and PS externalization is well known as a characteristic of apoptosis and as a molecular signal for phagocytes to engulf apoptotic cells (Segawa and Nagata, 2015). Besides its comprehensively described role in apoptosis, PS exposure is also known as an essential signal in various other processes (e.g., fertilisation, bone mineralisation and synaptic pruning). These processes indicate that PS exposure is also an important signal under non-apoptotic conditions. Recently, PS exposure was shown to be an important regulatory signal for ADAM17-mediated substrate release (Sommer et al., 2016). Within this context, it was pertinent to assess whether the breakdown of plasma membrane asymmetry and PS exposure are also relevant for ADAM10-mediated substrate release.

It is known that PS exposure is induced by ionomycin (IO) and melittin (Mel), both activators of ADAM10 (Sommer et al., 2016). Also, the stimulation with IO has been shown to induce cell shrinkage,

as well as, the breakdown of plasma membrane asymmetry and PS exposure in human erythrocytes and keratinocytes (Lang et al., 2003, Sommer et al., 2016); suggesting that IO is able to induce PS exposure irrespective of the cell type. It seems reasonable to assume that calcium influx enhances PS exposure under non-apoptotic conditions (Elliott et al., 2005). Therefore, treatment with ionomycin or melittin, which induces calcium influx (Morgan and Jacob, 1994, Sommer et al., 2012), should lead to PS exposure.

Annexin-V labelling was performed on IO or Mel-stimulated cells and confirmed that both activators enhanced PS externalisation. The direct comparison of the Annexin-V signals for either of these two activators suggested that IO led to a consistent increase and constant PS exposure. Mel-induced Annexin-V signals seemed to decrease over time, suggesting that the stimulation with Mel led to a transient exposure of PS. These results are in line with previous observations showing that IO leads to a constant but irreversible PS exposure while stimulation with Mel leads to transient peaks of PS (Sommer et al., 2016). Although the Annexin-V signals obtained in this thesis confirmed PS exposure as a result of either IO or Mel stimulation, the observed staining pattern differed from that reported by Sommer et al. (2016). They described that IO and Mel-induced PS exposure occurred ubiquitously along the plasma membrane in HaCaT cells (Sommer et al., 2016). However, Annexin-V labelling of COS7 cells incubated with the same stimuli showed a rather punctual than ubiquitous PS signal. These deviations in the obtained PS signals indicate that COS7 cells express other or less scramblases than HaCaT cells. However, a possible difference in the expression of scramblases between COS7 cells and HaCaT cells requires further analysis since the expression of scramblases (e.g., TMEM16F/ANO6) in COS7 cells was not further evaluated. Another explanation for the differences in PS signals may be the different experimental setups used to visualize PS exposure. For example, Sommer et al. (2016) described PS exposure with a live cell image approach using pSIVA (Kim et al., 2010) to label PS under IO and Mel stimulation. Alternative labelling techniques to Annexin-V to visualise PS exposure may allow further validation of the PS pattern observed in this thesis. For instance, lactadherin visualises PS exposure by binding calcium-independent to PS (Dasgupta et al., 2006). Thus, to evaluate whether the differences between PS patterns, under both ADAM10 activators, are indeed a result of the labelling method, lactadherin and pSIVA could be used, in addition to Annexin-V.

As shown in this thesis, stimulation with IO and Mel led to PS exposure and enhanced shedding of endogenous and overexpressed ADAM10 substrates: Epithelial cadherin (E-Cad), betacellulin (BTC), and VE-cadherin (VE-Cad). This thesis, therefore, addressed the question whether IO or Mel induced PS exposure is the actual regulator of ADAM10-mediated substrates release. To address this question OPS was used to inhibit PS interaction with ADAM10 competitively, and therefore show the importance of this interaction for the protease activity.

Spiegel et al. (2004) reported that OPS successfully inhibits Factor VIII C2 domain interaction with PS, suggesting that OPS acts as a competitive inhibitor. The inhibitory effect of OPS is presumably

ubiquitous rather than protein specific and should commonly inhibit the proteins ability to bind to PS. Indeed, incubation with OPS led to competitive inhibition of ADAM10-mediated shedding of endogenous and overexpressed substrates, indicating that the protease shedding activity is under the tight control of PS. Interestingly, it has been noted that the interaction between the Factor VIII C2 domain and PS was abolished upon concentrations of ~10 mM OPS (Spiegel et al., 2004). These results are in line with those presented in this thesis, where a substantial inhibition of ADAM10-mediated substrate release was observed upon 10 mM OPS. Moreover, the headgroup of phosphatidylcholine (OPC) showed no significant inhibitory effect. These results underline the specific inhibitory nature of OPS and at the same time highlights ADAM10 as a PS regulated protein.

Nevertheless, OPS is seldom used to inhibit protein interaction with PS. An alternative to OPS is the PS binding protein lactadherin, which can also inhibit the interaction of proteins with PS depending on the dosage (Zaitseva et al., 2017, Brummer et al., 2018). For example, lactadherin was shown to compete with the factor IXa for PS interaction, indicating that its binding to PS reduces the accessibility of factor IX to bind to PS (Brummer et al., 2018). Moreover, incubation with lactadherin led to a dosage-dependent reduction of HIV-1 viral envelope glycoprotein interaction with PS in vitro (Zaitseva et al., 2017). Although both studies highlight the inhibitory properties of lactadherin on PS interaction, the effect of lactadherin strongly relies on the experimental setup. Using a defined concentration of PS-liposomes Brummer et al. (2018) showed that low concentrations of lactadherin seemed sufficient to inhibit PS interaction. In contrast, in an in vitro setup, lactadherin inhibited PS interaction only at a high concentration (from 4 μ M on, Zaitseva et al., 2017). Both studies suggest a differential capacity of lactadherin to inhibit PS interaction, which depends on the experimental setup. However, lactadherin may be used as an additional tool to support the OPS results and to further confirm that PS exposure regulates ADAM10 shedding activity.

The stimulation with ionomycin or melittin is a standard method to enhance ADAM10 shedding activity. However, ionomycin and melittin are rather artificial in contrast to physiological activators enhancing the protease shedding activity. This thesis introduced a simple rabbit erythrocyte model in combination with pVCC as a readout system, to test whether stimulation of rabbit erythrocytes with BzATP leads to PS exposure, via P2 receptor activation and to show that PS exposure is the main driver of ADAM10-mediated substrate cleavage. Physiological stimuli, such as ATP, are described to expose PS through calcium influx (Di Garbo et al., 2012) and to activate ADAM10-mediated release of CD23 and CXCL16 (Pupovac et al., 2013, Pupovac et al., 2015). The stimulation with ATP or its potent analogue benzoyl ATP (BzATP), however, requires the expression of the respective P2 receptors whose activation facilitates calcium influx, thus triggering PS externalisation (Pupovac and Sluyter, 2016). Sluyter et al. (2007a, 2007b) showed that human and canine erythrocytes express functional P2X7R, implying that P2X7R receptors are ubiquitously expressed by erythrocytes of different species. Moreover, Fries (2013) showed that the stimulation of rabbit erythrocytes with BzATP induces PS exposure through P2

receptor activation. Furthermore, Fries showed that pVCC cleaving drives VCC-related hemolysis of rabbit erythrocytes upon P2 receptor stimulation.

Indeed, the stimulation with BzATP resulted in PS exposure in rabbit erythrocytes and incubation of rabbit erythrocytes with P2 receptor inhibitor PPADS abolished PS exposure, thus indicating an explicit P2 receptor dependence of the PS signal. Based on the results that BzATP led to enhanced PS exposure through P2 receptor activation, this thesis focused on the question whether PS is in the main driver of ADAM10-mediated cleavage of pVCC. In a simple wash experiment, the pVCC incubated rabbit erythrocytes were stimulated with BzATP. To avoid ADAM10-mediated cleavage of pVCC, during the stimulation, the cells were treated in the presence of broad-spectrum metalloproteinase inhibitor marimastat (MM). The respective rabbit erythrocytes became PS-positive, while ADAM10 remained inactive. ADAM10 remained inactive, indeed, within the time of stimulation and no shedding of pVCC and VCC related hemolysis occurred. The removal of the stimuli and the metalloproteinase inhibitor enabled ADAM10-mediated cleavage of pVCC. Consequently, the enhanced PS levels penultimately triggered ADAM10-dependent cleavage of pVCC. As a result of the cleavage of pVCC, an increase of mature VCC was accompanied by enhanced rabbit erythrocytes hemolysis. Thus, indicating that rabbit erythrocytes stimulated with BzATP enabled PS exposure through P2 receptor activation.

Given that most studies described PS exposure on human erythrocytes, rabbit erythrocytes in combination with pVCC may seem as a less favourable methodological combination to analyse ADAM10 shedding activity. However, rabbit erythrocytes, unlike human erythrocytes, express ADAM10 (Reiss et al., 2011). Moreover, the activity of ADAM10 on rabbit erythrocytes in combination with pVCC is an established system to analyse the protease activity (Reiss et al., 2011). The alteration of the composition of rabbit erythrocyte membranes by increasing or depleting the cholesterol content showed a corresponding reduction or enhancement of ADAM10 cleavage of pVCC (Reiss et al., 2011). Although this research showed no connection between PS exposure and ADAM10 activity, it indicated that pVCC on rabbit erythrocytes is actively cleaved by ADAM10. Based on the evidence presented in this thesis, it can be suggested that nucleotide stimulation (e.g., BzATP) enables via P2 receptor activation PS exposure which controls ADAM10-mediated cleavage of pVCC.

5.2 Phospholipid scramblase TMEM16F/ANO6 contributes to ADAM10 shedding activity through enhanced PS exposure

As previously mentioned, calcium influx is an important step to induce PS exposure. Among calcium-activated proteins, the phospholipid scramblase anoctamin-6 (TMEM16F/ANO6) is a comprehensively described phospholipid translocase (Suzuki et al., 2010). Upon calcium influx TMEM16F/ANO6 is activated and shows enhanced scrambling activity which leads to the externalisation of PS from the inner to the outer plasma membrane (Suzuki et al., 2010). Therefore, it was asked whether an increased expression of TMEM16F/ANO6 would lead to increased PS exposure and enhanced ADAM10-mediated shedding activity. Confocal microscopic analysis of TMEM16F/ANO6 overexpressing cells

and visualisation of PS exposure with Annexin-V showed no clear response. However, Annexin-V labelling and flow cytometry analysis of TMEM16F/ANO6 overexpressing cells showed, in fact, that more cells reacted upon IO-induced calcium influx. Both, microscopic imaging and flow cytometry, in combination with Annexin-V, are standard methods for the analyses of PS exposure. However, flow cytometry seems to be the more efficient method for detecting small shifts in PS exposure. Suzuki et al. showed via flow cytometry that overexpression of TMEM16F/ANO6 in Ba/F3 cells leads to an enhanced Annexin-V signal in comparison to respective control cells. On the contrary, as a consequence of siRNA-induced knockdown of TMEM16F/ANO6 expression in lymphocytes, TMEM16F/ANO6-mediated PS exposure was reduced under calcium ionophore treatment (Yang et al., 2012b, Kmit et al., 2013). Both studies showed that calcium ionophore-induced PS exposure depends on the expression of TMEM16F/ANO6, although they used different approaches.

Interestingly, the results presented in this thesis suggest that more cells became reactive to the IO stimulation, due to TMEM16F/ANO6 overexpression. In fact, there was an increase in the number cells that reacted to the stimulus but only a slight increase in overall PS signal per cell. In this context, it seems feasible to hypothesise that overexpression of TMEM16F/ANO6 leads to an increased sensitivity of cells to react to external stimuli, which were otherwise unresponsive. The responsiveness of cells, clearly, also depends on the concentration of the stimuli. The general ability of cells to react to calcium ionophore stimulation was shown to depend on the stimuli concentration (Yang et al., 2012b, Kmit et al., 2013). On the one hand, stimulation with low concentrations of the calcium ionophore A23187 (1 μ M) only led to PS exposure in 50 percent of stimulated platelets. On the other hand, high concentrations of the ionophore (10 μ M) led to 100 percent PS-positive platelets. High concentrations of calcium ionophores might be inappropriate to determine how TMEM16F/ANO6 overexpression contributes to PS exposure. The ionomycin (IO) stimulated cells presented in this thesis, therefore, might provide a clearer picture about the effect of TMEM16F/ANO6 overexpression under calcium ionophore-induced calcium influx, given that the cells were stimulated with low rather than high concentrations of IO. All in all, the results by Suzuki et al. together with the results presented in this thesis support a connection between the expression of TMEM16F/ANO6 and the ability of cells to expose PS.

In contrast to TMEM16F/ANO6, TMEM16A/ANO1 is mainly described as a calcium-activated chloride channel. Functional data on TMEM16A/ANO1 furthermore imply that calcium only activates its channel function (Brunner et al., 2014). Overexpression of TMEM16A/ANO1 was therefore not expected to have an impact on PS exposure, in contrast to TMEM16F/ANO6. However, cells overexpressing TMEM16A/ANO1 also showed enhanced Annexin-V levels, although the signal was lower than for the TMEM16F/ANO6 overexpressing cells. This result was unexpected, since Suzuki et al. (2010) demonstrated that TMEM16A/ANO1 showed no effect to calcium ionophore-induced PS exposure. Moreover, recently published TMEM16A/ANO1 structures indicate that the constitution of the TMEM16A/ANO1 transmembrane pore does not allow TMEM16A/ANO1 to act as a phospholipid

scramblase (Paulino et al., 2017). Most convincingly, although TMEM16A/ANO1 and TMEM16F/ANO6 show high sequential similarity in their calcium binding domains, a scrambling domain is only reported for TMEM16F/ANO6 (Yu et al., 2015). Nonetheless, Yu et al. (2015) suggested that TMEM16A/ANO1 may not act directly as a phospholipid scramblase but instead, it interacts with other proteins, thus affecting the activity of other scramblases. The elevated PS exposure due to the overexpression of TMEM16A/ANO1 might support such an indirect contribution of TMEM16A/ANO1 to PS exposure. Since TMEM16A/ANO1 overexpressing cells showed enhanced PS exposure in comparison to control cells, but lower PS exposure than TMEM16F/ANO6 overexpressing cells; the question arose whether this stepwise increase (from control, over TMEM16A/ANO1, to TMEM16F/ANO6) could be used to assess whether the levels of PS exposure determine the levels of ADAM10-mediated substrate release. If PS exposure regulates ADAM10 shedding activity, the amount of substrate released in TMEM16A/ANO1 overexpressing cells should be between that obtained for the control cells and those overexpressing TMEM16F/ANO6, since the intensity of the PS signal for TMEM16A/ANO1 cells is between these two groups.

Indeed, BTC and VE-Cad shedding by ADAM10 in TMEM16A/ANO1 overexpressing cells was higher compared to the control cells but lower than in TMEM16F/ANO6 overexpressing cells. Though TMEM16A/ANO1 is mainly described to function as a calcium-activated chloride channel, the results presented in this thesis suggest that TMEM16A/ANO1 also had an effect on PS exposure. Interestingly, downregulation of TMEM16A/ANO1 has been shown to reduce the release of EGF and TGF- α in breast cancer cell lines, suggesting that the activity of TMEM16A/ANO1 may affect the release of these two ADAM10 substrates (Britschgi et al., 2013). It would be interesting to analyse whether the downregulation of TMEM16A/ANO1 in breast cancer cell lines also affects PS exposure in these cell lines. Based on the importance of TMEM16A/ANO1 in the context of breast cancer progression and the presented data, further evaluation of TMEM16A/ANO1 overexpression in other cell lines and validation of the PS signal with other labelling techniques is recommendable. Moreover, the role of ADAM10 in the context of breast cancer progression should be further investigated. Overall, the results for TMEM16A/ANO1 and TMEM16F/ANO6 demonstrate a compelling connection between cells cellular capacity to expose PS and ADAM10 shedding activity. It seems intuitive that increasing amounts of PS on the outer leaflet would lead to a gradual increase of ADAM10 shedding activity and that ADAM10-mediated substrate release is modified according to the amount of PS on the outer plasma membrane leaflet.

The data for overexpressed TMEM16F/ANO6 and TMEM16A/ANO1 indicated that the levels of PS exposure had a positive effect on the amounts of ADAM10-mediated substrate shed from the cell surface. Though the linear regression model showed an apparent link between PS exposure and ADAM10 shedding activity, caution in the interpretation is advised because the total number of replicates is low. Increasing the number of data points in the linear regression model will further underline the

correlation between the levels of PS and ADAM10 shedding activity. Noticeably, TMEM16F/ANO6 requires calcium influx (e.g., through IO stimulation) to expose PS. In 2010, described a hyperactive mutant of the mouse TMEM16F/ANO6 which showed enhanced PS exposure under resting calcium levels. They argued that this was due to a point mutation leading to an amino acid exchange of aspartic acid at position 409 to glycine. This exchange was suggested to increase the calcium affinity of TMEM16F/ANO6, thus enhancing the proteins capacity to expose PS. In this thesis, it was shown that the respective point mutation in the human TMEM16F/ANO6 (human TMEM16F/ANO6 D408G) also led to consistently high PS exposure under resting calcium conditions in the overexpressing cells. Which to the best of the authors knowledge is the first description of the respective mutation in the human TMEM16F/ANO6 mimicking that described by Suzuki et al. (2010) for the mouse TMEM16F/ANO6 mutant. Although the ability to expose PS of both TMEM16F/ANO6 mutants was not compared in this thesis, it seems reasonable that a similar mutation in the human TMEM16F/ANO6 may lead to a similar effect described for the mouse TMEM16F/ANO6 mutant. In addition to the constitutively exposed PS, overexpression of the human TMEM16F/ANO6 D408G also resulted in a constantly high ADAM10-mediated release of overexpressed substrates BTC and VE-Cad over time. Moreover, it was also shown that OPS had a competitive inhibitory effect on the release of ADAM10 substrates, indicating that the constant PS exposure is responsible for the constant high substrate release.

Interestingly, Yang et al. (2012b) could not show that the overexpression of the mouse TMEM16F/ANO6 mutant (mouse TMEM16F/ANO6 D409G) in a human cell line led to constant PS exposure. HEK-293T cells overexpressing the mouse TMEM16F/ANO6 D409G showed no enhanced PS exposure under resting calcium conditions (Yang et al., 2012b). The authors speculated that the reason behind this might be that mouse TMEM16F/ANO6 D409G ability to expose PS is different in blood cells than in HEK-293T cells (Yang et al., 2012b). However, data from our lab with the human TMEM16F/ANO6 D409G mutant overexpressed in HEK-293T led to constantly enhanced PS exposure. One explanation may be that the mouse TMEM16F/ANO6 D409G is differently regulated than the human TMEM16F/ANO6 D408G mutant. Another explanation might be that mouse version of hyperactive ANO6 (TMEM16F/ANO6 D409G) is not functional in a human cell line and *vice versa*. However, both hypotheses are somewhat speculative, and further research should be carried out to shed light on the differential capacity of the mouse and the human hyperactive TMEM16F/ANO6 to scramble PS. Since the human TMEM16F/ANO6 also led to enhanced PS exposure in COS7, the general ability of the human hyperactive TMEM16F/ANO6 to constantly scramble PS was further verified.

Though the results in this thesis show that overexpression of human TMEM16F/ANO6 D408G mutant led to a constantly enhanced shedding of overexpressed ADAM10 substrates, via constantly high PS exposure, the effect of this mutant on endogenously expressed substrates remains to be further evaluated. Overexpression of the human TMEM16F/ANO6 D408G mutant in human keratinocytes represents an appealing approach to analyze the effect of constant PS exposure on the shedding of E-cadherin. As

shown in this thesis, PS exposure regulates ADAM10-mediated E-cadherin shedding. However, an experimental approach to analyze the effect of human TMEM16F/ANO6 D408G for the shedding of E-cadherin requires certain caution. For instance, the analysis of E-cadherin C-terminal fragment by Western Blot analysis as an indicator of ADAM10 activity seems to be a suitable method. However, since the C-terminal fragment of E-cadherin is further processed by the gamma-secretase complex, these experiments should be carried out in the presence of respective gamma-secretase inhibitors. Nevertheless, the human TMEM16F/ANO6 D408G mutant showed intriguing similarities to mouse TMEM16F/TMEM16F/ANO6 D409G in its ability to constantly expose PS under resting calcium conditions. Moreover, human TMEM16F/ANO6 D408G-related constant PS exposure led to enhanced ADAM10-mediated substrate release, as competitive inhibition with OPS indicated. This, indeed assures that a gain of function of TMEM16F/ANO6-related PS exposure is the cause for the constant enhanced ADAM10 shedding activity.

5.3 Loss of TMEM16F/ANO6 scrambling activity is related to impaired ADAM10-mediated substrate release

Human TMEM16F/ANO6 D408G showed enhanced PS exposure under constitutive conditions, although it was not known whether a loss of PS scrambling activity would lead to reduced ADAM10-mediated substrate release. The Scott syndrome is a rare genetic disorder with minor effects on blood coagulation which primarily affect blood cells (Zwaal et al., 2004). The cause of the coagulation deficiency in these patients was shown to be a result of the expression of functionally impaired TMEM16F/ANO6 (Suzuki et al., 2010). Because of the absence of functional TMEM16F/ANO6 in B-cells from Scott patients (Zwaal et al., 2004), these cells represent an important tool for studying the effect of missing TMEM16F/ANO6-mediated PS exposure on ADAM10 shedding activity.

B-cells are described to express CXCL16 and CD23, two major substrates of ADAM10 (Pupovac et al., 2013, Pupovac et al., 2015). The expression and shedding of CD23 from B-cells was firstly described by Gu et al. (1998) and Weskamp et al. (2006) identified ADAM10 as the responsible sheddase of CD23. Moreover, stimulation of P2X7R with ATP or its analogue BzATP is known to lead to PS exposure and activate ADAM10, thus facilitating the release of CD23 from the cell surface of human and mouse B-cells (Pupovac et al., 2015). This thesis showed that PS exposure is the required signal for ADAM10-mediated release of CD23. Nucleotide stimulation (e.g., BzATP) of human B-cells led to PS exposure and the release of CD23 from the cell surface as a result of ADAM10 shedding activity. To analyze whether PS exposure is the relevant trigger of ADAM10-mediated release of CD23, the ability to expose PS, and thus trigger ADAM10 mediated shedding of CD23, was compared in B-cells from a Scott patient and human control B-cells. Scott B-cells showed comparable levels of CD23 at the cell surface, compared to the human control B-cells. However, nucleotide stimulation showed no effect; neither on the cells ability to expose PS nor on the CD23 surface levels. The absence of PS exposure and impaired shedding of CD23 on the Scott patient B-cells seems to be a clear result of impaired TMEM16F/ANO6-

mediated PS exposure. Given that the expression of the P2X7R receptor and ADAM10 was comparable among Scott patient B-cells and control B-cells, these cells seem to be unable to expose PS under enhanced calcium influx as previously observed by Kmit et al. (2013).

However, Williamson et al. (2001) showed that the induction of apoptosis in Scott B-cells leads to PS-exposure, presumably through the activation of a calcium-independent scramblase. The Scott patient B-cells were therefore incubated with an antibody against the Fas receptor (FasR) to induce apoptosis and to shed light on the hypothesis that PS exposure regulates ADAM10 shedding activity independently of TMEM16F/ANO6. As described in this thesis, Scott patient B-cells incubated with the FasR antibody also exposed PS and showed for the first time that ADAM10 is the responsible sheddase of CD23 under apoptosis. This was not an unexpected result as Steinhusen et al. (2001) showed that ADAM10 is active under apoptosis. For example, the induction of apoptosis enhances the cleavage of ADAM10 substrate E-cadherin (Steinhusen et al., 2001). Incubation with metalloproteinase inhibitor TAPI abolished the cleavage of E-cadherin under apoptosis, indicating that the cause of the cleavage was due to the activity of a metalloproteinase (Steinhusen et al., 2001). Likewise, ADAM10 inhibitor GI254023X abolished the shedding of CD23 from the surface of Scott patient B-cells, clearly indicating that ADAM10 is the protease responsible for the shedding of CD23 under apoptosis; however, the scramblase responsible for the PS exposure under apoptosis remains unknown. The caspase activated scramblase Xkr8 was shown to scramble PS under apoptotic conditions (Suzuki et al., 2013). It seems feasible to suggest that Scott syndrome patients B-cells expose PS through a scramblase like Xkr8, although this remains to be further investigated. Nevertheless, the data presented in this thesis for the Scott syndrome patients B-cells further highlight the functional connection between PS exposure and ADAM10-mediated substrate release.

5.4 ADAM10 stalk domain facilitates the interaction with PS

Using multiple methodological approaches, different cell types and various substrates this thesis showed that PS exposure is an important functional trigger of ADAM10 shedding activity. In addition to the functional importance of PS, this thesis focused on inferring the interaction mechanism between ADAM10 and PS. The evidence in this thesis showed that the stalk domain of ADAM10 is of mechanical importance and is directly involved in the interaction with PS. Different biophysical analyses (ITC, SAW, and FRET) with ADAM10 stalk domain peptide were carried out by our research collaborators from the research centre in Borstel. Isothermal calorimetry (ITC) is a highly recommendable technique to measure the interaction capacity of membrane proteins with the plasma membrane (Rajarathnam and Rosgen, 2014). ITC measures the actual interaction of unmodified proteins in a solution, therefore, avoiding artefacts related to labelling. ITC was also shown to be a reliable technique to measure the interaction between PS and PS-binding proteins, e.g., Annexin-V (Capila et al., 1999). The interaction of Annexin-V with PS-liposomes was enhanced with the application of

calcium into the experimental setup (Capila et al., 1999). However, ADAM10 interaction with PS seems to be organised differently than the interaction mechanism of Annexin-V with PS.

The ITC experiments with a peptide version of ADAM10 stalk domain were carried out with different liposomes (PS and PC liposomes). In the presence of calcium, the interaction of the stalk domain of ADAM10 with the PS-liposomes was abolished. A reasonable explanation for the inhibition of the interaction between the ADAM10 stalk peptide and the PS-liposomes might be the saturation of the system. The positively charged calcium binds to the negatively charged PS headgroup and may block the direct interaction between the overall positively charged ADAM10 stalk peptide to PS. In the case of Annexin-V, an increase in the binding capacity through the introduction of calcium seems plausible, since the binding of Annexin-V to PS is described to occur via calcium bridges (Tait and Gibson, 1992). Based on the results of this thesis this seems an unlikely mechanism behind the interaction between ADAM10 and PS. However, the titration of the ADAM10 stalk peptide onto PS-liposomes produced a measurable release of energy which decreased over time, indicating a direct interaction of the peptide with PS which was abolished upon saturation of the system. In contrast, titration of the stalk domain onto PC-liposomes did not produce measurable energy release, pointing out that the ADAM10 stalk domain specifically binds to negatively charged PS. Interestingly, the introduction of calcium halted the capacity of the ADAM10 stalk domain to bind with PS, indicating that for the interaction to occur calcium is not required and that it has rather an inhibitory effect on the interaction. These results suggest that ADAM10 stalk domain binds to PS in a calcium-independent fashion.

The interaction of other proteins (e.g., HIV-1 Nef protein and c-Src) with PS is facilitated via electrostatic interaction (Sigal et al., 1994, Gerlach et al., 2010), which could be the mechanism behind the interaction between the stalk domain of ADAM10 and PS. Dimeric positively charged amino acids were shown to be the minimum prerequisite for proteins to interact with PS (Caberoy et al., 2009). Since ADAM10 stalk contains such a triplet motif and shows an overall positive charge, it could be argued that ADAM10 interacts with PS via electrostatic interaction. Further examination of the interaction between ADAM10 stalk peptide and PS-liposomes, with a surface acoustic wave experimental setup, pointed out that the peptide interaction occurs in a biphasic way. First, the peptide interacts with the PS liposomes, in the following stage increasing concentration of the peptide leads to intercalation into the liposomal bilayer. Notably, the second stage of this interaction indicates that the ADAM10 stalk domain sinks further into the membrane. To further investigate this second stage of intercalation, a FRET analysis of the ADAM10 stalk domain titrated onto PS liposomes was carried out. FRET analysis is described as a conventional method to analyse spatial changes in the phospholipid membrane caused by peptide insertion (Loura and Prieto, 2011). This analysis was carried out to elucidate further the results of the SAW experiments presented in this thesis. It was shown that the distance between donor and acceptor labelled PS headgroups indeed increased when the ADAM10 stalk domain was added to the PS liposomes, but not when the ADAM10 stalk peptide was titrated on the PC-liposomes. Based on this

it can be concluded that the increasing space between donor and acceptor shows that the stalk domain of ADAM10 sinks into the differently labelled phospholipids and increases the distance between them. These results suggested that ADAM10 interaction with PS is somehow similar to the interaction of ADAM17 with PS.

A sensible interpretation of the ITC, SAW, and FRET results from this thesis is that PS drags the ADAM10 stalk domain into the membrane. This interpretation is similar to what was reported for ADAM17 alpha-helical CANDIS, although the alpha-helical structure of ADAM10 stalk domain seems to be less pronounced (Dusterhoft et al., 2015). These results indicated that the stalk domain of ADAM10 is not only involved in the interaction with PS but also, upon increasing concentrations of PS, ADAM10 stalk domain intercalates into the plasma membrane. Nevertheless, caution needs to be exercised when interpreting the results regarding the ADAM10 stalk domain peptide, given that the ITC, SAW and FRET analyses were performed with the peptide version of the ADAM10 stalk domain and not with the complete protease. Independently of that recommendation, these results indicate that ADAM10 binds via electrostatic interaction to PS in a biphasic way. The first step is interaction with PS, followed by a second step, where an increase in PS drags the stalk domain of ADAM10 into the plasma membrane, thus enabling the proteases shedding activity.

5.5 The stalk domain of ADAM10 is essential for substrate shedding

To further test the hypothesis that the stalk domain is the relevant domain for the interaction with PS, in the context of substrate release, mutations of the positively charged amino acids in the stalk domain of full-length ADAM10 were performed. Stepwise mutation of one amino acid (R647N), a cationic triplet motif (R657N, K659N, and K660N) and a combination of both showed a gradual reduction of BTC release for each ADAM10 stalk mutant when compared to wtADAM10. Results showed that replacement of the positively charged amino acids in the stalk domain of ADAM10 led to reduced substrate release and supported the assumption that the stalk domain ADAM10 is essential for the proteases shedding activity. These results demonstrate that the mechanism of interaction between ADAM10 and PS is likely orchestrated via electrostatic interaction between the positively charged amino acids and PS. In agreement with these findings Lemmon (2008) and Caberoy et al. (2009) showed that the electrostatic interaction enables PS interaction with proteins through positively charged amino acids. For instance, HIV Nef-1 protein interacts with PS via a cationic motif, thus facilitating the protein attachment to the cell membrane; although replacement of the positively charged amino acids by alanine impaired the ability of HIV Nef-1 to interact with PS (Gerlach et al., 2010). This research is in line with the results shown in this thesis, although asparagine replaced the positively charged amino acids in ADAM10 stalk domain.

Noticeably, the exchange to asparagine in the stalk domain of ADAM10 had a positive effect on the protease levels at the cell surface. Asparagine residues (N) of ADAM10 are posttranslationally modified

through N-linked glycosylation (Escrevente et al., 2008). These posttranslational modifications were reported to play an important role for the proteases traffic and stabilisation on the cell surface (Escrevente et al., 2008). Therefore, a considerable number of asparagine residues, due to the mutations in the ADAM10 stalk domain, might have affected the susceptibility of the protease to increased glycosylation, thus affecting trafficking and stabilization of ADAM10 on the cell surface (Escrevente et al., 2008). Although this hypothesis seems reasonable, additional glycosylation would manifest itself in altered molecular weight of the respective mutant when compared to the wild-type. This was, however, not the case for any of the ADAM10 stalk mutants. In fact, glycosylation was reported as a rather specific modification, and simple mutations lead to impaired rather than enhanced traffic. Nevertheless, lysates from mADAM10 Stalk 2 mutant transfected should be treated with PNGase F to rule out that the elevated surface levels were caused by enhanced glycosylation. Other factors may also explain the enhanced surface levels of the mADAM10 Stalk 2 mutant. For example, tetraspanins (Tspans) are important for ADAM10 trafficking and stabilisation on the surface of the cell (Matthews et al., 2017b). It is known that Tspan15 directly interacts with ADAM10 stalk domain and the overexpression of Tspan15 enhances ADAM10-mediated shedding of N-cadherin (Noy et al., 2016). However, since the introduced mutation to the stalk domain led to more ADAM10 on the cell surface, it can be assumed that these mutations enhance ADAM10 interaction with Tspan15 rather than decrease it. Subsequently, this should lead to increased ADAM10 shedding activity. Nevertheless, ADAM10 shedding activity decreased under IO stimulation, indicating that even if the mutations affected ADAM10 interaction with Tspan15 at the cell surface this is less relevant for the protease interaction with PS. In addition to post-translational modifications or Tspans affecting the protease expression on the cell surface, ADAM10 itself is reported to be a substrate for other metalloproteinases (Tousseyn et al., 2009). In fact, the metalloproteinases ADAM9 and ADAM15 are described to shed ADAM10 in close proximity to the plasma membrane (Tousseyn et al., 2009). Although no particular cleavage motif has been described, where either of the two proteases may cleave ADAM10, it seems plausible that impaired shedding of ADAM10 by other proteases may lead to higher surface levels of ADAM10. In addition, ADAM10 was described to shed itself (Brummer et al., 2018). Given that mutations to the stalk domain directly affect ADAM10 shedding, it seems plausible that ADAM10-mediated autoproteolysis may be impaired.

However, even though the mutations in the stalk domain led to more ADAM10 at the cell surface, the shedding activity was clearly reduced. The successive mutation of positively charged amino acids to asparagine led to the respective reduction of ADAM10 shedding activity and highlighted the functional importance of stalk domain for ADAM10-mediated substrate release. Whether this is because of a reduced capacity of ADAM10 to interact with PS needs to be further analysed. Nonetheless, electrostatic interaction with negatively charged phospholipids was reported to be catalysed by the occurrence of a minimum of two cationic amino acids (Caberoy et al., 2009). Therefore, it seems justifiable to assume that this also occurs for the cationic triplet motif in the stalk domain of ADAM10.

5.6 A model behind PS regulation of ADAM10 shedding activity

Structural data on ADAM10 extracellular domains should provide a better understanding of the mechanism controlling ADAM10 shedding activity, given that the cytoplasmic domain of ADAM10 is neglectable for the process of substrate shedding. Recent research describing the entire extracellular structure of ADAM10 (Seegar et al., 2017) allows for the first time to analyse the protease structure in relation to its function. Based on the recently published structural data of ADAM10 (Seegar et al., 2017) and the results presented in this thesis a model explaining PS activation of ADAM10-mediated substrate release can be proposed. The negatively charged phospholipid phosphatidylserine (PS) is mainly localized at the inner plasma membrane leaflet. Upon enhanced calcium influx or induction of apoptosis, which leads to the activation of calcium-dependent scramblases like TMEM16F/ANO6 or caspase-dependent scramblases like Xkr8, PS is translocated from the inner to the outer plasma membrane leaflet. At the outer leaflet PS interacts via electrostatic interaction with the positively charged amino acids of the ADAM10 stalk domain and pulls this domain in close proximity to the plasma membrane. The PS initiated pulling could change the orientation of the ADAM10 stalk domain, thereby affecting the position of the following cysteine-rich domain. This domain was suggested to autoinhibit ADAM10 metalloproteinase domain and its removal may be the penultimate trigger for substrate shedding (Fig. 29). The data presented in this thesis suggest that the ADAM10 stalk domain interaction with PS is the major regulatory step. This activation mechanism for ADAM10 shedding activity shows particular similarities with the one described for ADAM17. For example, ADAM17 interacts with the negatively charged PS via a cationic triplet motif localised in the proteases membrane-proximal domain (MPD) (Sommer et al., 2016). While ADAM17 interacts with PS via a cationic motif localised in the proteases MPD (the equivalent to ADAM10 cysteine-rich domain), ADAM10 seems to interact with PS via a cationic motif localised in the protease stalk domain (the equivalent to ADAM17 CANDIS). Also for ADAM17, the stalk domain (ADAM17 CANDIS) was shown to be of particular importance for the protease shedding activity (Dusterhoft et al., 2015). The amphipathic alpha-helical structure of the CANDIS domain interacts with the plasma membrane and brings the protease in closer proximity to the plasma membrane (Dusterhoft et al., 2015), where then the protease MPD can interact with PS (Sommer et al., 2016). This two-way mechanism to activate ADAM17 shedding activity is different to what is suggested in this thesis for ADAM10. This brings up the question of whether there may be an additional mechanism involved in the regulation of ADAM10 shedding activity. Interestingly, ADAM10 stalk domain also shows minor alpha helical elements, although the alpha-helical characteristics of ADAM10 stalk domain seem less pronounced than the helical elements of ADAM17 CANDIS (Dusterhoft et al., 2015). However, ITC, SAW and FRET experiments with ADAM10 stalk domain peptide suggested that ADAM10 not only interacts with PS but, upon increasing concentrations of the peptide, it intercalates into the PS-enriched liposomal bilayer. These results, indeed, suggest that also ADAM10 stalk domain shows characteristics of an amphipathic helix and fulfils two functions. First, the interaction of the positively charged amino acids with negatively charged PS and second, the intercalation of the stalk

domain into the phospholipid bilayer. In this context, the stalk domain of ADAM10, unlike for ADAM17 where PS interaction and intercalation are regulated by different domains, might fulfil both functions.

The recent published structure of ADAM10 suggests that the cysteine-rich domain of ADAM10 acts as an auto inhibitor of the protease metalloproteinase domain (Seegar et al., 2017). Incubation of this ADAM10 structure with an antibody directed against the cysteine-rich domain increased the proteolytic activity (Seegar et al., 2017). In this case, PS might facilitate a transient breakdown of ADAM10 autoinhibition by dragging the stalk domain in close proximity to plasma domain and thereby removing the cysteine-rich domain from the ADAM10 metalloproteinase domain, thus activating the proteolytic activity. In this case, a two-step function of the ADAM10 stalk domain may provide the mechanical force to enable the breakdown of ADAM10 autoinhibition and enable substrate shedding. This two-step function of the ADAM10 stalk domain is even more necessary considering that electrostatic interaction alone is insufficient to fully attach e.g. the HIV-1 Nef protein to the plasma membrane (Gerlach et al., 2010). Only in combination with an amphipathic helix the interaction between HIV-1 Nef proteins and the membrane was achieved (Gerlach et al., 2010). The proposed modus of activation for ADAM10 shows, therefore, intriguing similarities to the one described for the ADAM17 (Sommer et al., 2016). However, whether only the stalk domain of ADAM10 alone is involved in the regulation of the protease shedding activity or if other domains also play a role in ADAM10 activation needs to be further evaluated. Since the mutation of the positively charged amino acids in the stalk domain of ADAM10 led to a clear but not entire reduction in substrate shedding, the involvement of other regulatory elements for the process of substrate shedding seems possible.

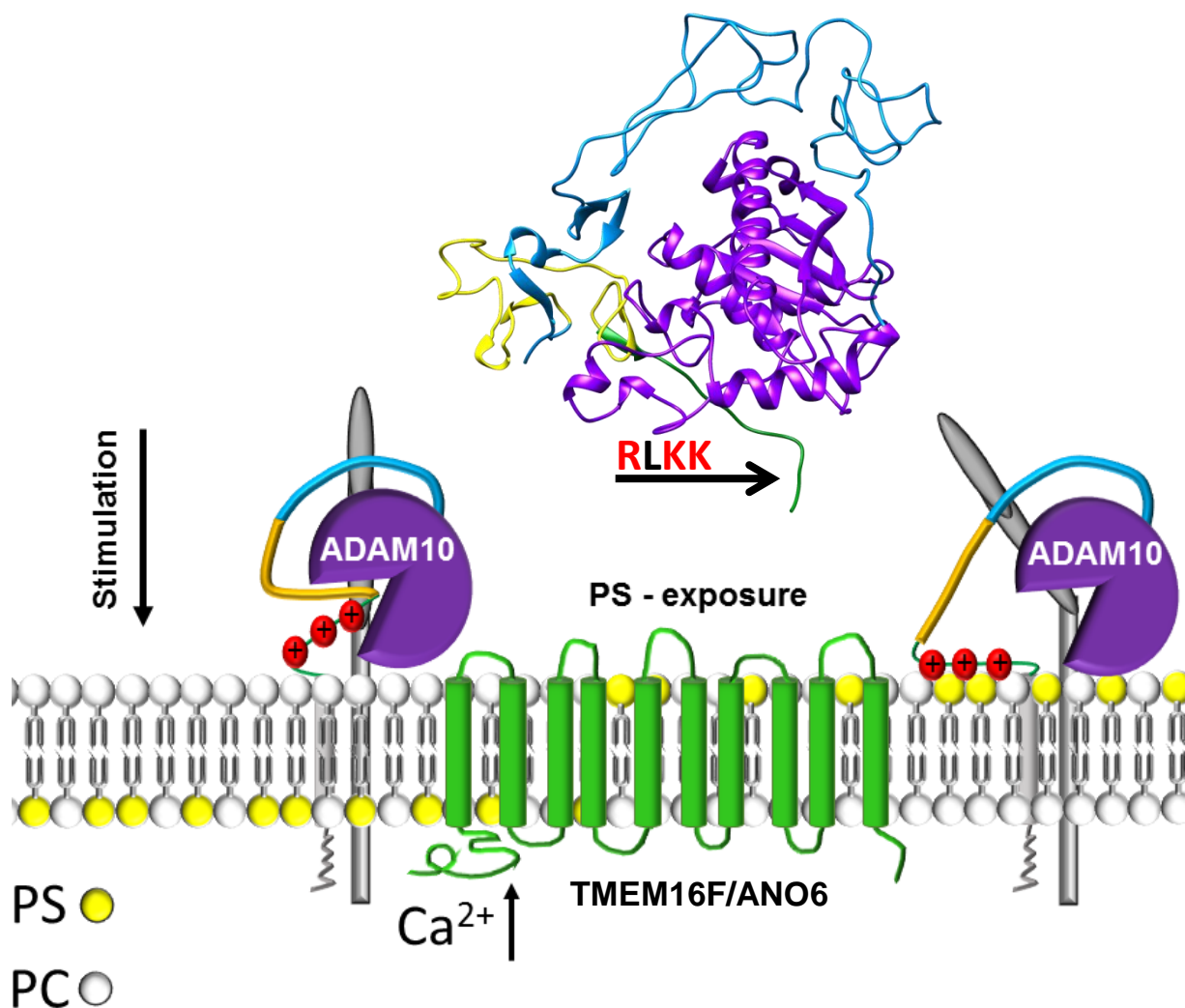


Figure 29. PS exposure and interaction with ADAM10 initialise substrate processing.

The phospholipids of the plasma membrane show an asymmetrical distribution, with phosphatidylserine (PS) mainly located at the inner leaflet and phosphatidylcholine (PC) mainly located at the outer leaflet. Under these constitutive conditions ADAM10 seems to be in an inactive state with the cysteine-rich domain (yellow) autoinhibiting the protease metalloproteinase domain (purple). The stimulation of cells with activators of ADAM10 leads then to increasing concentrations of intracellular calcium thus activating scramblases like TMEM16F/ANO6 (green) and enhance PS externalisation. ADAM10 stalk domain (green) contains a cationic triplet motif (RXKK) in close proximity to the plasma membrane. The cationic triplet motif seems to interact directly with the negatively charged PS via electrostatic interactions. The interaction of the cationic triplet motif with PS drags the ADAM10 stalk domain to the plasma membrane and thereby disables the autoinhibitory function of the cysteine domain. This results in full substrate accessibility to the ADAM10 metalloproteinase domain and enables substrate shedding.

Based on the model of ADAM10 activation proposed in this thesis, aside from ADAM10 shedding activity, the protease general *bona fide* enzymatic activity might be also regulated through PS exposure. For example, recent results for ADAM17 suggest that PS exposure only regulates the protease shedding activity but leaves the *bona fide* enzymatic activity unaffected (Sommer et al., 2016). Since the modus

of activation of ADAM10 and ADAM17 shows many similarities, the question arose whether ADAM10 enzymatic activity might also be regulated through PS exposure. The model of ADAM10 activation, as proposed in this thesis (Fig. 29), implies that under constant PS exposure ADAM10 is in an active state and shedding can take place. Indeed, stimuli like IO, Mel or BzATP led to a continuous and ubiquitous PS exposure, with a concomitant enhanced substrate release. If the model of how ADAM10 is activated proposed in this thesis held to be true, ADAM10 enzymatic activity should also increase under enhanced PS exposure.

Noticeably, incubation with an ADAM10 specific fluorescent peptide substrate showed that neither OPS (which reduced ADAM10 shedding activity) nor the mADAM10 Stalk 2 mutant (the mutated PS interaction motif) affected the ability of ADAM10 to cleave the fluorescent peptide substrate. These observations are in line with those reported for ADAM17 (Sommer et al., 2016) and suggest that also ADAM10 enzymatic activity is PS-independent. However, the results for ADAM10 enzymatic activity were only described under constitutive conditions, where PS is mainly localised at the inner plasma membrane leaflet. The nanoscale levels of PS on the outer leaflet would therefore only lead to a minimum of shedding as well as enzymatic activity of ADAM10 under constitutive conditions. Stimulation, however, should result in enhanced PS exposure. Given that ADAM10 shedding activity increased under stimuli-induced PS exposure, analysing ADAM10 *bona fide* enzymatic activity under stimuli inducing PS exposure would be necessary. Stimulation of platelets, with collagen-related peptide and collagen or convulxin (all stimuli of ADAM10), only enhanced ADAM10-mediated shedding of glycoprotein VI but did not increase the protease enzymatic ability to cleave a soluble fluorescent peptide substrate (Facey et al., 2016). These results suggest that even under stimulated conditions, ADAM10 substrate shedding and enzymatic activity are two differently regulated mechanisms. However, stimulation of platelets with NEM, another potent activator of ADAM10, led to both: enhanced shedding of the glycoprotein VI and enhanced *bona fide* enzymatic cleavage of the soluble fluorescent peptide substrate (Facey et al., 2016). Moreover, the enhanced enzymatic activity of ADAM10 under the stimulation with NEM was inhibited with broadspectrum metalloproteinase inhibitors, GM6001 and GI254023X (GI), suggesting that ADAM10 mediated the enzymatic cleavage of the fluorescent peptide substrate. A possible explanation for the differences of these diverse stimuli in enhancing ADAM10 *bona fide* enzymatic activity might be their different ability to expose PS. In this context, it could be suggested, that ADAM10 enzymatic activity depends on the potency of the stimuli to induce PS exposure. As it was shown for ADAM17, stimuli like FGF7 only led to a mild and local PS exposure (Sommer et al., 2016). Other, more potent stimuli (e.g., IO), lead to a robust, ubiquitous and constant PS exposure (Sommer et al., 2016). Since a stimulus like FGF7 has a physiological relevance and a stimulus like IO is irrelevant in the physiological context, a stimuli independent increase in PS exposure might provide the most accurate insight on whether PS exposure also controls ADAM10 enzymatic activity. ADAM10 enzymatic activity was therefore analysed using the hyperactive human TMEM16F/ANO6 D408G. As overexpression of this mutant led to constant

stimuli independent PS scrambling, under basic intracellular calcium levels, this might present a more accurate way to determine whether ADAM10 *bona fide* enzymatic activity increases under PS exposure. Indeed, overexpression of the human TMEM16F/ANO6 D408G mutant led to enhanced ADAM10 *bona fide* enzymatic activity. Moreover, the mADAM10 Stalk 2 mutant enzymatic activity seemed to be lower than that of the ADAM10 wild-type. These results for ADAM10 suggest that, indeed, PS exposure regulates the protease shedding and enzymatic activity. However, given that the samples transfected with the inactive mADAM10 E/A mutant also showed enhanced cleavage of the fluorescent peptide substrate, the analysis of ADAM10 enzymatic activity in the context of overexpressed TMEM16F/ANO6 D408G might be not as adequate as presumed to determine whether ADAM10 enzymatic activity is also enhanced under PS exposure. Although HEK-293T cells transfected with the human hyperactive scrambling mutant TMEM16F/ANO6 D408G showed high PS exposure (Martin Veit, personal communication), the unspecificity of the ADAM10 fluorescent peptide substrate cannot allow to ascertain whether ADAM10 enzymatic activity is also PS-regulated. The currently available tools to measure ADAM10 enzymatic activity are too insensitive and/or too unspecific to measure ADAM10 enzymatic activity. It is therefore essential to develop new assays that allow specific discrimination between ADAM10 shedding and enzymatic activity, and to differentiate whether both are regulated through PS exposure. Nevertheless, this thesis offers several lines of evidence sustaining that PS exposure is a significant regulatory event for ADAM10-mediated substrate shedding.

6. Outlook

The results presented in this thesis clearly show that PS exposure is the primary regulatory event controlling ADAM10 shedding activity. The mutation of the polycationic motif in the stalk domain of ADAM10 led to a reduced shedding of betacellulin, likely through an impaired interaction between PS and ADAM10. However, in addition to the description of PS exposure as the major regulatory event for ADAM10-mediated substrate shedding *in vitro*, a respective *in vivo* model could provide further insights about the relevance of this mechanism. ADAM10-deficient mice have been described to die during embryonal development, indicating the vital importance of ADAM10-mediated shedding activity. The mutation of the polycationic motif in ADAM10, however, should not manifest in such a severe way. As the *in vitro* results in this thesis show, ADAM10 shedding activity is drastically but not entirely reduced, indicating remaining minor shedding activity. This new ADAM10 stalk model organism might, therefore, provide with a unique chance to study the impact of a sharply reduced ADAM10 shedding activity on many physiological processes and at the same time avoid the severe effects to embryonal development that are caused by knock-out of ADAM10.

Aside from the ADAM10 stalk *in vivo* model, further research should focus on ADAM10 and ADAM17 shedding activity under physiological and pathophysiological conditions, where PS exposure is naturally enhanced. As it was shown in this thesis, the induction of apoptosis, where PS exposure is described as a hallmark, led to the enhanced ADAM10-mediated shedding of CD23. These results brought up the idea that also in other physiological or pathophysiological processes and diseases, where PS exposure is enhanced, ADAM10 and ADAM17 shedding activity may be also increased. In conjunction to apoptosis, enhanced PS exposure was described as a characteristic of various cancer types (Vallabhapurapu et al., 2015, Sharma and Kanwar, 2017). Interestingly, also increased ADAM10 shedding activity was described for various cancer types (Crawford et al., 2009). It seems plausible to suggest that the enhanced PS levels on cancer cells might be the responsible trigger for the increased ADAM10 shedding activity. However, such suggestion should be taken with caution since not every cancer cell type might show enhanced PS levels or elevated ADAM10 activity. It is, therefore, necessary, in a first step, to identify cancer types that show both, enhanced PS exposure and increased ADAM10 shedding activity. In a second step, the data for PS exposure and ADAM10 shedding activity need to be compared to a respective non-cancerous control. Nevertheless, whether enhanced PS exposure leads to increase ADAM10 shedding activity, in particular in the context of cancer development and progression, should be further investigated.

In addition to further describe the relevance of PS exposure for ADAM10-mediated substrate shedding *in vivo*, the identification and description of other PS-regulated proteases would highlight PS exposure as a general controlling mechanism. After ADAM17, ADAM10 was the second member of the ADAM protease family for which breakdown of plasma membrane asymmetry and PS exposure could be described as the penultimate step for the activation of ADAM10 and ADAM17. In this context, it seems

reasonable to ask whether PS exposure might also regulate the shedding activity of other ADAM proteases. Based on the results indicating that PS exposure controls ADAM17 and ADAM10 shedding activity, a subset of criteria to be fulfilled by ADAM proteases, to become a PS-regulated protease candidate, could be enumerated. The primary observations from the analysis of ADAM10 and ADAM17 were that the stimulation with calcium ionophore ionomycin (IO) led to enhanced PS-externalization and to a concurrent increase of substrate release. It is important to rule in or out whether PS exposure also controls their shedding activity, therefore the shedding activity of other ADAM proteases should be analysed under the stimulation with IO. For example, recent research for ADAM9 suggest that PS exposure is not the responsible mechanism controlling its shedding activity, as stimulation with IO showed no effect on ADAM9-mediated shedding of EphB4 (Maretzky et al., 2017). On the other hand, the shedding activity of ADAM15 seemed to increase under IO stimulation which in turn leads to the increased shedding of FGFR2b (Maretzky et al., 2014). Although the authors claim that the increase might be due to enhanced ADAM10 or ADAM17-mediated shedding of FGFR2b, it could be argued that stimulation with IO led to enhanced ADAM15-mediated shedding of the substrate. It is possible that IO directly enhances ADAM15 shedding, since the authors did not use any metalloproteinase inhibitor to confirm the involvement of ADAM10 and/or ADAM17 in the shedding of FGFR2b. Another feature that ADAM10 and ADAM17 share, that could be taken as another general criterion to identify other PS regulated ADAM proteases, is that both seem to interact with PS via a polycationic motif. The motifs, identified in ADAM10 and ADAM17, are localised in close proximity to the plasma membrane. Since this is a common feature in both proteases, other members of the ADAM proteases, which might also be regulated through PS exposure, should possess a similar motif. Indeed, also ADAM15 contains multiple positively charged amino acids close to its transmembrane domain. Although the occurrence of a polycationic motif in ADAM15 alone is not sufficient to declare the protease as another PS-regulated ADAM protease, mutation of this motif and the effect to ADAM15-mediated substrate shedding could provide further insights. As mentioned before and in addition to the first two criteria, it was shown that ADAM10 and ADAM17 shedding activity increased under conditions where PS exposure is enhanced (e.g., apoptosis). The data presented in this thesis showed that ADAM10-mediated shedding of CD23 increased under the induction of apoptosis. Moreover, Steinhilber et al. (2001) showed that the induction of apoptosis led to the enhanced ADAM10-mediated shedding of E-cadherin. Similar to ADAM10, the induction of apoptosis also resulted in an increased ADAM17 mediated shedding of L-selectin (Sommer et al., 2016). An increase of the shedding activity of other ADAM proteases under conditions where PS exposure is naturally enhanced might be therefore another indicator to define new PS-regulated ADAM proteases. Although such studies might represent the ultimate criteria to identify other PS-regulated ADAM proteases, data for the shedding activity under apoptosis primarily exist for ADAM10 and ADAM17 and should be obtained for possible candidate proteases.

To sum up, further research on ADAM10 and on the importance of PS exposure *in vivo* is urgent. The importance of PS exposure as the primary trigger of ADAM10-mediated substrate shedding should,

therefore, be further investigated with an *in vivo* model containing the previously described mutations in the stalk domain of ADAM10. The relevance of PS exposure for ADAM10 and ADAM17 shedding activity in a pathophysiological context would provide further insights to question if ADAM10 and ADAM17 shedding activity have a distinct role in the onset and development of various diseases. Finally, it is likely that next to ADAM10 and ADAM17 also other proteases are regulated by PS exposure, independent of whether they are members of the ADAM or another protease family. Furthermore, the identification of another protease whose activity is also regulated by PS exposure, would further support PS exposure as a more general mechanism of activation.

7. Summary

The “*a disintegrin and metalloproteinase 10*” (ADAM10) mediates the release of the vast majority of transmembrane bound or GPI-anchored substrates, together with its close homologue ADAM17. The protease is vital for several physiological and pathophysiological processes. Although ADAM10 activity in these processes is comprehensively described, little is known about the mechanism controlling the protease shedding activity. Given that the cytoplasmic domain of ADAM10 is negligible for substrate shedding, the focus of current research has shifted to the extracellular domains. In this context, also the plasma membrane itself may play an essential role in the regulation of ADAM10 shedding activity. This novel concept of the plasma membrane acting as a regulator has been recently described to be the penultimate step controlling ADAM17 shedding activity. The exposure of the phospholipid phosphatidylserine (PS) and its direct interaction with ADAM17 was identified as the primary trigger for substrate release. Based on this newly acquired knowledge for ADAM17 and the common structural and functional similarities between ADAM17 and ADAM10, this thesis focuses on the question of whether PS exposure also regulates ADAM10-mediated substrate shedding.

In the context of this overall aim, the first question was whether PS exposure regulates ADAM10-mediated substrate shedding. A series of experiments with different cell types were carried out; these showed that stimulation with different activators of ADAM10 led to enhanced externalisation of PS with a concomitant increase in substrate release. The headgroup of PS (OPS) showed a competitive inhibitory effect on ADAM10-mediated substrate release, presumably by abolishing ADAM10 interaction with PS. This inhibitory effect of OPS on ADAM10-mediated substrate release was shown for multiple ADAM10 substrates and stimuli, indicating that PS exposure is in general essential for ADAM10 shedding activity. Finally, using a rabbit erythrocyte – pVCC model, PS exposure was highlighted as the primary trigger of ADAM10-mediated substrate shedding.

Furthermore, the question arose whether calcium-activated phospholipid scramblases (e.g. anoctamin 6, TMEM16F/ANO6) might contribute to PS exposure and thereby affect ADAM10-mediated substrate release. Overexpression of phospholipid scramblase TMEM16F/ANO6 was shown to contribute to PS exposure and related enhanced ADAM10-mediated substrate release. In an approach of gain - and loss of function of TMEM16F/ANO6 scrambling activity, PS exposure was shown to be directly connected to ADAM10 shedding activity. On the one hand, the human hyperactive TMEM16F/ANO6 mutant (human ANO6 D408G) showed enhanced PS exposure in conjunction with increased ADAM10-mediated substrate release, under constitutive conditions. On the other hand, B-cells from a patient with the Scott syndrome showed TMEM16F/ANO6-related impaired PS scrambling, resulting in the absence of ADAM10 shedding activity.

The final aim was to identify the mechanism behind the interaction between ADAM10 and PS. For ADAM17, it was shown that the protease intercalates via an amphipathic helix into the lipid bilayer and interacts through a polycationic motif directly with PS. The stalk domain of ADAM10 combines these two attributes, by showing the characteristics of an amphipathic helix and containing a polycationic motif. Biophysical experiments with a peptide version of the ADAM10 stalk domain indicated a direct interaction of ADAM10 with PS and its intercalation into the phospholipid bilayer. Furthermore, the mutation of the positively charged amino acids in the stalk domain of ADAM10 significantly reduced the ability of the proteases to release its substrate betacellulin. These results highlight the importance of positively charged amino acids in the ADAM10 stalk domain for the interaction with PS and substrate shedding.

The results presented in this thesis show for the first time that the cell membrane plays an important role in the ADAM10-mediated substrate release; they also highlight PS exposure as a general regulatory mechanism for two of the most prominent proteases: ADAM10 and ADAM17.

8. Zusammenfassung

Die „*a disintegrin and metalloproteinase 10*“ (ADAM10) ist, zusammen mit seinem nächsten Verwandten ADAM17, für die Freisetzung eines Großteils der membranständigen und GPI-verankerten Substraten ist von essentieller Bedeutung. Die Aktivität der Protease ist dabei für verschiedenste physiologische und pathophysiologische Prozesse von essentieller Bedeutung. Die Aktivität von ADAM10 in diesen Prozessen wurde umfangreich beschrieben; dabei ist jedoch wenig über den Mechanismus bekannt, der die proteolytische Aktivität der Protease reguliert. Die Erkenntnis, dass die zyttoplasmatische Domäne von ADAM10 für den Prozess der Substratfreisetzung vernachlässigbar ist, verdeutlicht die Rolle der extrazellulären Domänen für die Regulation der proteolytischen Aktivität von ADAM10. In diesem Zusammenhang kommt auch der extrazellulären Seite der Zellmembran eine mögliche essentielle Rolle in der Regulation der ADAM10-vermittelten Substratfreisetzung zu. Dieses neue Konzept, das die Zellmembran als Regulator der proteolytischen Aktivität einer Protease beschreibt, wurde vor kurzem erstmals für die Metalloprotease ADAM17 gezeigt. Dabei wurde die Externalisierung des Phospholipids Phosphatidylserin (PS) und die direkte Interaktion mit ADAM17 als entscheidender regulatorischer Mechanismus für die Substratfreisetzung beschrieben. Ausgehend von diesen Ergebnissen sowie den strukturellen und funktionellen Gemeinsamkeiten von ADAM17 und ADAM10 stellt diese Arbeit die Frage in den Mittelpunkt, ob die PS-Externalisierung auch der entscheidende Aktivierungsmechanismus für die ADAM10-vermittelten Substratfreisetzung ist.

In diesem Zusammenhang stellte sich die Frage, ob ein Zusammenhang zwischen der PS-Externalisierung und der ADAM10-vermittelte Substratfreisetzung besteht. Mittels verschiedener Experimente mit unterschiedlichen Zelllinien und verschiedenen Aktivatoren von ADAM10 konnte gezeigt werden, dass eine erhöhte PS-Externalisierung zu einem Anstieg der ADAM10-vermittelte Substratfreisetzung führte. Die Inkubation von Zellen mit der Kopfgruppe von PS (OPS) führte zu einer kompetitiven Inhibition der ADAM10-induzierten Substratfreisetzung und verdeutlichte die grundlegende Bedeutung der PS-Externalisierung für die ADAM10-vermittelte Substratfreisetzung. Mit Hilfe eines Erythrozyten-Modells wurde weiterhin gezeigt, dass die PS-Externalisierung der initiale Schritt für die ADAM10-vermittelte Substratfreisetzung ist.

Aufbauend auf den Ergebnissen das die PS-Externalisierung der primäre Regulator der ADAM10-vermittelten Substratfreisetzung ist, stellte sich die Frage, ob Kalzium-aktivierte Phospholipid-Scramblasen (z.B. TMEM16F/ANO6) zur Externalisierung von PS beitragen und inwiefern dieser erhöhte Anteil von PS auf der Außenseite der Zellmembran zu einer gesteigerten ADAM10-vermittelten Substratfreisetzung führt. Die Überexpression des Phospholipid-Scramblase TMEM16F/ANO6 führte, unter induziertem Kalziumeinstrom, zu einer erhöhten PS-Externalisierung und damit verbunden zu einer Steigerung der ADAM10-Aktivität. Mit Hilfe von Experimenten, die sich eine erhöhte oder verminderte Aktivität von TMEM16F/ANO6 zu Nutzen machten, konnte die direkte Verbindung zwischen PS-Externalisierung und ADAM10-vermittelter Substratfreisetzung beschrieben werden.

Zunächst wurde mittels einer hyperaktiven Mutante von TMEM16F/ANO6 gezeigt, dass eine erhöhte Externalisierung von PS, unter basalen (intrazellulär) Kalziumkonzentration, zu einem gleichzeitigen Anstieg der Aktivität von ADAM10 führte. Weiterhin wurde mit Hilfe von B-Zellen eines Patienten mit dem Scott-Syndrom gezeigt, dass das Ausbleiben der TMEM16F/ANO6-vermittelten PS-Externalisierung zu einem Verlust der ADAM10-vermittelten Substratfreisetzung führte.

Abschließend wurde die Fragestellung nach einem möglichen Mechanismus, wie PS die proteolytische Aktivität von ADAM10 reguliert, weitergehend untersucht. Für ADAM17 konnte gezeigt werden, dass die Protease mittels einer amphipathischen Helix in die Membran inseriert und über ein polykationisches Motiv direkt mit PS interagiert. Die Stalk-Domäne von ADAM10 besitzt ein polykationisches Motiv und die Eigenschaften einer amphipathischen Helix; damit weist diese Domäne die strukturellen Voraussetzungen für eine Interaktion mit PS und eine Inserierung in die Membran auf. Mittels biophysikalischer Experiment konnte gezeigt werden, dass die Stalk-Domäne von ADAM10 direkt mit PS interagiert und in die Membran inseriert. Des Weiteren konnte gezeigt werden, dass die Mutation der positiv-geladenen Aminosäuren der ADAM10-Stalk-Domäne zu einer reduzierten Freisetzung des ADAM10-Substrates Betacellulin führte. Diese Ergebnisse deuten darauf hin, dass die positive geladenen Aminosäuren der ADAM10-Stalk-Domäne für den Prozess der Substratfreisetzung von essentieller Bedeutung sind.

Zusammenfassend weisen die Ergebnisse dieser Arbeit erstmalig nach, dass die Zellmembran eine entscheidende Rolle für die ADAM10-vermittelte Substratfreisetzung spielt und veranschaulichen dabei die PS-Externalisierung als grundlegendes regulatorisches Prinzip für zwei der meist beschriebenen Metalloproteasen: ADAM17 und ADAM10.

9. References:

- Adinolfi E, Callegari MG, Cirillo M, Pinton P, Giorgi C, Cavagna D, Rizzuto R, Di Virgilio F (2009) Expression of the P2X7 receptor increases the Ca²⁺ content of the endoplasmic reticulum, activates NFATc1, and protects from apoptosis. *J Biol Chem* 284:10120-10128.
- Adinolfi E, Callegari MG, Ferrari D, Bolognesi C, Minelli M, Wieckowski MR, Pinton P, Rizzuto R, Di Virgilio F (2005) Basal activation of the P2X7 ATP receptor elevates mitochondrial calcium and potential, increases cellular ATP levels, and promotes serum-independent growth. *Mol Biol Cell* 16:3260-3272.
- Altmepfen HC, Prox J, Krasemann S, Puig B, Kruszewski K, Dohler F, Bernreuther C, Hoxha A, Linsenmeier L, Sikorska B, Liberski PP, Bartsch U, Saftig P, Glatzel M (2015) The sheddase ADAM10 is a potent modulator of prion disease. *Elife* 4.
- Anders A (2001) Regulation of the α -secretase ADAM10 by its prodomain and proprotein convertases. *The FASEB Journal*.
- Andra J, Bohling A, Gronewold TM, Schlecht U, Perpeet M, Gutschmann T (2008) Surface acoustic wave biosensor as a tool to study the interaction of antimicrobial peptides with phospholipid and lipopolysaccharide model membranes. *Langmuir : the ACS journal of surfaces and colloids* 24:9148-9153.
- Arribas J, Borroto A (2002) Protein ectodomain shedding. *Chemical reviews* 102:4627-4638.
- Asai M, Hattori C, Szabó B, Sasagawa N, Maruyama K, Tanuma S-i, Ishiura S (2003) Putative function of ADAM9, ADAM10, and ADAM17 as APP -secretase. *Biochem Biophys Res Co* 301:231-235.
- Atapattu L, Saha N, Chheang C, Eissman MF, Xu K, Vail ME, Hii L, Llerena C, Liu Z, Horvay K, Abud HE, Kusebauch U, Moritz RL, Ding BS, Cao Z, Rafii S, Ernst M, Scott AM, Nikolov DB, Lackmann M, Janes PW (2016) An activated form of ADAM10 is tumor selective and regulates cancer stem-like cells and tumor growth. *J Exp Med* 213:1741-1757.
- Barger SW, Harmon AD (1997) Microglial activation by Alzheimer amyloid precursor protein and modulation by apolipoprotein E. *Nature* 388:878-881.
- Beyers EM, Wiedmer T, Comfurius P, Shattil SJ, Weiss HJ, Zwaal RF, Sims PJ (1992) Defective Ca(2+)-induced microvesiculation and deficient expression of procoagulant activity in erythrocytes from a patient with a bleeding disorder: a study of the red blood cells of Scott syndrome. *Blood* 79:380-388.
- Black RA, Rauch CT, Kozlosky CJ, Peschon JJ, Slack JL, Wolfson MF, Castner BJ, Stocking KL, Reddy P, Srinivasan S, Nelson N, Boiani N, Schooley KA, Gerhart M, Davis R, Fitzner JN, Johnson RS, Paxton RJ, March CJ, Cerretti DP (1997) A metalloproteinase disintegrin that releases tumour-necrosis factor- α from cells. *Nature* 385:729-733.
- Blaydon DC, Biancheri P, Di WL, Plagnol V, Cabral RM, Brooke MA, van Heel DA, Ruschendorf F, Toynbee M, Walne A, O'Toole EA, Martin JE, Lindley K, Vulliamy T, Abrams DJ, MacDonald TT, Harper JI, Kelsell DP (2011) Inflammatory skin and bowel disease linked to ADAM17 deletion. *The New England journal of medicine* 365:1502-1508.
- Blobel CP, Wolfsberg TG, Turck CW, Myles DG, Primakoff P, White JM (1992) A potential fusion peptide and an integrin ligand domain in a protein active in sperm-egg fusion. *Nature* 356:248-252.
- Borchelt DR, Rogers M, Stahl N, Telling G, Prusiner SB (1993) Release of the cellular prion protein from cultured cells after loss of its glycoinositol phospholipid anchor. *Glycobiology* 3:319-329.
- Britschgi A, Bill A, Brinkhaus H, Rothwell C, Clay I, Duss S, Rebhan M, Raman P, Guy CT, Wetzel K, George E, Popa MO, Lilley S, Choudhury H, Gosling M, Wang L, Fitzgerald S, Borawski J, Baffoe J, Labow M, Gaither LA, Bentires-Alj M (2013) Calcium-activated chloride channel ANO1 promotes breast cancer progression by activating EGFR and CAMK signaling. *Proc Natl Acad Sci U S A* 110:E1026-1034.
- Brouxhon SM, Kyrkanides S, Teng X, Athar M, Ghazizadeh S, Simon M, O'Banion MK, Ma L (2014) Soluble E-cadherin: a critical oncogene modulating receptor tyrosine kinases, MAPK and PI3K/Akt/mTOR signaling. *Oncogene* 33:225-235.
- Brummer T, Pignoni M, Rossello A, Wang H, Noy PJ, Tomlinson MG, Blobel CP, Lichtenthaler SF (2018) The metalloprotease ADAM10 (a disintegrin and metalloprotease 10) undergoes rapid, postlysis autocatalytic degradation. *Faseb J* fj201700823RR.

- Brunner JD, Lim NK, Schenck S, Duerst A, Dutzler R (2014) X-ray structure of a calcium-activated TMEM16 lipid scramblase. *Nature* 516:207-212.
- Caberoy NB, Zhou Y, Alvarado G, Fan X, Li W (2009) Efficient identification of phosphatidylserine-binding proteins by ORF phage display. *Biochem Biophys Res Commun* 386:197-201.
- Cai HB, Wang YS, McCarthy D, Wen HJ, Borchelt DR, Price DL, Wong PC (2001) BACE1 is the major beta-secretase for generation of A beta peptides by neurons. *Nat Neurosci* 4:233-234.
- Capila I, VanderNoot VA, Mealy TR, Seaton BA, Linhardt RJ (1999) Interaction of heparin with annexin V. *Febs Lett* 446:327-330.
- Chantray A, Gregson NA, Glynn P (1989) A Novel Metalloproteinase Associated with Brain Myelin Membranes - Isolation and Characterization. *J Biol Chem* 264:21603-21607.
- Checler F, Vincent B (2002) Alzheimer's and prion diseases: distinct pathologies, common proteolytic denominators. *Trends in neurosciences* 25:616-620.
- Chow VW, Mattson MP, Wong PC, Gleichmann M (2009) An Overview of APP Processing Enzymes and Products. *NeuroMolecular Medicine* 12:1-12.
- Crawford H, Dempsey P, Brown G, Adam L, Moss M (2009) ADAM10 as a Therapeutic Target for Cancer and Inflammation. *Curr Pharm Design* 15:2288-2299.
- Dasgupta SK, Guchhait P, Thiagarajan P (2006) Lactadherin binding and phosphatidylserine expression on cell surface-comparison with annexin A5. *Transl Res* 148:19-25.
- De S, Olson R (2011) Crystal structure of the *Vibrio cholerae* cytolysin heptamer reveals common features among disparate pore-forming toxins. *P Natl Acad Sci USA* 108:7385-7390.
- Deng W, Cho S, Su P-C, Berger BW, Li R (2014) Membrane-enabled dimerization of the intrinsically disordered cytoplasmic domain of ADAM10. *Proceedings of the National Academy of Sciences* 111:15987-15992.
- Devaux PF (1991) Static and dynamic lipid asymmetry in cell membranes. *Biochemistry-U.S.* 30:1163-1173.
- Di Garbo A, Alloisio S, Nobile M (2012) P2X7 receptor-mediated calcium dynamics in HEK293 cells: experimental characterization and modelling approach. *Physical biology* 9:026001.
- Dornier E, Coumailleau F, Ottavi JF, Moretti J, Boucheix C, Mauduit P, Schweisguth F, Rubinstein E (2012) TspanC8 tetraspanins regulate ADAM10/Kuzbanian trafficking and promote Notch activation in flies and mammals. *J Cell Biol* 199:481-496.
- Drozdetskiy A, Cole C, Procter J, Barton GJ (2015) JPred4: a protein secondary structure prediction server. *Nucleic acids research* 43:W389-394.
- Duffy MJ, Mullyooly M, O'Donovan N, Sukor S, Crown J, Pierce A, McGowan PM (2011) The ADAMs family of proteases: new biomarkers and therapeutic targets for cancer? *Clinical proteomics* 8:9.
- Dusterhoft S, Hobel K, Oldefest M, Lokau J, Waetzig GH, Chalaris A, Garbers C, Scheller J, Rose-John S, Lorenzen I, Grotzinger J (2014) A disintegrin and metalloprotease 17 dynamic interaction sequence, the sweet tooth for the human interleukin 6 receptor. *J Biol Chem* 289:16336-16348.
- Dusterhoft S, Jung S, Hung CW, Tholey A, Sonnichsen FD, Grotzinger J, Lorenzen I (2013) Membrane-proximal domain of a disintegrin and metalloprotease-17 represents the putative molecular switch of its shedding activity operated by protein-disulfide isomerase. *J Am Chem Soc* 135:5776-5781.
- Dusterhoft S, Michalek M, Kordowski F, Oldefest M, Sommer A, Roseler J, Reiss K, Grotzinger J, Lorenzen I (2015) Extracellular Juxtamembrane Segment of ADAM17 Interacts with Membranes and Is Essential for Its Shedding Activity. *Biochemistry-U.S.* 54:5791-5801.
- Edwards DR, Handsley MM, Pennington CJ (2008) The ADAM metalloproteinases. *Molecular aspects of medicine* 29:258-289.
- Elliott JI, Surprenant A, Marelli-Berg FM, Cooper JC, Cassady-Cain RL, Wooding C, Linton K, Alexander DR, Higgins CF (2005) Membrane phosphatidylserine distribution as a non-apoptotic signalling mechanism in lymphocytes. *Nat Cell Biol* 7:808-816.
- Endres K, Fahrenholz F (2012) Regulation of alpha-secretase ADAM10 expression and activity. *Exp Brain Res* 217:343-352.
- Escrevente C, Morais VA, Keller S, Soares CM, Altevogt P, Costa J (2008) Functional role of N-glycosylation from ADAM10 in processing, localization and activity of the enzyme. *Biochimica et Biophysica Acta (BBA) - General Subjects* 1780:905-913.
- Evan GI, Vousden KH (2001) Proliferation, cell cycle and apoptosis in cancer. *Nature* 411:342-348.

- Facey A, Pinar I, Arthur JF, Qiao J, Jing J, Mado B, Carberry J, Andrews RK, Gardiner EE (2016) A-Disintegrin-And-Metalloproteinase (ADAM) 10 Activity on Resting and Activated Platelets. *Biochemistry-Us* 55:1187-1194.
- Fisher SI, Hartzell HC (2017) Poring over furrows. *Elife* 6.
- Fries A (2013) Über den Einfluss von Melittin auf die Funktion membranständiger Proteasen der ADAM-Familie.
- Garbers C, Janner N, Chalaris A, Moss ML, Floss DM, Meyer D, Koch-Nolte F, Rose-John S, Scheller J (2011) Species specificity of ADAM10 and ADAM17 proteins in interleukin-6 (IL-6) trans-signaling and novel role of ADAM10 in inducible IL-6 receptor shedding. *J Biol Chem* 286:14804-14811.
- Gerlach H, Laumann V, Martens S, Becker CF, Goody RS, Geyer M (2010) HIV-1 Nef membrane association depends on charge, curvature, composition and sequence. *Nature chemical biology* 6:46-53.
- Gibb DR, El Shikh M, Kang DJ, Rowe WJ, El Sayed R, Cichy J, Yagita H, Tew JG, Dempsey PJ, Crawford HC, Conrad DH (2010) ADAM10 is essential for Notch2-dependent marginal zone B cell development and CD23 cleavage in vivo. *J Exp Med* 207:623-635.
- Giebler N, Zigrino P (2016) A Disintegrin and Metalloprotease (ADAM): Historical Overview of Their Functions. *Toxins (Basel)* 8:122.
- Groot AJ, Vooijs MA (2012) The Role of Adams in Notch Signaling. *727:15-36*.
- Grosdidier A, Zoete V, Michielin O (2011) SwissDock, a protein-small molecule docking web service based on EADock DSS. *Nucleic acids research* 39:W270-277.
- Gu B, Bendall LJ, Wiley JS (1998) Adenosine triphosphate-induced shedding of CD23 and L-selectin (CD62L) from lymphocytes is mediated by the same receptor but different metalloproteases. *Blood* 92:946-951.
- Guo J, He L, Yuan P, Wang P, Lu Y, Tong F, Wang Y, Yin Y, Tian J, Sun J (2012) ADAM10 overexpression in human non-small cell lung cancer correlates with cell migration and invasion through the activation of the Notch1 signaling pathway. *Oncol Rep* 28:1709-1718.
- Halbleib JM, Nelson WJ (2006) Cadherins in development: cell adhesion, sorting, and tissue morphogenesis. *Genes & Development* 20:3199-3214.
- Harris B, Pereira I, Parkin E (2009) Targeting ADAM10 to lipid rafts in neuroblastoma SH-SY5Y cells impairs amyloidogenic processing of the amyloid precursor protein. *Brain Res* 1296:203-215.
- Hartmann D, de Strooper B, Serneels L, Craessaerts K, Herreman A, Annaert W, Umans L, Lubke T, Illert AL, von Figura K, Saftig P (2002) The disintegrin/metalloprotease ADAM 10 is essential for Notch signalling but not for alpha-secretase activity in fibroblasts. *Hum Mol Genet* 11:2615-2624.
- Hinkle CL, Mohan MJ, Lin P, Yeung N, Rasmussen F, Milla ME, Moss ML (2003) Multiple metalloproteinases process protransforming growth factor-alpha (proTGF-alpha). *Biochemistry-Us* 42:2127-2136.
- Hooper NM (2005) Roles of proteolysis and lipid rafts in the processing of the amyloid precursor protein and prion protein. *Biochem Soc Trans* 33:335-338.
- Horiuchi K, Le Gall S, Schulte M, Yamaguchi T, Reiss K, Murphy G, Toyama Y, Hartmann D, Saftig P, Blobel CP (2006) Substrate Selectivity of Epidermal Growth Factor-Receptor Ligand Sheddases and their Regulation by Phorbol Esters and Calcium Influx. *Mol Biol Cell* 18:176-188.
- Howard L, Lu XH, Mitchell S, Griffiths S, Glynn P (1996) Molecular cloning of MADM: A catalytically active mammalian disintegrin-metalloprotease expressed in various cell types. *Biochem J* 317:45-50.
- Huxley-Jones J, Clarke TK, Beck C, Toubaris G, Robertson DL, Boot-Handford RP (2007) The evolution of the vertebrate metzincins; insights from *Ciona intestinalis* and *Danio rerio*. *Bmc Evol Biol* 7:63.
- Irwin JJ, Sterling T, Mysinger MM, Bolstad ES, Coleman RG (2012) ZINC: a free tool to discover chemistry for biology. *Journal of chemical information and modeling* 52:1757-1768.
- Janes PW, Saha N, Barton WA, Kolev MV, Wimmer-Kleikamp SH, Nievergall E, Blobel CP, Himanen JP, Lackmann M, Nikolov DB (2005) Adam meets Eph: an ADAM substrate recognition module acts as a molecular switch for ephrin cleavage in trans. *Cell* 123:291-304.

- Jorissen E, Prox J, Bernreuther C, Weber S, Schwanbeck R, Serneels L, Snellinx A, Craessaerts K, Thathiah A, Tesseur I, Bartsch U, Weskamp G, Blobel CP, Glatzel M, De Strooper B, Saftig P (2010) The disintegrin/metalloproteinase ADAM10 is essential for the establishment of the brain cortex. *J Neurosci* 30:4833-4844.
- Jouannet S, Saint-Pol J, Fernandez L, Nguyen V, Charrin S, Boucheix C, Brou C, Milhiet PE, Rubinstein E (2016) TspanC8 tetraspanins differentially regulate the cleavage of ADAM10 substrates, Notch activation and ADAM10 membrane compartmentalization. *Cell Mol Life Sci* 73:1895-1915.
- Kim YE, Chen J, Chan JR, Langen R (2010) Engineering a polarity-sensitive biosensor for time-lapse imaging of apoptotic processes and degeneration. *Nature methods* 7:67-73.
- Kmit A, van Kruchten R, Ousingasawat J, Mattheij NJ, Senden-Gijsbers B, Heemskerk JW, Schreiber R, Bevers EM, Kunzelmann K (2013) Calcium-activated and apoptotic phospholipid scrambling induced by Ano6 can occur independently of Ano6 ion currents. *Cell Death Dis* 4:e611.
- Kojima H, Newton-Nash D, Weiss HJ, Zhao J, Sims PJ, Wiedmer T (1994) Production and characterization of transformed B-lymphocytes expressing the membrane defect of Scott syndrome. *J Clin Invest* 94:2237-2244.
- Kojro E, Gimpl G, Lammich S, Marz W, Fahrenholz F (2001) Low cholesterol stimulates the nonamyloidogenic pathway by its effect on the α -secretase ADAM 10. *Proceedings of the National Academy of Sciences* 98:5815-5820.
- Kuhn PH, Wang H, Dislich B, Colombo A, Zeitschel U, Ellwart JW, Kremmer E, Rossner S, Lichtenthaler SF (2010) ADAM10 is the physiologically relevant, constitutive α -secretase of the amyloid precursor protein in primary neurons. *Embo J* 29:3020-3032.
- Lam YH, Wassall SR, Morton CJ, Smith R, Separovic F (2001) Solid-state NMR structure determination of melittin in a lipid environment. *Biophys J* 81:2752-2761.
- Lang KS, Durantou C, Poehlmann H, Myssina S, Bauer C, Lang F, Wieder T, Huber SM (2003) Cation channels trigger apoptotic death of erythrocytes. *Cell Death Differ* 10:249-256.
- Lee SB, Schramme A, Doberstein K, Dummer R, Abdel-Bakky MS, Keller S, Altevogt P, Oh ST, Reichrath J, Oxmann D, Pfeilschifter J, Mihic-Probst D, Gutwein P (2010) ADAM10 is upregulated in melanoma metastasis compared with primary melanoma. *J Invest Dermatol* 130:763-773.
- Lemmon MA (2008) Membrane recognition by phospholipid-binding domains. *Nature reviews Molecular cell biology* 9:99-111.
- Leventis PA, Grinstein S (2010) The distribution and function of phosphatidylserine in cellular membranes. *Annual review of biophysics* 39:407-427.
- Lhermusier T, Chap H, Payrastre B (2011) Platelet membrane phospholipid asymmetry: from the characterization of a scramblase activity to the identification of an essential protein mutated in Scott syndrome. *J Thromb Haemost* 9:1883-1891.
- Li X, Perez L, Pan Z, Fan H (2007) The transmembrane domain of TACE regulates protein ectodomain shedding. *Cell Res* 17:985-998.
- Linsenmeier L, Altmepfen HC, Wetzel S, Mohammadi B, Saftig P, Glatzel M (2017) Diverse functions of the prion protein - Does proteolytic processing hold the key? *Biochimica et biophysica acta*.
- Linsenmeier L, Mohammadi B, Wetzel S, Puig B, Jackson WS, Hartmann A, Uchiyama K, Sakaguchi S, Endres K, Tatzelt J, Saftig P, Glatzel M, Altmepfen HC (2018) Structural and mechanistic aspects influencing the ADAM10-mediated shedding of the prion protein. *Mol Neurodegener* 13:18.
- Liu H, Shim AH, He X (2009) Structural characterization of the ectodomain of a disintegrin and metalloproteinase-22 (ADAM22), a neural adhesion receptor instead of metalloproteinase: insights on ADAM function. *J Biol Chem* 284:29077-29086.
- Lorenzen I, Lokau J, Dusterhoft S, Trad A, Garbers C, Scheller J, Rose-John S, Grotzinger J (2012) The membrane-proximal domain of A Disintegrin and Metalloprotease 17 (ADAM17) is responsible for recognition of the interleukin-6 receptor and interleukin-1 receptor II. *FEBS Lett* 586:1093-1100.
- Loura LM, Prieto M (2011) FRET in Membrane Biophysics: An Overview. *Frontiers in physiology* 2:82.
- Marambaud P, Shioi J, Serban G, Georgakopoulos A, Sarnier S, Nagy V, Baki L, Wen P, Efthimiopoulos S, Shao Z, Wisniewski T, Robakis NK (2002) A presenilin-1/ γ -secretase cleavage

- releases the E-cadherin intracellular domain and regulates disassembly of adherens junctions. *Embo J* 21:1948-1956.
- Maretzky T, Blobel CP, Guaiquil V (2014) Characterization of oxygen-induced retinopathy in mice carrying an inactivating point mutation in the catalytic site of ADAM15. *Invest Ophthalmol Vis Sci* 55:6774-6782.
- Maretzky T, Evers A, Le Gall S, Alabi RO, Speck N, Reiss K, Blobel CP (2015) The cytoplasmic domain of a disintegrin and metalloproteinase 10 (ADAM10) regulates its constitutive activity but is dispensable for stimulated ADAM10-dependent shedding. *J Biol Chem* 290:7416-7425.
- Maretzky T, Reiss K, Ludwig A, Buchholz J, Scholz F, Proksch E, de Strooper B, Hartmann D, Saftig P (2005) ADAM10 mediates E-cadherin shedding and regulates epithelial cell-cell adhesion, migration, and beta-catenin translocation. *Proc Natl Acad Sci U S A* 102:9182-9187.
- Maretzky T, Swendeman S, Mogollon E, Weskamp G, Sahin U, Reiss K, Blobel CP (2017) Characterization of the catalytic properties of the membrane-anchored metalloproteinase ADAM9 in cell-based assays. *Biochem J* 474:1467-1479.
- Maretzky T, Yang G, Ouerfelli O, Overall CM, Worpenberg S, Hassiepen U, Eder J, Blobel CP (2009) Characterization of the catalytic activity of the membrane-anchored metalloproteinase ADAM15 in cell-based assays. *Biochem J* 420:105-113.
- Matthews AL, Noy PJ, Reyat JS, Tomlinson MG (2017a) Regulation of A disintegrin and metalloproteinase (ADAM) family sheddases ADAM10 and ADAM17: The emerging role of tetraspanins and rhomboids. *Platelets* 28:333-341.
- Matthews AL, Szyroka J, Collier R, Noy PJ, Tomlinson MG (2017b) Scissor sisters: regulation of ADAM10 by the TspanC8 tetraspanins. *Biochem Soc Trans* 45:719-730.
- Morgan AJ, Jacob R (1994) Ionomycin enhances Ca²⁺ influx by stimulating store-regulated cation entry and not by a direct action at the plasma membrane. *Biochem J* 300 (Pt 3):665-672.
- Moss ML, Bomar M, Liu Q, Sage H, Dempsey P, Lenhart PM, Gillispie PA, Stoeck A, Wildeboer D, Bartsch JW, Palmisano R, Zhou P (2007) The ADAM10 prodomain is a specific inhibitor of ADAM10 proteolytic activity and inhibits cellular shedding events. *J Biol Chem* 282:35712-35721.
- Moss ML, Jin SLC, Milla ME, Burkhart W, Carter HL, Chen W-J, Clay WC, Didsbury JR, Hassler D, Hoffman CR, Kost TA, Lambert MH, Leesnitzer MA, McCauley P, McGeehan G, Mitchell J, Moyer M, Pahel G, Rocque W, Overton LK, Schoenen F, Seaton T, Su J-L, Warner J, Willard D, Becherer JD (1997) Cloning of a disintegrin metalloproteinase that processes precursor tumour-necrosis factor-[alpha]. *Nature* 385:733-736.
- Moulder K, Barton A, Weston B (1993) CD23-mediated homotypic cell adhesion: the role of proteolysis. *European journal of immunology* 23:2066-2071.
- Nagata S, Suzuki J, Segawa K, Fujii T (2016) Exposure of phosphatidylserine on the cell surface. *Cell Death Differ* 23:952-961.
- North RA (2002) Molecular physiology of P2X receptors. *Physiological reviews* 82:1013-1067.
- Noy PJ, Yang J, Reyat JS, Matthews AL, Charlton AE, Furnston J, Rogers DA, Rainger GE, Tomlinson MG (2016) TspanC8 Tetraspanins and A Disintegrin and Metalloprotease 10 (ADAM10) Interact via Their Extracellular Regions: EVIDENCE FOR DISTINCT BINDING MECHANISMS FOR DIFFERENT TspanC8 PROTEINS. *J Biol Chem* 291:3145-3157.
- Olson R, Gouaux E (2005) Crystal structure of the *Vibrio cholerae* cytolysin (VCC) pro-toxin and its assembly into a heptameric transmembrane pore. *J Mol Biol* 350:997-1016.
- Ousingsawat J, Wanitchakool P, Kmit A, Romao AM, Jantarajit W, Schreiber R, Kunzelmann K (2015) Anoctamin 6 mediates effects essential for innate immunity downstream of P2X7 receptors in macrophages. *Nat Commun* 6:6245.
- Paulino C, Neldner Y, Lam AK, Kalienkova V, Brunner JD, Schenck S, Dutzler R (2017) Structural basis for anion conduction in the calcium-activated chloride channel TMEM16A. *Elife* 6.
- Postina R, Schroeder A, Dewachter I, Bohl J, Schmitt U, Kojro E, Prinzen C, Endres K, Hiemke C, Blessing M, Flamez P, Dequenne A, Godaux E, van Leuven F, Fahrenholz F (2004) A disintegrin-metalloproteinase prevents amyloid plaque formation and hippocampal defects in an Alzheimer disease mouse model. *J Clin Invest* 113:1456-1464.
- Primakoff P, Hyatt H, Tredick-Kline J (1987) Identification and purification of a sperm surface protein with a potential role in sperm-egg membrane fusion. *J Cell Biol* 104:141-149.

- Pruessmeyer J, Ludwig A (2009) The good, the bad and the ugly substrates for ADAM10 and ADAM17 in brain pathology, inflammation and cancer. *Semin Cell Dev Biol* 20:164-174.
- Puente XS, Sanchez LM, Overall CM, Lopez-Otin C (2003) Human and mouse proteases: a comparative genomic approach. *Nature reviews Genetics* 4:544-558.
- Pupovac A, Foster CM, Sluyter R (2013) Human P2X7 receptor activation induces the rapid shedding of CXCL16. *Biochem Biophys Res Commun* 432:626-631.
- Pupovac A, Geraghty NJ, Watson D, Sluyter R (2015) Activation of the P2X7 receptor induces the rapid shedding of CD23 from human and murine B cells. *Immunol Cell Biol* 93:77-85.
- Pupovac A, Sluyter R (2016) Roles of extracellular nucleotides and P2 receptors in ectodomain shedding. *Cell Mol Life Sci* 73:4159-4173.
- R Core T (2017) R: A Language and Environment for Statistical Computing.
- Rajaratnam K, Rosgen J (2014) Isothermal titration calorimetry of membrane proteins - progress and challenges. *Biochimica et biophysica acta* 1838:69-77.
- Reiss K, Bhakdi S (2012) Pore-forming bacterial toxins and antimicrobial peptides as modulators of ADAM function. *Medical microbiology and immunology* 201:419-426.
- Reiss K, Cornelsen I, Husmann M, Gimpl G, Bhakdi S (2011) Unsaturated fatty acids drive disintegrin and metalloproteinase (ADAM)-dependent cell adhesion, proliferation, and migration by modulating membrane fluidity. *J Biol Chem* 286:26931-26942.
- Reiss K, Maretzky T, Ludwig A, Tousseyn T, de Strooper B, Hartmann D, Saftig P (2005) ADAM10 cleavage of N-cadherin and regulation of cell-cell adhesion and beta-catenin nuclear signalling. *Embo J* 24:742-752.
- Reiss K, Saftig P (2009) The "a disintegrin and metalloprotease" (ADAM) family of sheddases: physiological and cellular functions. *Semin Cell Dev Biol* 20:126-137.
- Rosing J, Bevers EM, Comfurius P, Hemker HC, van Dieijen G, Weiss HJ, Zwaal RF (1985) Impaired factor X and prothrombin activation associated with decreased phospholipid exposure in platelets from a patient with a bleeding disorder. *Blood* 65:1557-1561.
- Saftig P, Lichtenthaler SF (2015) The alpha secretase ADAM10: A metalloprotease with multiple functions in the brain. *Prog Neurobiol* 135:1-20.
- Saftig P, Reiss K (2011) The "A Disintegrin And Metalloproteases" ADAM10 and ADAM17: novel drug targets with therapeutic potential? *Eur J Cell Biol* 90:527-535.
- Sahin U, Weskamp G, Kelly K, Zhou H-M, Higashiyama S, Peschon J, Hartmann D, Saftig P, Blobel CP (2004) Distinct roles for ADAM10 and ADAM17 in ectodomain shedding of six EGFR ligands. *The Journal of Cell Biology* 164:769-779.
- Sala-Rabanal M, Yurtsever Z, Nichols CG, Brett TJ (2015) Secreted CLCA1 modulates TMEM16A to activate Ca²⁺-dependent chloride currents in human cells. *Elife* 4.
- Sanderson MP, Erickson SN, Gough PJ, Garton KJ, Wille PT, Raines EW, Dunbar AJ, Dempsey PJ (2005) ADAM10 Mediates Ectodomain Shedding of the Betacellulin Precursor Activated by p-Aminophenylmercuric Acetate and Extracellular Calcium Influx. *J Biol Chem* 280:1826-1837.
- Saraceno C, Marcello E, Di Marino D, Borroni B, Claeysen S, Perroy J, Padovani A, Tramontano A, Gardoni F, Di Luca M (2014) SAP97-mediated ADAM10 trafficking from Golgi outposts depends on PKC phosphorylation. *Cell Death and Disease* 5:e1547.
- Schulz B, Pruessmeyer J, Maretzky T, Ludwig A, Blobel CP, Saftig P, Reiss K (2008) ADAM10 regulates endothelial permeability and T-Cell transmigration by proteolysis of vascular endothelial cadherin. *Circ Res* 102:1192-1201.
- Seegar TCM, Killingsworth LB, Saha N, Meyer PA, Patra D, Zimmerman B, Janes PW, Rubinstein E, Nikolov DB, Skinotis G, Kruse AC, Blacklow SC (2017) Structural Basis for Regulated Proteolysis by the alpha-Secretase ADAM10. *Cell* 171:1638-1648 e1637.
- Segawa K, Nagata S (2015) An Apoptotic 'Eat Me' Signal: Phosphatidylserine Exposure. *Trends in cell biology* 25:639-650.
- Segawa K, Suzuki J, Nagata S (2011) Constitutive exposure of phosphatidylserine on viable cells. *Proc Natl Acad Sci U S A* 108:19246-19251.
- Sharma B, Kanwar SS (2017) Phosphatidylserine: A cancer cell targeting biomarker. *Seminars in cancer biology*.
- Sigal CT, Zhou W, Buser CA, McLaughlin S, Resh MD (1994) Amino-terminal basic residues of Src mediate membrane binding through electrostatic interaction with acidic phospholipids. *Proc Natl Acad Sci U S A* 91:12253-12257.

- Sluyter R, Shemon AN, Hughes WE, Stevenson RO, Georgiou JG, Eslick GD, Taylor RM, Wiley JS (2007a) Canine erythrocytes express the P2X7 receptor: greatly increased function compared with human erythrocytes. *American journal of physiology Regulatory, integrative and comparative physiology* 293:R2090-2098.
- Sluyter R, Shemon AN, Wiley JS (2007b) P2X(7) receptor activation causes phosphatidylserine exposure in human erythrocytes. *Biochem Biophys Res Commun* 355:169-173.
- Sommer A, Fries A, Cornelsen I, Speck N, Koch-Nolte F, Gimpl G, Andra J, Bhakdi S, Reiss K (2012) Melittin modulates keratinocyte function through P2 receptor-dependent ADAM activation. *J Biol Chem* 287:23678-23689.
- Sommer A, Kordowski F, Buch J, Maretzky T, Evers A, Andra J, Dusterhoft S, Michalek M, Lorenzen I, Somasundaram P, Tholey A, Sonnichsen FD, Kunzelmann K, Heinbockel L, Nehls C, Gutschmann T, Grotzinger J, Bhakdi S, Reiss K (2016) Phosphatidylserine exposure is required for ADAM17 sheddase function. *Nat Commun* 7:11523.
- Spiegel PC, Kaiser SM, Simon JA, Stoddard BL (2004) Disruption of protein-membrane binding and identification of small-molecule inhibitors of coagulation factor VIII. *Chemistry & biology* 11:1413-1422.
- Stein TD, Anders NJ, DeCarli C, Chan SL, Mattson MP, Johnson JA (2004) Neutralization of transthyretin reverses the neuroprotective effects of secreted amyloid precursor protein (APP) in APPSW mice resulting in tau phosphorylation and loss of hippocampal neurons: support for the amyloid hypothesis. *J Neurosci* 24:7707-7717.
- Steinhusen U, Weiske J, Badock V, Tauber R, Bommert K, Huber O (2001) Cleavage and shedding of E-cadherin after induction of apoptosis. *J Biol Chem* 276:4972-4980.
- Suzuki J, Denning DP, Imanishi E, Horvitz HR, Nagata S (2013) Xk-related protein 8 and CED-8 promote phosphatidylserine exposure in apoptotic cells. *Science* 341:403-406.
- Suzuki J, Imanishi E, Nagata S (2016) Xkr8 phospholipid scrambling complex in apoptotic phosphatidylserine exposure. *Proc Natl Acad Sci U S A* 113:9509-9514.
- Suzuki J, Umeda M, Sims PJ, Nagata S (2010) Calcium-dependent phospholipid scrambling by TMEM16F. *Nature* 468:834-838.
- Tait JF, Gibson D (1992) Phospholipid binding of annexin V: effects of calcium and membrane phosphatidylserine content. *Arch Biochem Biophys* 298:187-191.
- Toti F, Satta N, Fressinaud E, Meyer D, Freyssinet JM (1996) Scott syndrome, characterized by impaired transmembrane migration of procoagulant phosphatidylserine and hemorrhagic complications, is an inherited disorder. *Blood* 87:1409-1415.
- Tousseyn T, Thathiah A, Jorissen E, Raemaekers T, Konietzko U, Reiss K, Maes E, Snellinx A, Serneels L, Nyabi O, Annaert W, Saftig P, Hartmann D, De Strooper B (2009) ADAM10, the rate-limiting protease of regulated intramembrane proteolysis of Notch and other proteins, is processed by ADAMS-9, ADAMS-15, and the gamma-secretase. *J Biol Chem* 284:11738-11747.
- Turk B (2006) Targeting proteases: successes, failures and future prospects. *Nature reviews Drug discovery* 5:785-799.
- Valeva A, Walev I, Weis S, Boukhallouk F, Wassenaar TM, Endres K, Fahrenholz F, Bhakdi S, Zitzer A (2004) A cellular metalloproteinase activates *Vibrio cholerae* pro-cytolysin. *J Biol Chem* 279:25143-25148.
- Vallabhapurapu SD, Blanco VM, Sulaiman MK, Vallabhapurapu SL, Chu Z, Franco RS, Qi X (2015) Variation in human cancer cell external phosphatidylserine is regulated by flippase activity and intracellular calcium. *Oncotarget* 6:34375-34388.
- van Engeland M, Ramaekers FC, Schutte B, Reutelingsperger CP (1996) A novel assay to measure loss of plasma membrane asymmetry during apoptosis of adherent cells in culture. *Cytometry* 24:131-139.
- van Meer G, Voelker DR, Feigenson GW (2008) Membrane lipids: where they are and how they behave. *Nature reviews Molecular cell biology* 9:112-124.
- von Kugelgen I, Hoffmann K (2016) Pharmacology and structure of P2Y receptors. *Neuropharmacology* 104:50-61.
- Weber S, Saftig P (2012) Ectodomain shedding and ADAMs in development. *Development* 139:3693-3709.

- Wente (2010) Expression of A disintegrin and metalloprotease 10 in pancreatic carcinoma. *Int J Mol Med* 26.
- Weskamp G, Ford JW, Sturgill J, Martin S, Docherty AJ, Swendeman S, Broadway N, Hartmann D, Saftig P, Umland S, Sehara-Fujisawa A, Black RA, Ludwig A, Becherer JD, Conrad DH, Blobel CP (2006) ADAM10 is a principal 'shedase' of the low-affinity immunoglobulin E receptor CD23. *Nat Immunol* 7:1293-1298.
- Williamson P (2015) Phospholipid Scramblases. *Lipid insights* 8:41-44.
- Williamson P, Christie A, Kohlin T, Schlegel RA, Comfurius P, Harmsma M, Zwaal RF, Bevers EM (2001) Phospholipid scramblase activation pathways in lymphocytes. *Biochemistry-Us* 40:8065-8072.
- Wong GE, Zhu X, Prater CE, Oh E, Evans JP (2001) Analysis of Fertilin α (ADAM1)-mediated Sperm-Egg Cell Adhesion during Fertilization and Identification of an Adhesion-mediating Sequence in the Disintegrin-like Domain. *J Biol Chem* 276:24937-24945.
- Xu P, Liu J, Sakaki-Yumoto M, Derynck R (2012) TACE activation by MAPK-mediated regulation of cell surface dimerization and TIMP3 association. *Science signaling* 5:ra34.
- Yang CL, Jiang FQ, Xu F, Jiang GX (2012a) ADAM10 overexpression confers resistance to doxorubicin-induced apoptosis in hepatocellular carcinoma. *Tumour biology : the journal of the International Society for Oncodevelopmental Biology and Medicine* 33:1535-1541.
- Yang H, Kim A, David T, Palmer D, Jin T, Tien J, Huang F, Cheng T, Coughlin SR, Jan YN, Jan LY (2012b) TMEM16F forms a Ca²⁺-activated cation channel required for lipid scrambling in platelets during blood coagulation. *Cell* 151:111-122.
- You B, Shan Y, Shi S, Li X, You Y (2015) Effects of ADAM10 upregulation on progression, migration, and prognosis of nasopharyngeal carcinoma. *Cancer Sci* 106:1506-1514.
- Yu K, Whitlock JM, Lee K, Ortlund EA, Cui YY, Hartzell HC (2015) Identification of a lipid scrambling domain in ANO6/TMEM16F. *Elife* 4:e06901.
- Yu P, Kosco-Vilbois M, Richards M, Kohler G, Lamers MC (1994) Negative feedback regulation of IgE synthesis by murine CD23. *Nature* 369:753-756.
- Zaitseva E, Zaitsev E, Melikov K, Arakelyan A, Marin M, Villasmil R, Margolis LB, Melikyan GB, Chernomordik LV (2017) Fusion Stage of HIV-1 Entry Depends on Virus-Induced Cell Surface Exposure of Phosphatidylserine. *Cell Host Microbe* 22:99-110 e117.
- Zhuang J, Wei Q, Lin Z, Zhou C (2015) Effects of ADAM10 deletion on Notch-1 signaling pathway and neuronal maintenance in adult mouse brain. *Gene* 555:150-158.
- Zwaal RF, Comfurius P, Bevers EM (2004) Scott syndrome, a bleeding disorder caused by defective scrambling of membrane phospholipids. *Biochimica et biophysica acta* 1636:119-128.

10. List of figures

Figure 1. Overview of the zinc-dependent proteases superfamilies.....	8
Figure 2. Structural overview and characteristics of ADAM10.....	10
Figure 3. ADAM10-mediated substrate release and its implications for cell signalling.	14
Figure 4. Anoctamins and phospholipid scrambling.....	21
Figure 5. COS7 cells expose PS under ionomycin and melittin stimulation.	47
Figure 6. OPS inhibits ADAM10-mediated BTC-AP shedding.	49
Figure 7. OPS inhibits ADAM10-mediated VE-Cad-AP shedding.....	50
Figure 8. OPS inhibits ADAM10-mediated shedding of endogenous N-cadherin and E-cadherin.	52
Figure 9. ADAM10 bona fide enzymatic activity remains functional under OPS.....	54
Figure 10. Rabbit erythrocyte – pVCC mode1	55
Figure 11. P2 receptor activation leads to PS exposure on rabbit erythrocytes.	56
Figure 12. P2 receptor activation leads to VCC driven hemolysis.....	58
Figure 13. PS regulates ADAM10-mediated cleavage of pVCC and rabbit erythrocytes hemolysis.	59
Figure 14. Overexpression of TMEM16/FANO6GFP increases PS exposure in COS7 cells.	60
Figure 15. Stimulation of TMEM16F/ANO6GFP and TMEM16A/ANO1GFP overexpressing COS7 cells leads to enhanced PS exposure.	62
Figure 16. Overexpression of TMEM16F/ANO6GFP leads to a significant increase in PS exposure.....	63
Figure 17. TMEM16F/ANO6 and TMEM16A/ANO1 overexpression enhance ADAM10- mediated substrate release.....	64
Figure 18. PS levels determined ADAM10-mediated shedding activity.....	65
Figure 19. Hyperactive TMEM16F/ANO6 D408 leads to constitutive high PS exposure.....	67
Figure 20. TMEM16F/ANO6 D408G overexpression led to constantly enhanced substrate shedding.....	68
Figure 21. TMEM16F/ANO6 D408G overexpression drives ADAM10-mediated substrate shedding.....	69
Figure 22. Loss of function of TMEM16F/ANO6 abolishes ADAM10-mediated shedding of CD23.	71
Figure 23. Impaired shedding of CD23 from Scott B-cells is unrelated to ADAM10 or P2X7R expression.....	72
Figure 24. ADAM10 stalk domain is predestined for the interaction with PS.	74
Figure 25. ADAM10 stalk domain interacts with PS.	76
Figure 26. ADAM10 shedding activity requires a positively charged stalk domain.	78
Figure 27. The mADAM10 Stalk 2 mutant is expressed and transported to the cell surface.	79
Figure 28. ADAM10 enzymatic activity alters under enhanced PS exposure.....	82
Figure 29. PS exposure and interaction with ADAM10 initialise substrate processing.....	97

11.List of tables

Table 1. Substrates released by ADAM10 and their relevance in diseases.	15
Table 2. Eukaryotic plasma membrane phospholipids abundance and localisation*.	18
Table 3. Consumables.	23
Table 4. Laboratory standard equipment.	24
Table 5. Chemicals and provider.	25
Table 6. Commercial kits and provider.	27
Table 7. Software and developer.	27
Table 8. Stimuli and inhibitors.	28
Table 9. Primary antibodies.	28
Table 10. Secondary antibodies.	29
Table 11. Plasmids.	29
Table 12. Buffer recipes.	30
Table 13. Cells and cell lines used in this thesis.	32
Table 14. List of the ADAM10wt mutagenesis and sequencing primers.	35
Table 15. SDS page composition.	38

12. Abbreviations

% (v/v)	Percentage volume/volume
% (w/v)	Percentage weight/volume
°C	degree Celsius
μ	Micro
ABB	Annexin binding buffer
ADAM10	A disintegrin and metalloproteinase 10
ADAM17	A disintegrin and metalloproteinase 17
ADAMDEC-1	ADAM-like decysin 1
ADAMTS	A disintegrin and metalloproteinase with a thrombospondin motif
AEBSF	4-(2-Aminoethyl)benzenesulfonylfluorid
ANOVA	Analysis of variance
AP	Alkaline phosphatase
APC	Allophycocyanin
APP	Amyloid precursor protein
ATP	adenosine 5'-triphosphate
BACE	Beta-secretase
BSA	Bovine serum albumin
BTC	Betacellulin
bzATP	Benzoyl adenosine 5'-triphosphate
CANDIS	Conserved ADAM-SeventeenN Dynamic Interaction Sequence
CD	Cluster of differentiation (e.g., CD23)
CH	Switzerland
CO	Control
COS7	Fibroblast-like cell line from <i>C. aethiops</i>
CTF	Carboxyl terminal fragment
CXCL16	Chemokine (C-X-C motif) ligand 16
DAPI	4',6-Diamidin-2-phenylindol
DMEM	Dulbecco's Modified Eagle's Medium
DNA	Deoxyribonucleic acid
E-, N-, VE-cadherin	Epithelial-, neuronal-, vascular endothelial-cadherin
EGF	Epidermal growth factor
EGFR	Epidermal growth factor receptor
EGFR	Epidermal growth factor receptor
ER	Endoplasmic reticulum
ER	Endoplasmic reticulum
ErbB2	Erb-B2 Receptor Tyrosine Kinase 2
FACS	Fluorescence-activated cell sorting
FBS	Fetal bovine serum
FITC	Fluorescein isothiocyanate
FRET	Fluorescence resonance energy transfer
g	gramm
GAPDH	Glyceraldehyde -3-phosphate dehydrogenase
GER	Germany
GPI	Glycophosphatidylinositol
HEK293T	Human embryonic kidney cells 293T

HIV	Human immunodeficiency virus
HIV-1	Human immunodeficiency virus type 1
HRP	Horse-raddish peroxidase
IgE	Immunoglobulin E
IO	Ionomycin
iRhoms	inactive rhomboid proteases
JPN	Japan
l	Liter
LB-medium	Lysogeny broth medium
L-selectin	Leukocyte selectin
M	Molarity
Mef	Murine embryonic fibroblast
Mel	Melittin
MM	Marimastat
MPD	Membrane proximal domain
N-Cad, E-Cad, VE-Cad	Neuronal cadherin, epithelial cadherin, vascular endothelial cadherin
Nef	Negative Regulatory Factor
NS	Non-significant
OPC	Ortho-phosphocholine
OPC	O-phosphocholine
OPS	Ortho-phosphoserine
OPS	O-phosphoserine
P2 receptor	ATP activated purinergic receptor
PA	Phosphatidic acid
PBS	Phosphate buffered saline
PC	Phosphatidylcholine
PCR	Polymerase chain reaction
PDI	Protein disulfide-isomerase
PE	Phosphatidylethanolamin
PE	Phosphatidylethanolamine
Pen/Strep	Penicillin/Streptomycin
PI	Propidium iodide
PI	Phosphatidylinositol
PKC- α	Protein kinase alpha
p-NP	p-nitrophenyl
p-NPP	p-nitrophenyl phosphate
PrP ^c	Cellular prion protein
PrP ^c	Cellular prion protein
PS	Phosphatidylserine
pVCC	Pro <i>Vibrio cholerae</i> cytolysin
PVDF	Polyvinylidene difluoride
RPMI	Roswell Park Memorial Institute medium
s.e.m	Standard error of mean
SAP97	synapse-associated protein 97
SAW	Surface acoustic wave
SDS-Page	Sodium dodecyl sulfate polyacrylamide
siRNA	Small interfering RNA
SM	Sphingomyelin

SM	Sphingomyelin
SOC medium	SOB medium with glucose
Stalk	Extracellular juxtamembrane
SVMP	Snake venom metalloproteinase
SVMP	Snake venom metalloprotease
TACE	Tumor necrosis factor-alpha-converting enzyme
TAPI	Metalloprotease broad spectrum inhibitor
TBS	Tris-buffered saline
TBST	Tris-buffered saline with Tween20,
TGF-alpha	Transforming growth factor alpha
TGF- α	Transforming growth factor alpha
TMD	Transmembrane domain
TMEM16A/ANO1	Anoctamin 1
TMEM16F/ANO6	Anoctamin 6
TNF- α	Tumor necrosis factor alpha
Tspan	Tetraspanin
UK	United Kingdom
USA	United States of America
VE-Cad	Vascular endothelial cadherin
WB	Western Blot
wt	Wildtype
xg	gravitational force
Xkr8	Xk-related protein 8

13.Acknowledgments

First, I want to thank my supervisor Karina Reiss for being part of her group and the opportunity to work on my thesis project. Her scientific support, the constructive discussions and her trust in my abilities guided me through the entire time as a PhD student.

My gratefulness is also dedicated to Anselm Sommer, Felix Kordowski and Joscha Büch. First for their input in the ADAM10 project but most importantly for the good friends they became over the years.

I also want to thank my colleagues in the department of dermatology. In particular: Maria Sperrhacker for her critical review of the ADAM10 data and the time and effort she invested in proof-reading versions of my manuscript. Björn Ahrens for his technical support and his help with the ADAM10 project. Lena Baumecker, for being strong enough over the last years to share the office with me and for the multiple conversations about and beyond science. Martin Veit for the production of the ANO6 mutant. Furthermore, I want to thank him and Hagen Rövekamp for the X-challenges over the years.

My special thanks are also dedicated to the working group of Thomas Gutschmann. In particular Christian Nehls and Wilmar-Alexander Correa-Vargas for their work with the ADAM10 stalk peptide and their additional time and effort for data preparation.

I also want to thank Joachim Grötzinger, as my Co-supervisor in the IRTG of the SFB877 and for the many enlightening conversations about the ADAM10 structure.

My special gratitude is to Thomas Roeder for agreeing to be the first supervisor of my thesis

Furthermore, I want to thank the SFB877 and the IRTG for financial support. In particular to Christine Desel for being a good cooperation partner.

Finally, I want to thank my family. Most importantly my grandmother Ingrid Ruder. Your support gave me the opportunity to follow my ideas that built the fundament for this thesis. I am thankful for your trust and I hope you will be proud.

Most importantly, my greatest gratitude goes to Glenda Mendieta Leiva: Su papel en mi vida está más allá de esta tesis. Novia, mentor, apoyo moral. La roca en la orilla. Mi amor, gracias por todo y que eres parte de mi vida.

14. Erklärung

Hiermit bestätige ich, Florian Bleibaum, dass die vorliegende Arbeit – abgesehen von der wissenschaftlichen Beratung durch meine BetreuerInnen – nach Inhalt und Form, und nur unter Zuhilfenahme der angegebenen Quellen und Hilfsmittel, von mir persönlich verfasst wurde. Die Arbeit wurde unter Einhaltung der Regeln guter wissenschaftlicher Praxis der Deutschen Forschungsgemeinschaft (DFG) verfasst. Die vorliegende Arbeit wurde keiner anderen Universität, weder teilweise noch vollständig im Rahmen eines anderen Prüfungsverfahrens, zur Begutachtung vorgelegt.

Ein Manuskript, das Daten dieser Arbeit enthält wird zur Einreichung vorbereitet:

Florian Bleibaum, Anselm Sommer, Martin Veit, Jörg Andrä, Karl Kunzelmann, Christian Nehls, Wilmar Correa, Thomas Gutschmann, Joachim Grötzinger, Sucharit Bhakdi, Karina Reiss

ADAM10 sheddase activation is controlled by cell membrane asymmetry

Kiel, April 2018

(Florian Bleibaum)

15. Curriculum vitae

Name: Florian Bleibaum
Date of Birth: 26.10.1984
Born in: Hameln
Citizenship: German

Education:

01/2015 – currently Doctoral researcher at the University of Kiel
AG Cellular Pathobiochemistry, Department of Dermatology, UKSH, Kiel
Thesis: “On the relevance of PS exposure as a regulatory event for ADAM10-mediated substrate release”

05/2014 – 12/2014 Scientific assistant at the University of Oldenburg
AG Neurosensorik (Animal Navigation)

10/2010 – 05/2014 Master of Biology at the University of Oldenburg
AG Neurosensorik (Animal Navigation), IBU, Oldenburg
Thesis: “Characterization, identification and siRNA induced regulation of Erithacus rubecula cryptochromes”

10/2006 – 10/2010 Bachelor of Environmental Sciences at the Leuphana University
AG Ecosystem Functions, Institute of Ecology, Lüneburg
Thesis: “The impact of changing environmental factors on host – parasite communities. Parameters for further laboratory tests”

10/2002 – 07/2005 Abitur graduation
Elisabeth-Selbert-Schule Hameln
Fachgymnasium für Gesundheit und Soziales